

Title	Crystalline properties of gallium oxide thin films epitaxially grown by mist chemical vapor deposition( Dissertation_全文 )
Author(s)	Lee, Sam-Dong
Citation	京都大学
Issue Date	2016-03-23
URL	<a href="https://doi.org/10.14989/doctor.k19721">https://doi.org/10.14989/doctor.k19721</a>
Right	許諾条件により本文は2017-01-01に公開
Type	Thesis or Dissertation
Textversion	ETD

**Crystalline properties of gallium oxide thin films  
epitaxially grown by mist chemical vapor deposition**

**SAM-DONG LEE**

**Crystalline properties of gallium oxide thin films  
epitaxially grown by mist chemical vapor deposition**

**2016**

**SAM-DONG LEE**

# **Crystalline properties of gallium oxide thin films epitaxially grown by mist chemical vapor deposition**

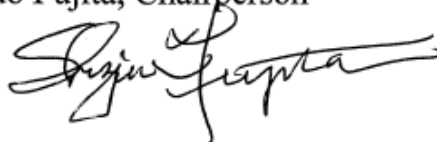
**By Sam-dong Lee**

A thesis submitted to the Graduate School of Kyoto University in partial fulfillment  
of the requirements for the degree of Doctor of Philosophy in Electronic Science and  
Engineering

Thesis Advisor: Professor Shizuo Fujita

Examining Committee:

Professor Shizuo Fujita, Chairperson



Professor Takaoka Gikan



Professor Jun Suda



Kyoto University  
February 2016

# CONTENTS

<b>Chapter 1. Introduction</b> .....	1
1.1 Backgrounds .....	1
1.2 Purpose of this study .....	4
1.3 Synopsis .....	5
References .....	7
<b>Chapter 2. Literature survey: Growth methods and properties of Ga<sub>2</sub>O<sub>3</sub> and     fundamental study</b> .....	13
2.1 Fundamental properties of Ga <sub>2</sub> O <sub>3</sub> .....	13
2.2 Technical background for growth method of Ga <sub>2</sub> O <sub>3</sub> .....	16
2.3 Power devices with wide-bandgap semiconductors .....	17
References .....	20
<b>Chapter 3. Growth of hetero-epitaxial β-Ga<sub>2</sub>O<sub>3</sub> thin films on cubic substrates</b> .....	23
3.1 Introduction .....	23
3.2 Growth of β-Ga <sub>2</sub> O <sub>3</sub> thin films on YSZ substrates as a function of growth temperature .....	24
3.3 Growth of β-Ga <sub>2</sub> O <sub>3</sub> thin films on cubic substrates as a function of substrate direction .....	27
3.4 Summary .....	41
References .....	42
<b>Chapter 4. Growth of homo-epitaxial and conductive Sn-doped β-Ga<sub>2</sub>O<sub>3</sub> thin     films</b> .....	45
4.1 Introduction .....	45
4.2 Basic growth conditions of homo-epitaxial β-Ga <sub>2</sub> O <sub>3</sub> films .....	46
4.2.1 Sample preparation .....	46
4.2.2 Structural properties of β-Ga <sub>2</sub> O <sub>3</sub> as a function of growth temperature .....	47

4.3 Unintentionally doped $\beta$ -Ga <sub>2</sub> O <sub>3</sub> homo-epitaxial films on conductive substrates .....	50
4.3.1 Sample preparation .....	50
4.3.2 Structural properties of homo-epitaxial unintentionally doped $\beta$ -Ga <sub>2</sub> O <sub>3</sub> films .....	50
4.3.3 Optical properties of homo-epitaxial unintentionally doped $\beta$ -Ga <sub>2</sub> O <sub>3</sub> films .....	55
4.3.4 $\beta$ -Ga <sub>2</sub> O <sub>3</sub> -based Schottky barrier diodes .....	56
4.4 Conductive Sn-doped $\beta$ -Ga <sub>2</sub> O <sub>3</sub> homo-epitaxial films on semi-insulating substrates .....	58
4.4.1 Sample preparation .....	58
4.4.2 Structural properties of homo-epitaxial Sn-doped $\beta$ -Ga <sub>2</sub> O <sub>3</sub> films ..	58
4.4.3 Electrical properties of homo-epitaxial Sn-doped $\beta$ -Ga <sub>2</sub> O <sub>3</sub> films ..	60
4.5 Summary .....	63
References .....	64
<b>Chapter 5. Growth of <math>\alpha</math>-Ga<sub>2</sub>O<sub>3</sub> thin films on c-sapphire substrate .....</b>	<b>67</b>
5.1 Introduction .....	67
5.2 $\alpha$ -Ga <sub>2</sub> O <sub>3</sub> films on <i>c</i> -Al <sub>2</sub> O <sub>3</sub> substrate .....	68
5.2.1 Sample preparation .....	68
5.2.2 Crystallinity of $\alpha$ -Ga <sub>2</sub> O <sub>3</sub> as a function of carrier gas flow rate .....	68
5.3 Thermal stability of $\alpha$ -Ga <sub>2</sub> O <sub>3</sub> against annealing process .....	71
5.3.1 Sample preparation .....	71
5.3.2 Structural properties after annealing .....	71
5.3.3 Optical properties after annealing .....	73
5.3.4 Surface morphology .....	75
5.4 Summary .....	76
References .....	77
<b>Chapter 6. Effect of Al doping for enhanced thermal stability of <math>\alpha</math>-Ga<sub>2</sub>O<sub>3</sub> thin films .....</b>	<b>79</b>
6.1 Introduction .....	79
6.2 Fabrication and characterization of Al-doped $\alpha$ -Ga <sub>2</sub> O <sub>3</sub> films .....	80

6.2.1 Sample preparation .....	80
6.2.2 Structural properties .....	81
6.3 Thermal stability for Al-doped $\alpha$ -Ga <sub>2</sub> O <sub>3</sub> films .....	83
6.4 Summary .....	91
References .....	93
<b>Chapter 7. Conclusions</b> .....	<b>95</b>
<b>LIST OF ACHIEVEMENTS</b> .....	<b>100</b>
<b>ACKNOLWEDGEMENTS</b> .....	<b>105</b>



# Chapter 1

## Introduction

### 1.1 Backgrounds

World energy consumption is rapidly increasing with expanded world population and a high standard of living. This apparently has led the increased consumption of fossil fuel because most of energy comes from it as shown Fig.1.1 [1], and this causes global warming by CO<sub>2</sub> emissions [2]. In order to slow down the global warming, in December 2015, 195 nations negotiated the establishment of Paris Agreement to govern the emission of greenhouse gases, as a new and up-to-date standard for future sustainable development of the society after Kyoto protocol forged in 1999 [3,4]. Therefore, advanced nations are starting to act in renewable green energy and enhanced energy efficiency [5].

Power electronics could help enhancing energy generation and conversion efficiency, and this area is now attracting focused interest as a key technology to save electronic energy. Power electronics has been supported by power semiconductor devices. In the 1960s, rectifier diodes and thyristors became commercially available [6-8]. The power efficiency has improved greatly due to supply of the inverter with insulated gate bipolar transistors developed in the late 1980s [9]. Then challenges to use new semiconductor materials other than silicon (Si), which had been the only materials supporting the development of a variety of electronics devices over fifty years, have been become active because Si-based power devices are almost facing to their physical limit.

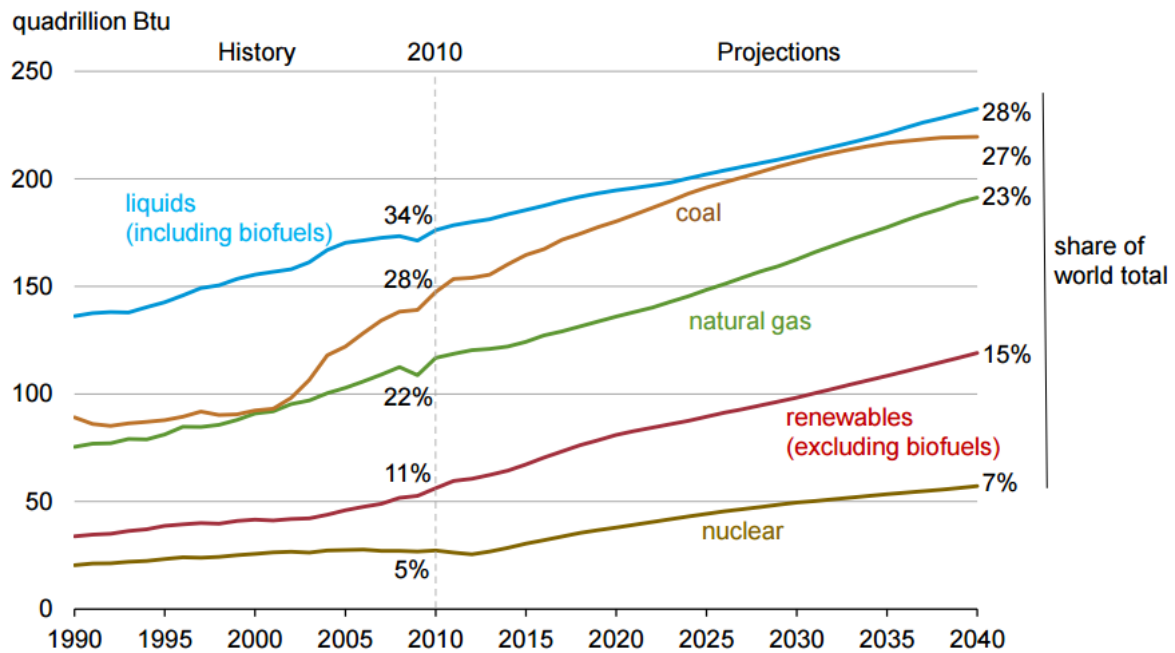


Figure 1.1. Energy information administration (EIA), Annual energy outlook 2105.

([www.eia.gov/forecasts/aeo/](http://www.eia.gov/forecasts/aeo/))

Many researchers have paid attention to wide bandgap semiconductors as candidate materials for power devices [10-14]. Silicon carbide (SiC) and gallium nitride (GaN), possessing the bandgap of 3.3 and 3.4 eV, respectively, as well as strong chemical bonding, are the most promising material [15-22]. Practical device operation showing high power conversion efficiency has already been demonstrated [23-27], but SiC- and GaN-based devices still possess several remaining problems for mass production and cost due to complicated growth techniques, extremely limited growth environments, and expensive substrates.

In the last years, gallium oxide ( $\text{Ga}_2\text{O}_3$ ) has attracted increasing attention as a promising new candidate for application to power semiconductor devices [13,14,28-31]. Moreover,  $\text{Ga}_2\text{O}_3$  has also been studied as transparent conducting layers [32-35], ultraviolet photodetectors [36-44], and gas

sensors [45-51]. Ga<sub>2</sub>O<sub>3</sub> has the largest bandgap of all oxide semiconductors, and its large bandgap is expected to increase performance of power devices compared to those of SiC and GaN [52-61]. The estimated Baliga's figure of merit, which is a good guideline for an effective power semiconductor material, is several times greater for Ga<sub>2</sub>O<sub>3</sub> than for SiC and GaN [62-64]. In addition, Ga<sub>2</sub>O<sub>3</sub>-based power devices are more attractive owing to the available high quality single-crystal substrates. Bulk Ga<sub>2</sub>O<sub>3</sub> substrates have been fabricated by using the floating zone, the edge-defined film-fed growth (EFG), and the Czochralski method [63-69]. Recently, new power devices with epitaxial Ga<sub>2</sub>O<sub>3</sub> film on a single-crystal Ga<sub>2</sub>O<sub>3</sub> substrates have been demonstrated such as metal oxide semiconductor field effect transistors (MOSFETs) and metal semiconductor FETs (MESFETs) [14,63,70-72]. Molecular beam epitaxy (MBE) and metal organic chemical vapor deposition (MOCVD) have been mainly used for the growth of Ga<sub>2</sub>O<sub>3</sub> thin films [14,63,70-72], however, these techniques are generally expensive, energy consuming, and extremely limiting the growth environments.

The use of mist CVD has been proposed and investigated for the growth of Ga<sub>2</sub>O<sub>3</sub> for power devices. It has been shown that the mist CVD method with non-vacuum system is a very simple and cost-effective process with easy set-up for the growth compared to MBE and MOCVD [73]. For the growth of various oxide materials, it just needs safe and soluble source precursors such as metal-acetylacetonate, -chloride dehydrate, and -acetate. This is also applicable for doping processes.

## 1.1 Purpose of this study

In this study, the author emphasizes the crystalline properties of  $\text{Ga}_2\text{O}_3$  thin films epitaxially grown by mist CVD aiming at their future applications to power devices. As will be explained later, there are five different phases (crystal structures) for  $\text{Ga}_2\text{O}_3$ . Among them, the most stable phase in thermodynamically is the monoclinic structure, which is labeled as  $\beta\text{-Ga}_2\text{O}_3$ . Bulk  $\text{Ga}_2\text{O}_3$  is constituted by the  $\beta$ -phase. The author will investigate the formation of  $\beta\text{-Ga}_2\text{O}_3$  by mist CVD and the emphasis will be given to control the electrical properties by doping. Other stable phase, though semi-stable phase, is the trigonal and corundum structure, which is labeled as  $\alpha\text{-Ga}_2\text{O}_3$ . High quality  $\alpha\text{-Ga}_2\text{O}_3$  has been demonstrated by the use of mist CVD on sapphire substrate [73,74]. However, the semi-stable phase is not suitable for the successive device processes such as metallization. The author will propose doping of aluminum (Al) to  $\alpha\text{-Ga}_2\text{O}_3$  aiming at solution hardening and show the enhanced thermal stability, contributing to widening the device process windows and to forming various high-performance devices.

The author strongly wishes and expects that, in coming years, the mist CVD method can be a useful technology for high performance  $\text{Ga}_2\text{O}_3$ -based power device saving our planet.

## 1.3 Synopsis

This thesis is organized as follows:

### **Chapter 2. Literature survey: Growth methods and properties of Ga<sub>2</sub>O<sub>3</sub> and fundamental study**

Chapter 2 presents introduction and principle of the mist CVD method and equipment as a growth method of Ga<sub>2</sub>O<sub>3</sub> thin films. Fundamental properties of Ga<sub>2</sub>O<sub>3</sub> will be summarized and the motivation and objective of this thesis will be clarified.

### **Chapter 3. Growth of hetero-epitaxial β-Ga<sub>2</sub>O<sub>3</sub> thin films on cubic substrates**

Chapter 3 describes growth of hetero-epitaxial β-Ga<sub>2</sub>O<sub>3</sub> thin films on cubic substrates by mist CVD as a fundamental study to realize β-Ga<sub>2</sub>O<sub>3</sub> films. First, optimization of the growth conditions for high quality β-Ga<sub>2</sub>O<sub>3</sub> thin films will be discussed in detail. Then, properties of β-Ga<sub>2</sub>O<sub>3</sub> thin films on various cubic substrates with different surface orientations are investigated to elucidate the growth behavior of β-Ga<sub>2</sub>O<sub>3</sub>.

### **Chapter 4. Growth of homo-epitaxial and conductive Sn-doped β-Ga<sub>2</sub>O<sub>3</sub> thin films**

Chapter 4 deals with homo-epitaxial and single-crystalline β-Ga<sub>2</sub>O<sub>3</sub> films grown by the mist CVD method. As a first step, fabrication of β-Ga<sub>2</sub>O<sub>3</sub> films is described as a function of the growth temperature. Furthermore, the fabrication of electrical conductive Sn-doped β-Ga<sub>2</sub>O<sub>3</sub> films on semi-insulating β-Ga<sub>2</sub>O<sub>3</sub> substrates is discussed, and the conductivity control will be demonstrated in terms of the Sn concentration in source solution.

## **Chapter 5. Growth of $\alpha$ -Ga<sub>2</sub>O<sub>3</sub> thin films on c-sapphire substrate**

Chapter 5 describes growth and thermal stability issues of  $\alpha$ -Ga<sub>2</sub>O<sub>3</sub> thin films on sapphire substrates at 470 °C as a function of the flow rate of carrier gas. Thermal stability of single-crystalline  $\alpha$ -Ga<sub>2</sub>O<sub>3</sub> films on *c*-plane Al<sub>2</sub>O<sub>3</sub> will be characterized by x-ray diffraction analysis and optical transmittance spectroscopy. Issues on the temperature limit for the successive device process will be discussed.

## **Chapter 6. Effect of Al doping for enhanced thermal stability of $\alpha$ -Ga<sub>2</sub>O<sub>3</sub> thin films**

Chapter 6 describes the attempts to enhance the thermal stability of  $\alpha$ -Ga<sub>2</sub>O<sub>3</sub> films on sapphire substrates by doping Al. Marked enhancement will be demonstrated and the prospect for future device applications will be discussed.

## **Chapter 7. Conclusions**

Finally, the conclusions of the work are presented in Chapter 7. Subjects to be investigated in the future study will also be discussed.

## References

- [1] <http://www.eia.gov/forecasts/aeo>
- [2] C. McGlade and P. Ekins, *Nature* **517**, 187 (2015).
- [3] T. Jayaraman and T. Kanitkar, *Econ. Polit. Weekly* **51**, 3 (2016).
- [4] S. H. Schneider and *Climatic Change* **39**, 1 (1998).
- [5] <https://www.iea.org/publications/insights/insightpublications/enabling-renewable-energy-and-energy-efficiency-technologies.html>
- [6] T. Misawa, *J. Electron. Control* **7**, 523 (1957).
- [7] G. D. Bergman, *Solid-St. Electron.* **8**, 757 (1965).
- [8] J.M. Garrett, M. J. Evans and M. S. Towers, *Solid-St. Electro.* **39**, 137 (1996).
- [9] A. R. Hefner Jr and D. L. Blackburn, *Solid State Electron.* **31**, 10 (1988).
- [10] R. Singh, D. C. Capell, A. R. Hefner, J. Lai and J. W. Palmour, *IEEE Trans. Electron Devices* **49**, 2054 (2002)
- [11] R. J. Callanan, A. Agarwal, A. Burk, M. Das, B. Hull, F. Husna, A. Powell, J. Richmond, S.-H. Ryu and Q. Zhang, *Proc. 34th Ind. Electron. Conf.* 2885 (2008)
- [12] P. Srivastava, J. Das, D. Visalli, M. Van Hove, P. E. Malinowski, D. Marcon, S. Lenci, K. Geens, K. Cheng, M. Leys, S. Decoutere, R. P. Mertens and G. Borghs, *IEEE Electron Dev. Lett.* **32**, 30 (2011)
- [13] K. Sasaki, M. Higashiwaki, A. Kuramata, T. Masui and S. Yamakoshi, *IEEE Electr. Device L.* **34**, 493 (2013).

- [14] M. Higashiwaki, K. Sasaki, A. Kuramata, T. Masui and S. Yamakoshi, *Phys. Status Solidi A* **211**, 21 (2014).
- [15] D. K. Ferry, *Phys. Rev. B* **12**, 2361 (1975).
- [16] K. Shenai, R. S. Scott and B. J. Balliga, *IEEE T. Electron Dev.* **36**, 1811 (1989).
- [17] M. Asif Khan, J. N. Kuznia, A. R. Bhattarai and D. T. Olson, *Appl. Phys. Lett.* **62**, 1786 (1993).
- [18] Ruff, Martin, Mitlehner, Heinz, Helbig and Reinhard, *IEEE T. Electron Dev.* **41**, 1040 (1994).
- [19] H. Morkoç, S. Strite, G. B. Gao, M. E. Lin, B. Sverdlov, and M. Burns. *J. Appl. Phys.* **76**, 1363 (1994).
- [20] T. P. Chow and R. Tyagi, *IEEE T. Ind. Appl.* **37**, 1282 (2001).
- [21] R. J. Trew, *Proc. IEEE* **90**, 1032 (2002).
- [22] H. Kambayashi, S. Yoshihiro, S. Ootomo, T. Kokawa, T. Nomura, S. Kato and T. P. Chow, *Solid State Electron.* **52**, 660 (2010).
- [23] H. Niwa, J. Suda and T. Kimoto, *Appl. Phys. Express* **5**, 064001 (2012).
- [24] R. Pengelly, S. M. Wood, J. W. Milligan, S. T. Sheppard and W. L. Pribble, *IEEE Trans. Microwave Theory Tech.* **60**, 1764 (2012).
- [25] B. J. Baliga and *Semicond. Sci. Tech.* **28**, 074011 (2013).
- [26] M. J. Scott, L. Fu, X. Zhang, J. Li, C. Yao, M. Sievers and J. Wang, *Semicond. Sci. Tech.* **28**, 074013 (2013).
- [27] S. Dimitrijević, J. Han, H. A. Moghadam and A. Aminbeidokhti, *MRS Bull.* **40**, 399 (2015).
- [28] M. H. Wong, K. Sasaki, A. Kuramata, S. Yamakoshi and M. Higashiwaki, *Appl. Phys. Lett.* **106**, 032105 (2015).

- [29] T. Kamimura, K. Sasaki, M. Hoi Wong, D. Krishnamurthy, A. Kuramata, T. Masui, S. Yamakoshi and M. Higashiwaki, *Appl. Phys. Lett.* **104**, 192104 (2014)
- [30] K. Sasaki, M. Higashiwaki, A. Kuramata, T. Masui and S. Yamakoshi, *Appl. Phys. Express* **6**, 086502 (2013).
- [31] N. Suzuki, S. Ohira, M. Tanaka, T. Sugawara, K. Nakajima, and T. Shishido, *Phys. Status Solidi C* **4**, 2310 (2007).
- [32] M. Orita, H. Ohta, M. Hirano and H. Hosono, *Appl. Phys. Lett.* **77**, 4166 (2000).
- [33] E. G. Villora, M. Yamaga, T. Inoue, S. Yabasi, Y. Masui, T. Sugawara and T. Fukuda, *Jpn. J. Appl. Phys.* **41**, L622 (2002)
- [34] H. Ohta, K. Nomura, H. Hiramatsu, K. Ueda, T. Kamiya, M. Hirano and H. Hosono, *Solid-State Electron.* **47**, 2261 (2003)
- [35] S. Ohira, N. Arai, M. Tanaka, T. Sugawara, K. Nakajima and T. Shishido, *Thin Solid Films* **516**, 5763 (2008)
- [36] T. Oshima, T. Okuno and S. Fujita, *Jpn. J. Appl. Phys. Lett.* **46**,11 (2007).
- [37] Y. Kokubun, K. Miura, F. Endo, S. Nakagomi, *Appl. Phys. Lett.* **90**, 031912 (2007)
- [38] M.-Y. Tsai, O. Bierwagen, M. E. White and J. S. Speck, *J. Vac. Sci. Technol. A* **28**, 354 (2010)
- [39] W. Y. Weng, T. J. Hsueh, S. J. Chang, G. J. Huang, H. T. Hsueh, *IEEE Sensors J.* **11**, 999 (2011)
- [40] R. Suzuki, S. Nakagomi and Y. Kokubun, *Appl. Phys. Lett.* **98**, 1114 (2011)
- [41] W. Y. Weng, T. J. Hsueh, S. J. Chang, G. J. Huang and H. T. Hsueh, *IEEE Photonics Technol. Lett.* **23**, 444 (2011)

- [42] S. Nakagomi and Y. Kokubun, *J. Cryst. Growth* **349**, 12 (2012)
- [43] L. Kong, J. Ma, C. Luan and W. Mi, Y. Lv, *Thin Solid Films*, **520**, 4270 (2012)
- [44] S.-L. Ou, D.-S. Wu, Y.-C. Fu, S.-P. Liu, R.-H. Horng, L. Liu and Z.-C. Feng, *Mater. Chem. Phys.* **133**, 700 (2012)
- [45] M. Fleischer and H. Meixner, *Sensor. Actuat. B* **4**, 437 (1991)
- [46] M. Fleischer and H. Meixner, *Sensor. Actuat. B* **6**, 257 (1992)
- [47] M. Fleischer, J. Giber and H. Meixner, *Appl. Phys.* **A54**, 560 (1992)
- [48] M. Ogita, N. Saika, Y. Nakanishi, Y. Hatanaka, *Appl. Surf. Sci.* **142**, 188 (1999)
- [49] M. Ogita, K. Higo, Y. Nakanishi and Y. Hatanaka, *Appl. Surf. Sci.* **175-176**, (2001).
- [50] A. Trinchi, W. Wlodarski, Y. X. Li, *Sensor. Actuat. B* **100**, 94 (2004)
- [51] S. Nakagomi, T. Sai, Y. Kokubun, *Sensor. Actuat. B: Chem.* **187**, 413 (2013)
- [52] H. H. Tippins, *Phys. Rev.* **140**, A316 (1965).
- [53] H. He, R. Orlando, M. A. Blanco, R. Pandey, E. Amazallag, I. Baraille, and M. Rérat, *Phys. Rev. B* **74**, 195123 (2006).
- [54] N. Ueda, H. Hosono, R. Waseda, and H. Kawazoe, *Appl. Phys. Lett.* **70**, 3561 (1997).
- [55] E. G. Villora, K. Shimamura, Y. Yoshikawa, T. Ujiie, and K. Aoki, *Appl. Phys. Lett.* **92**, 202120 (2008).
- [56] J. B. Varley, J. R. Weber, A. Janotti, and G. G. Van De Walle, *Appl. Phys. Lett.* **97**, 142106 (2010).
- [57] K. Yamaguchi, *Solid State Commun.* **131**, 739 (2004).
- [58] E.G. Villora, K. Shimamura, T. Ujiie, and K. Aoki, *Appl. Phys. Lett.* **92**, 202118 (2008).

- [59] T. Oshima, T. Okuno, N. Arai, Y. Kobayashi, and S. Fujita, *Jpn. J. Appl. Phys.* **48**, 070202 (2009)
- [60] T. Oshima, T. Okuno, N. Arai, N. Suzuki, S. Ohira, and S. Fujita, *Appl. Phys. Express* **1**, 011202 (2008)
- [61] T. Oshima, K. Kaminaga, A. Mukai, K. Sasaki, T. Masui, A. Kuramata, S. Yamakoshi, S. Fujita, and A. Ohtomo, **52**, 051101 (2013)
- [62] B. J. Baliga, *J. Appl. Phys.* **53**, 1759 (1982)
- [63] M. Higashiwaki, K. Sasaki, A. Kuramata, T. Masui, and S. Yamakoshi, *Appl. Phys. Lett.* **100**, 013504 (2012).
- [64] K. Sasaki, A. Kuramata, T. Masui, E. G. Villora, K. Shimamura, and S. Yamakoshi, *Appl. Phys. Express* **5**, 035502 (2012).
- [65] Y. Tamm, J. M. Ko, A. Yoshikawa, and T. Fukuda, *Sol. Energ. Mat. Sol. C.* **66**, 369 (2001).
- [66] E. G. Villora, K. Shimamura, Y. Yoshikawa, K. Aoki, and N. Ichinose, *J. Cryst. Growth* **270**, 420 (2004).
- [67] H. Aida, K. Nishiguchi, H. Takeda, N. Aota, K. Sunakawa, and Y. Yaguchi, *Jpn. J. Appl. Phys.* **47**, 8506 (2008).
- [68] Z. Galazka, R. Uecker, K. Imscher, M. Albrecht, D. Klimm, M. Pietsch, M. Brützm, R. Bertram, S. Ganschow, and R. Fornari, *Cryst. Res. Technol.* **45**, 1229 (2010).
- [69] K. Imscher, Z. Galazka, M. Pietsch, R. Uecker, and R. Fornari, *J. Appl. Phys.* **110**, 063720 (2011).

- [70] M. Higashiwaki, K. Sasaki, T. Kamimura, M. H. Wong, D. Krishnamurthy, A. Kuramata, T. Masui, and S. Yamakoshi, *Appl. Phys. Lett.* **103**, 123511 (2013).
- [71] K. Sasaki, M. Higashiwaki, A. Kuramata, T. Masui, and S. Yamakoshi, *J. Cryst. Growth* **378**, 591 (2013).
- [72] H. Murakami, K. Nomura, K. Goto, K. Sasaki, K. Kawara, Q. T. Thieu, R. Togashi, Y. Kumagai, M. Higashiwaki, A. Kuramata, S. Yamakoshi, B. Monemar, and A. Koukitu, *Appl. Phys. Express* **8**, 015503 (2015).
- [73] D. Shinohara and S. Fujita, *Jpn. J. Appl. Phys.* **47**, 9311 (2008).
- [74] K. Kaneko, H. Kawanowa, H. Ito, and S. Fujita, *Jpn. J. Appl. Phys.* **51**, 020201(2012).

## Chapter 2

### Literature survey: Growth methods and properties of Ga<sub>2</sub>O<sub>3</sub> and fundamental study.

#### 2.1 Fundamental properties of Ga<sub>2</sub>O<sub>3</sub>

Ga<sub>2</sub>O<sub>3</sub> is a compound semiconductor with wide bandgap of 4.9-5.3 eV [1-3]. The Ga<sub>2</sub>O<sub>3</sub> from the III-VI group is particularly interesting for its device potential because it is both transparent and conducting with a wide bandgap. Therefore, potential applications are strongly expected, for example, the interest in its electronic and optical properties has recently increased for various applications in semiconducting devices such as field-effect transistors, ultraviolet photo-detectors, transparent conducting films, and gas sensors as shown in Fig. 2.1 [4-7].

It is generally known that Ga<sub>2</sub>O<sub>3</sub> has five different crystalline phases,  $\alpha$ -,  $\beta$ -,  $\gamma$ -,  $\delta$ -, and  $\epsilon$  [2]. Among the five crystalline phases,  $\beta$ -Ga<sub>2</sub>O<sub>3</sub> is the thermodynamically most stable phase. Therefore, previous researches have not paid much attention for other phases of Ga<sub>2</sub>O<sub>3</sub> except for  $\beta$ -Ga<sub>2</sub>O<sub>3</sub>. Crystal structure of  $\beta$ -Ga<sub>2</sub>O<sub>3</sub> is monoclinic as shown in Fig 2.2.  $\beta$ -Ga<sub>2</sub>O<sub>3</sub> is known as a transparent semiconductor compound with a bandgap of 4.9 eV. One of the remarkable advantages of  $\beta$ -Ga<sub>2</sub>O<sub>3</sub> is that  $\beta$ -Ga<sub>2</sub>O<sub>3</sub> bulk substrates are available by the conventional solution methods such as floating zone (FZ), edge-defined film-fed growth (EFG), and Czochralski methods [8-11].

Corundum-structured  $\alpha$ -Ga<sub>2</sub>O<sub>3</sub> with the largest bandgap energy of 5.3 eV in oxide semiconductors as shown in Fig 2.3 is the thermodynamically semi-stable phase [2]. Therefore, it has not attracted

much attention owing to difficulty of the film synthesis. Nevertheless, the research group in Kyoto University, to which the author belongs, has shown that high-quality single crystalline  $\alpha$ -Ga<sub>2</sub>O<sub>3</sub> films were synthesized on sapphire ( $\alpha$ -Al<sub>2</sub>O<sub>3</sub>) substrates by the mist CVD method [1]. This has opened researches on  $\alpha$ -Ga<sub>2</sub>O<sub>3</sub>-based power devices which possess potential advantages of utilizing low-cost sapphire substrates and low-cost growth technology. In addition, corundum-structured  $\alpha$ -Ga<sub>2</sub>O<sub>3</sub> is attractive to fabricate alloys with other corundum-structured oxide materials such as Al<sub>2</sub>O<sub>3</sub>, In<sub>2</sub>O<sub>3</sub>, Cr<sub>2</sub>O<sub>3</sub>, and Fe<sub>2</sub>O<sub>3</sub> for bandgap engineering and function engineering. However, due to its semi-stable phase, inclusion of  $\beta$ -phase has been seen at the growth temperatures higher than 550 °C and at the successive annealing temperatures higher than 600 °C. This is a severe limit for  $\alpha$ -Ga<sub>2</sub>O<sub>3</sub>-based device processes because the process temperatures should be kept at lower than 600°C.

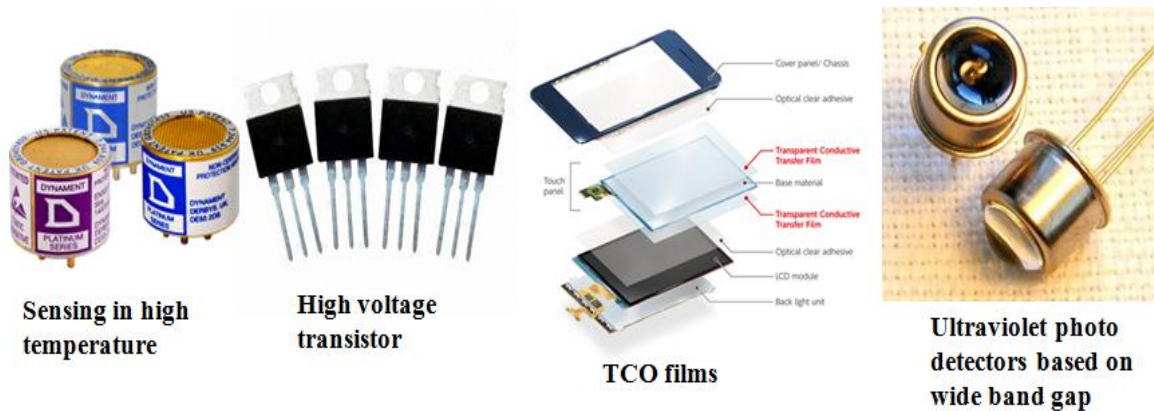


Figure 2.1. Several examples of potential device applications of Ga<sub>2</sub>O<sub>3</sub>. Of course the photographs are not real Ga<sub>2</sub>O<sub>3</sub> devices.

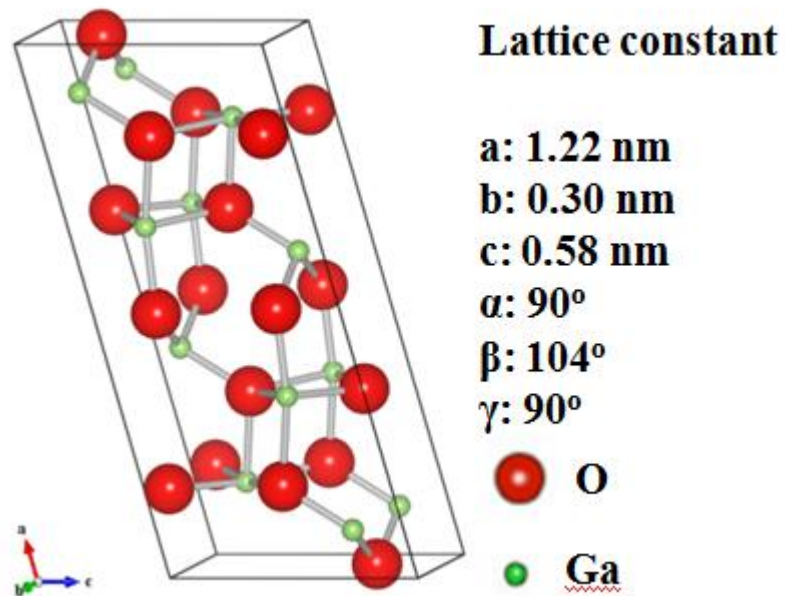


Figure 2.2. Illustration of crystalline structure of  $\beta$ -Ga<sub>2</sub>O<sub>3</sub>. Ga atoms are in green and O atoms in red.

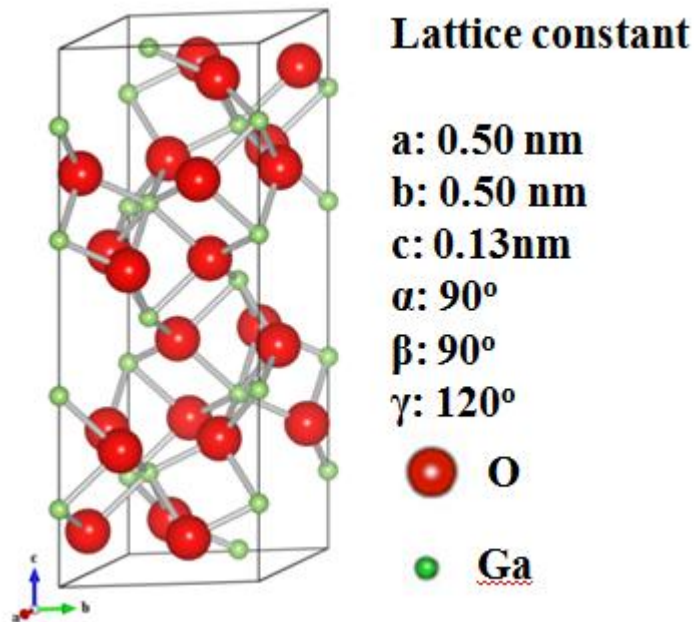


Figure 2.3. Illustration of crystalline structure of  $\alpha$ -Ga<sub>2</sub>O<sub>3</sub>. Ga atoms are in green and O atoms in red.

## 2.2 Technical background for growth method of Ga<sub>2</sub>O<sub>3</sub>

For growth equipments of Ga<sub>2</sub>O<sub>3</sub> thin films, MBE and MOCVD have been mainly used [12-14]. However, these techniques are generally expensive and energy consuming processes.

Mist CVD method with non-vacuum system is a very simple and cost-effective process with easy operation for growth compared to MBE and MOCVD [1]. A schematic drawing of a system for mist CVD is shown in Fig. 2.4. Mist CVD is one of the solution-based thin film fabrication techniques under atmospheric pressure. In the mist CVD system, there are two parts; a mist generator part and a reaction part. The mist generator part consists with a solution tank and ultrasonic generator(s). For the growth, source solution in the tank is atomized to micrometer-size droplet by the ultrasonic generator(s). Then, mist droplets are transferred from the mist generator part into the reaction part with a carrier gas, and then, thin films are fabricated by the thermal decomposition.. The reaction part is easily exchanged to various configurations according to the desired growth temperature and substrate size, allowing simple, fast-rate, and large-scale growth.

For growth of various oxide materials, as source precursors we can chose variety of chemicals containing the target metal element, as far as they are soluble to solvent (water or alcohol). Generally we chose such as metal-acetylacetonate, -chloride dehydrate, or -acetate as the source precursors.

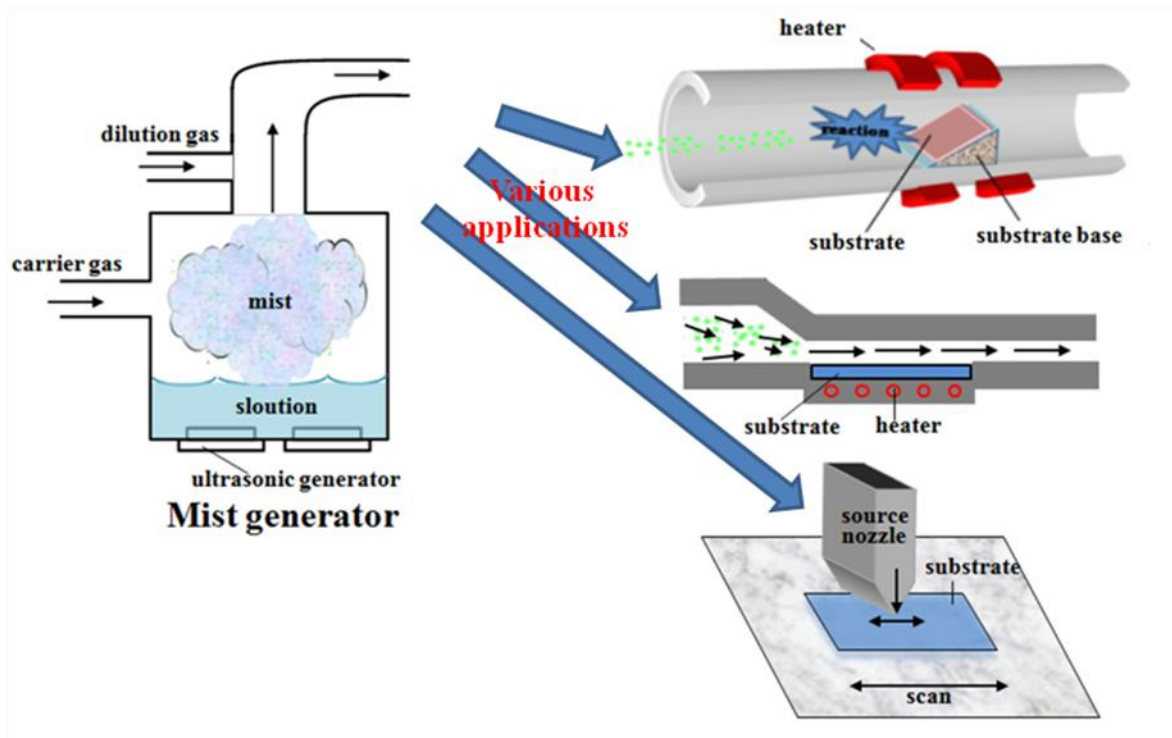


Figure 2.4. Schematic illustration of the mist CVD system used in this thesis.

### 2.3 Power devices with wide-bandgap semiconductors

Power devices, which can convert electric power with low energy consumption (that is, with high efficiency), have been required to promote the effective use of electric power and to achieve a low carbon and energy saving society. Wide bandgap semiconductors that have strong chemical bonding are promising candidates to be used as power devices because they can simultaneously achieve high breakdown voltage and low on-resistance compared to Si-based devices. Until now, SiC and GaN, having bandgaps of 3.3 and 3.4 eV, respectively [15-17], have been intensively investigated as the most promising candidates for practical power devices and several power devices and modules have already been in market [15-17].

However, SiC- and GaN-based devices still possess several remaining problems for mass production and cost because the growth techniques of them generally require extremely limited growth environments and the substrates are expensive. In the last years, Ga<sub>2</sub>O<sub>3</sub> has attracted increasing attention as a promising new candidate for application to power semiconductor devices [12,13]. Ga<sub>2</sub>O<sub>3</sub> has the largest bandgap of all oxide binary-compound semiconductors, and its large bandgap is expected to increase performance of power devices compared to those of SiC and GaN. Table 2.1 compares the important material properties of major semiconductors with those of β-Ga<sub>2</sub>O<sub>3</sub> [18]. The breakdown field of β-Ga<sub>2</sub>O<sub>3</sub> is expected to have a very large value of about 8 MV/cm.

The electron mobility of β-Ga<sub>2</sub>O<sub>3</sub> in Table 2.1 is estimated on the basis of the experimental data obtained for the Sn-doped epitaxial layers and n-type single-crystal substrates by M. Higashiwaki et al. [18]. From these material properties, the estimated Baliga's figure of merit, which is a good guideline for an effective power semiconductor material, for Ga<sub>2</sub>O<sub>3</sub> is several times greater than those for SiC and GaN [8,19]. These estimates indicate the great potential of Ga<sub>2</sub>O<sub>3</sub> for high power and high voltage device applications with low on-resistance. Furthermore, single crystal β-Ga<sub>2</sub>O<sub>3</sub> substrates can be fabricated from melt by the floating-zone (FZ), the edge-defined film-fed growth (EFG) methods [10,20]. This allows low-cost substrates in market and is favorable for growing high-quality β-Ga<sub>2</sub>O<sub>3</sub> layers by homo-epitaxy. Therefore, increasing interest is focusing on Ga<sub>2</sub>O<sub>3</sub>-based power devices which can achieve both high performance and low cost.

Table 2.1. Material properties of major semiconductors [18].

	<b>Si</b>	<b>SiC</b>	<b>GaN</b>	<b><math>\beta</math>-Ga<sub>2</sub>O<sub>3</sub></b>
<u>Bandgap</u> $E_g$ (eV)	1.12	3.26	3.4	<b>4.8~4.9</b>
Dielectric constant $\epsilon$	11.9	9.7	9.5	<b>10</b>
Electron mobility $\mu$ (cm <sup>2</sup> /Vs)	1350	1000	900	<b>300 (est.)</b>
<u>Thermal conductivity</u> ( W/cmK)	1.5	4.9	2	<b>0.14</b>
Breakdown voltage <u><math>E_b</math></u> (MV/cm)	0.3	2.7	3.5	<b>8 (est.)</b>
BFOM* ( $\epsilon\mu E_b^3$ )	1	340	870	<b>3444</b>

## References

- [1] D. Shinohara and S. Fujita, *Jpn. J. Appl. Phys.* **47**, 9311 (2008).
- [2] H. H. Tippins, *Phys. Rev.* **140**, A316 (1965).
- [3] M. Orita, H. Ohta, M. Hirano, and H. Hosono, *Appl. Phys. Lett.* **77**, 4166 (2000).
- [4] M. Higashiwaki, K. Sasaki, T. Kamimura, M. H. Wong, D. Krishnamurthy, A. Kuramata, T. Masui, and S. Yamakoshi, *Appl. Phys. Lett.* **103**, 123511 (2013).
- [5] T. Oshima, T. Okuno and S. Fujita, *Jpn. J. Appl. Phys. Lett.* **46**,11 (2007).
- [6] M. Orita, H. Ohta, M. Hirano and H. Hosono, *Appl. Phys. Lett.* **77**,4166 (2000).
- [7] M. Ogita, K. Higo, Y. Nakanishi and Y. Hatanaka, *Appl. Surf. Sci.* **175-176**, (2001).
- [8] K. Sasaki, A. Kuramata, T. Masui, E. G. Villora, K. Shimamura, and S. Yamakoshi, *Appl. Phys. Express* **5**, 035502 (2012).
- [9] Y. Tomm, J. M. Ko, A. Yoshikawa, and T. Fukuda, *Sol. Energ. Mat. Sol. C.* **66**, 369 (2001).
- [10] E. G. Villora, K. Shimamura, Y. Yoshikawa, K. Aoki, and N. Ichinose, *J. Cryst. Growth* **270**, 420 (2004).
- [11] Z. Galazka, R. Uecker, K. Irmscher, M. Albrecht, D. Klimm, M. Pietsch, M. Brützmam, R. Bertram, S. Ganschow, and R. Fornari, *Cryst. Res. Technol.* **45**, 1229 (2010).
- [12] M. Higashiwaki, K. Sasaki, T. Kamimura, M. H. Wong, D. Krishnamurthy, A. Kuramata, T. Masui, and S. Yamakoshi, *Appl. Phys. Lett.* **103**, 123511 (2013).
- [13] K. Sasaki, M. Higashiwaki, A. Kuramata, T. Masui, and S. Yamakoshi, *J. Cryst. Growth* **378**, 591 (2013).

- [14] H. Murakami, K. Nomura, K. Goto, K. Sasaki, K. Kawara, Q. T. Thieu, R. Togashi, Y. Kumagai, M. Higashiwaki, A. Kuramata, S. Yamakoshi, B. Monemar, and A. Koukitu, *Appl. Phys. Express* **8**, 015503 (2015).
- [15] H. Morkoç, S. Strite, G. B. GaO, M. E. Lin, B. Sverdlov and M. Burns, *J. Appl. Phys.* **76**, 1363 (1994).
- [16] H. Kambayashi, S. Yoshihiro, S. Ootomo, T. Kokawa, T. Nomura, S. Kato, and T. P. Chow, *Solid State Electron.* **52**, 660 (2010).
- [17] S. Dimitrijević, J. Han, H. A. Moghadam, and A. Aminbeidokhti, *MRS Bull.* **40**, 399 (2015).
- [18] M. Higashiwaki, K. Sasaki, A. Kuramata, T. Masui, and S. Yamakoshi, *Appl. Phys. Lett.* **100**, 013504 (2012).
- [19] B. J. Baliga, *J. Appl. Phys.* **53**, 1759 (1982).
- [20] H. Aida, K. Nishiguchi, H. Takeda, N. Aota, K. Sunakawa, and Y. Yaguchi, *J. Cryst. Growth* **47**, 8506 (2008).



## Chapter 3

### Growth of hetero-epitaxial $\beta$ -Ga<sub>2</sub>O<sub>3</sub> thin films on cubic substrates

#### 3.1 Introduction

Gallium oxide (Ga<sub>2</sub>O<sub>3</sub>) has attracted various applications such as ultraviolet optical devices, power electronic devices, transparent conducting layers, and gas sensors [1-4]. Ga<sub>2</sub>O<sub>3</sub> has five different phases ( $\alpha$ -,  $\beta$ -,  $\gamma$ -,  $\delta$ -, and  $\epsilon$ -phase) [5]. Among them,  $\beta$ -Ga<sub>2</sub>O<sub>3</sub> is the thermodynamically most stable phase [5].  $\beta$ -Ga<sub>2</sub>O<sub>3</sub> bulk substrates are becoming available by conventional met growth techniques such as the floating-zone (FZ), the edge-defined film-fed growth (EFG), and Czochralski (CZ) methods [6-9]. Furthermore, in the previous reports, homo-epitaxial  $\beta$ -Ga<sub>2</sub>O<sub>3</sub> thin films were grown by molecular-beam epitaxy (MBE) and metal organic chemical vapor deposition (MOCVD) techniques [10-12]. On the other hand,  $\alpha$ -Ga<sub>2</sub>O<sub>3</sub> was successfully grown by the mist CVD as being suitable for cost effective process, the mass production of oxide semiconductors, and low energy consuming process. So the author has shown his interest to fabricate and characterize homo-epitaxy  $\beta$ -Ga<sub>2</sub>O<sub>3</sub> semiconductors grown by mist CVD for the understanding of their structure and electrical properties. However,  $\beta$ -Ga<sub>2</sub>O<sub>3</sub> bulk substrates are under the development level and therefore they are still expensive for the fundamental research works.

In those regards, in this chapter, the author describes the properties of  $\beta$ -Ga<sub>2</sub>O<sub>3</sub> thin film on commercialized substrates such as yttrium-stabilized zirconia (YSZ), magnesium oxide (MgO), and spinel (MgAl<sub>2</sub>O<sub>4</sub>) where the surface structure is cubic, the same as that of rhombic  $\beta$ -Ga<sub>2</sub>O<sub>3</sub>. With the

growth on these substrates in terms of the substrate properties and its surface orientation  $\langle 111 \rangle$ ,  $\langle 110 \rangle$  and  $\langle 100 \rangle$ , the author aimed at investigating the fundamental growth behavior of  $\beta\text{-Ga}_2\text{O}_3$  on cubic substrates.

### **3.2 Growth of $\beta\text{-Ga}_2\text{O}_3$ thin film on YSZ substrates as a function of growth temperature**

The hetero-epitaxial  $\beta\text{-Ga}_2\text{O}_3$  films were grown on YSZ (111) substrates as a function of growth temperature by the mist CVD method. As a source solution, gallium acetylacetonate [ $\text{Ga}(\text{C}_5\text{H}_8\text{O}_3)_3$ ] of 0.05 mol/L solved in deionized water, with slight addition of hydrochloric acid [HCl] to solve the precursor completely was used. The  $\beta\text{-Ga}_2\text{O}_3$  films were synthesized at between 600 to 850 °C with 50 °C intervals during 60 min under the  $\text{O}_2$  gas in atmospheric pressure. Dilution gas flow rate and carrier gas flow rate were fixed at 1.0 L/min and 1.5 L/min, respectively. Structural properties of the  $\beta\text{-Ga}_2\text{O}_3$  films were investigated by X-ray diffraction (XRD). The morphology of samples was examined by field emission scanning electron microscopy (FE-SEM).

Figure 3.1 shows the XRD  $2\theta/\theta$  scan spectra of  $\beta\text{-Ga}_2\text{O}_3$  thin films on YSZ (111) substrates as a function of the growth temperature at between 600 and 850 °C. It was found that diffraction peaks originating from  $\beta\text{-Ga}_2\text{O}_3$  (-201) planes was observed for the samples grown at between 600 and 800 °C. This result suggests that the grown samples are  $\beta\text{-Ga}_2\text{O}_3$  with a single (-201) orientation. However, at the temperature higher than 800 °C, peaks originating from  $\beta\text{-Ga}_2\text{O}_3$  (-201) planes disappeared as shown Fig. 3.1. Figures 3.2 (a)-(d) show the FE-SEM images of the surface morphologies of the  $\beta\text{-Ga}_2\text{O}_3$  films deposited at 600, 650, 750 and 850 °C, respectively. In Figs. 3.2 (a), (b) and (c), which

correspond to the growth temperatures of 600, 650 and 750 °C, large and rough grains with well-defined grain boundaries were observed. On the other hand, at the growth temperature of 850 °C as shown in Fig 3.2 (d), the surface of the film is smoother, that is, fewer grain boundaries remain compared to other films.

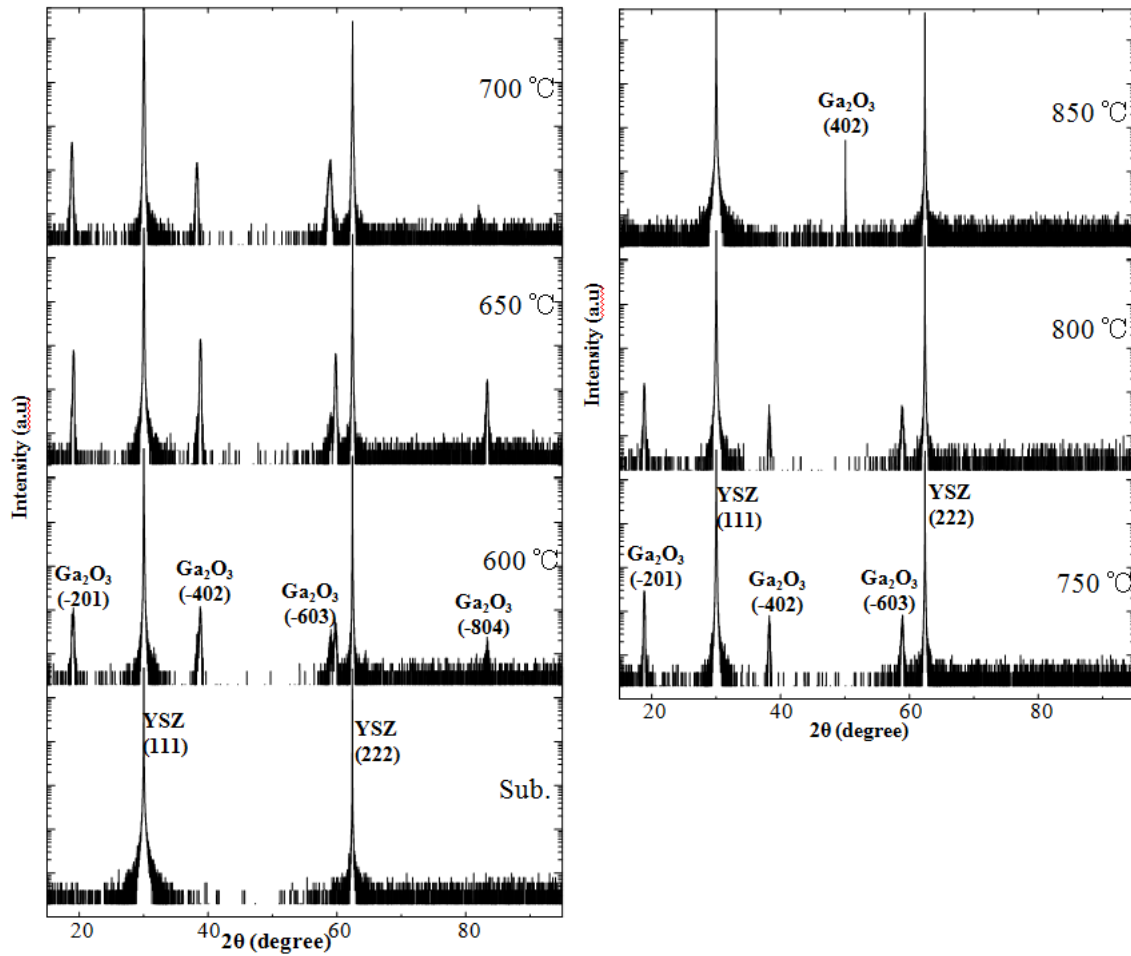


Figure 3.1. XRD 2θ/θ scan spectra for the hetero-epitaxial unintentionally doped β-Ga<sub>2</sub>O<sub>3</sub> films grown on YSZ (111) substrate as a function of growth temperatures

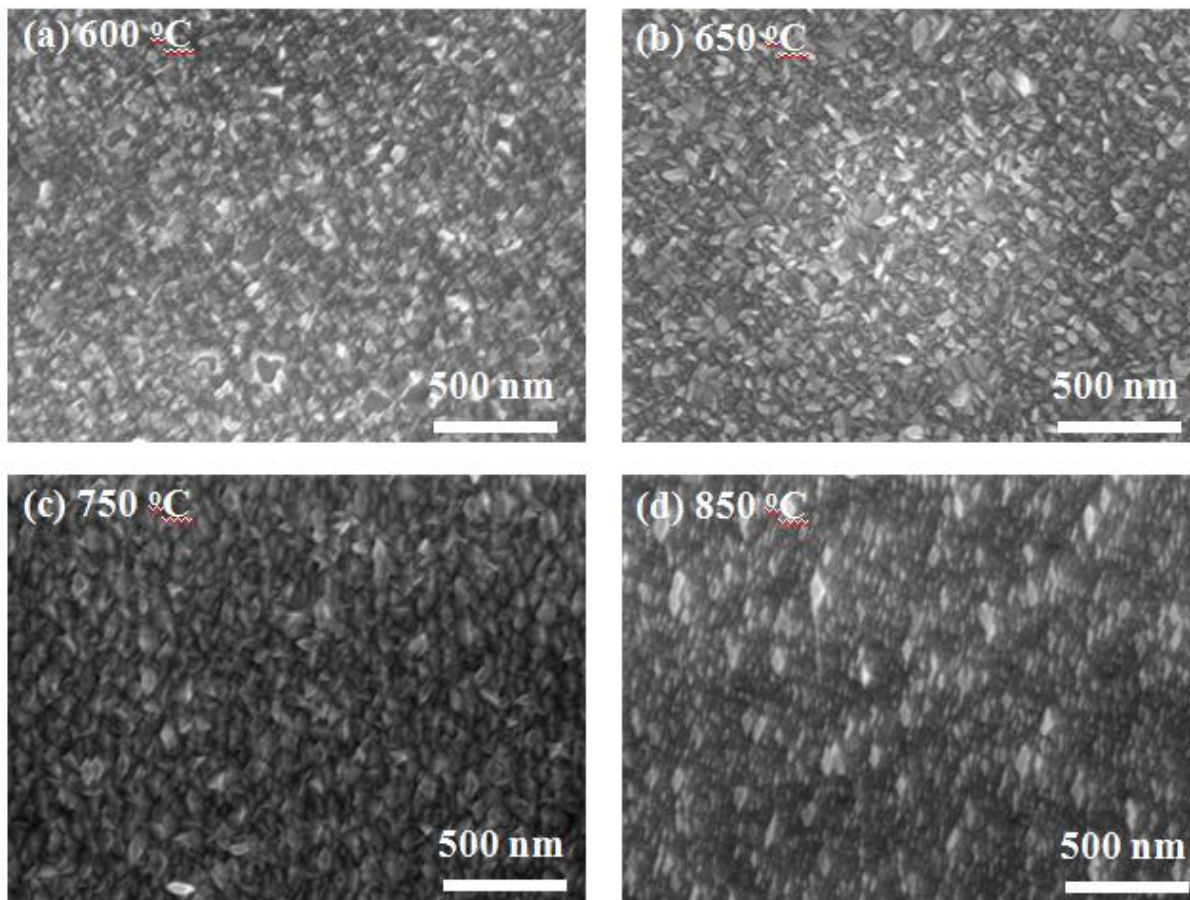


Figure 3.2. Plain-view FE-SEM images of  $\beta$ -Ga<sub>2</sub>O<sub>3</sub> films grown at temperatures of (a) 600 °C, (b) 650 °C, (c) 750 °C and (d) 850 °C.

### 3.3 Growth of $\beta$ -Ga<sub>2</sub>O<sub>3</sub> thin film on cubic substrates as a function of substrate direction

The hetero-epitaxial  $\beta$ -Ga<sub>2</sub>O<sub>3</sub> films were grown on various cubic substrates as a function of the substrate direction by the mist CVD method. The experimental condition is equal with chapter 3.2 except for the orientation of the substrate. As substrates, the author chose YSZ (111), (100), (110), MgAl<sub>2</sub>O<sub>4</sub> (111), and MgO (110). The growth temperature was set typically at 750 °C (or below), because well-crystallized  $\beta$ -Ga<sub>2</sub>O<sub>3</sub> was evidenced in section 3.2.

The XRD spectra of the  $\beta$ -Ga<sub>2</sub>O<sub>3</sub> films grown on YSZ (111), (100), (110), MgAl<sub>2</sub>O<sub>4</sub> (111), and MgO (110), are summarized in Fig. 3.3. As mentioned in section 3.2,  $\beta$ -Ga<sub>2</sub>O<sub>3</sub> (-201) was grown of YSZ (111). Similarly, on a MgAl<sub>2</sub>O<sub>4</sub> (111) substrate, single-phase  $\beta$ -Ga<sub>2</sub>O<sub>3</sub> (-201) was also grown. On a YSZ (100) substrate, a previous literature reported that, at the low growth temperature of 500 °C,  $\gamma$ -Ga<sub>2</sub>O<sub>3</sub> with cubic structure was grown on it [13]. However, in this experiments with high growth temperature over 600 °C, single-crystal  $\beta$ -Ga<sub>2</sub>O<sub>3</sub> (-201) was grown. In case on YSZ (110) and MgO (110), single-phase  $\beta$ -Ga<sub>2</sub>O<sub>3</sub> (-102) was grown. The overall results indicated that the growth behavior and direction of  $\beta$ -Ga<sub>2</sub>O<sub>3</sub> films grown on cubic structure greatly depend on the substrates. The physics in the background will be discussed later. The XRD full-width at half-maximum (FWHM) values of the  $\beta$ -Ga<sub>2</sub>O<sub>3</sub> films on YSZ (111), YSZ (110), and MgO (110) were 0.90, 0.50°, and 0.62°, respectively. The results imply that the crystallinity of  $\beta$ -Ga<sub>2</sub>O<sub>3</sub> films is affected by the substrates orientation.

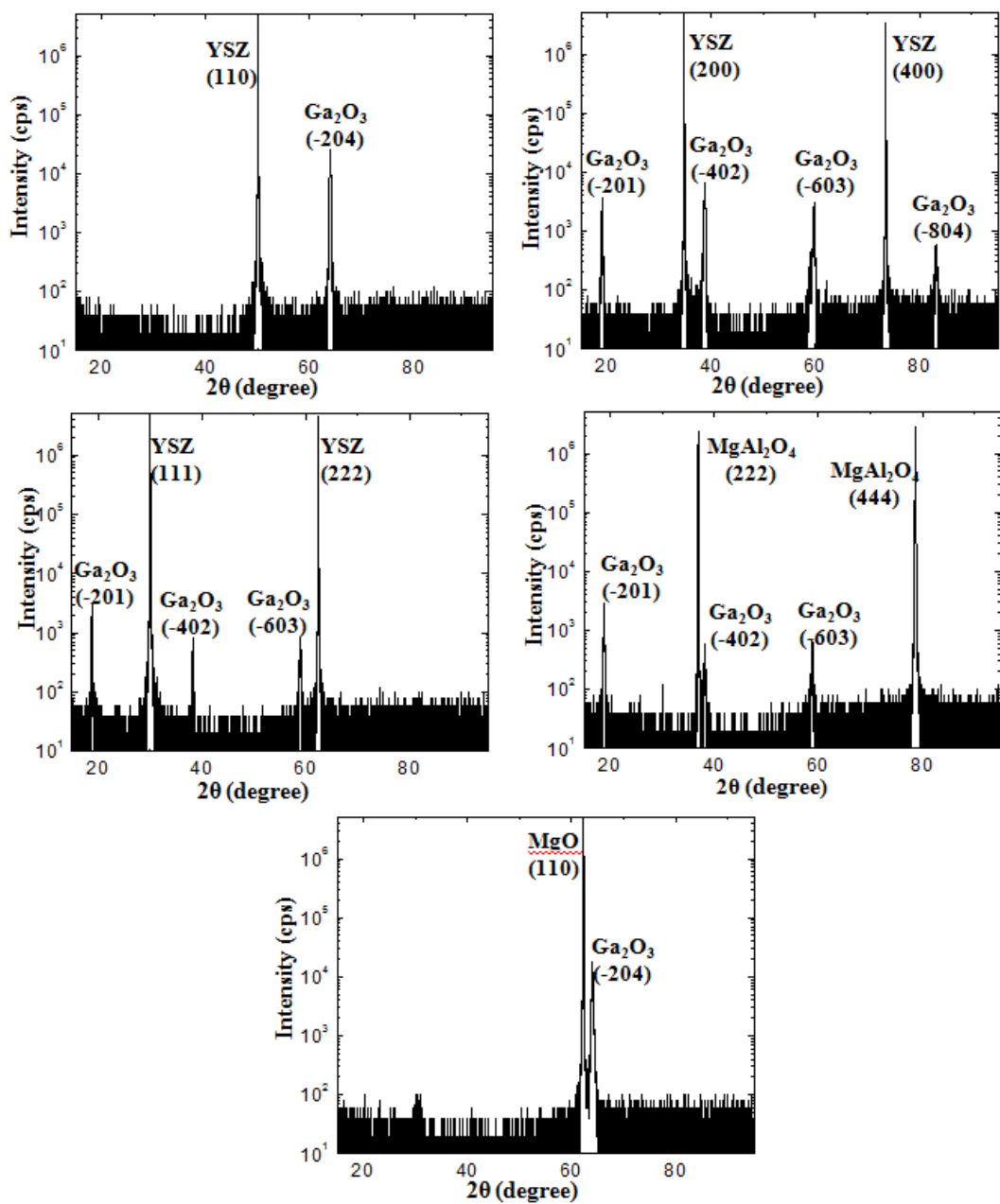


Figure 3.3. XRD 2θ/θ scan spectra for the hetero-epitaxial  $\beta$ -Ga<sub>2</sub>O<sub>3</sub> films grown on YSZ (110), (100), (111), MgAl<sub>2</sub>O<sub>4</sub> (111), and MgO (110), respectively.

Figure 3.4 shows the XRD off-specular phi-scan of YSZ (400) and  $\beta$ -Ga<sub>2</sub>O<sub>3</sub> (002) planes for the  $\beta$ -Ga<sub>2</sub>O<sub>3</sub> films grown on a YSZ (111) substrate. In YSZ (400), three peaks separated by 120° are measured as shown in Fig. 3.4 (b). The YSZ (400) was three-fold symmetrical along YSZ [111]. In  $\beta$ -Ga<sub>2</sub>O<sub>3</sub> (002) planes, six peaks separated by 60° are detected as shown in Fig. 3.4 (a). For single crystal  $\beta$ -Ga<sub>2</sub>O<sub>3</sub> without any domain structures, only one peak is supposed to appear in the measurement. Six peaks appeared in Fig. 3.4 (a) mean that six-fold domain structure is existed inside the film.

To explain structure relationship between a  $\beta$ -Ga<sub>2</sub>O<sub>3</sub> films and an YSZ substrate, the schematic diagram of geometrical epitaxial relationship between the film and the substrate was described in Fig. 3.5. The red balls were used to represent the O<sup>2-</sup> ions. The small balls with green color were used to represent the Ga<sup>3+</sup> and Zr<sup>4+</sup> ions because the radiuses of Ga<sup>3+</sup> and Zr<sup>4+</sup> ions are smaller than that of O<sup>2-</sup> ions. YSZ (111) has three equivalent directions [0-11], [-110], and [10-1] as shown in Fig. 3.5 (b).  $\beta$ -Ga<sub>2</sub>O<sub>3</sub> [010] growth direction has three equal opportunities along YSZ [0-11], [-110], and [10-1]. Since the  $\beta$ -Ga<sub>2</sub>O<sub>3</sub> is one-fold symmetrical,  $\beta$ -Ga<sub>2</sub>O<sub>3</sub> [010] growth direction along YSZ [-110] and [1-10] can get two different structures. Therefore, the six-fold domain structure was formed inside the film. The epitaxial relationship can be determined to be the  $\beta$ -Ga<sub>2</sub>O<sub>3</sub> (010)  $\parallel$  YSZ (110).

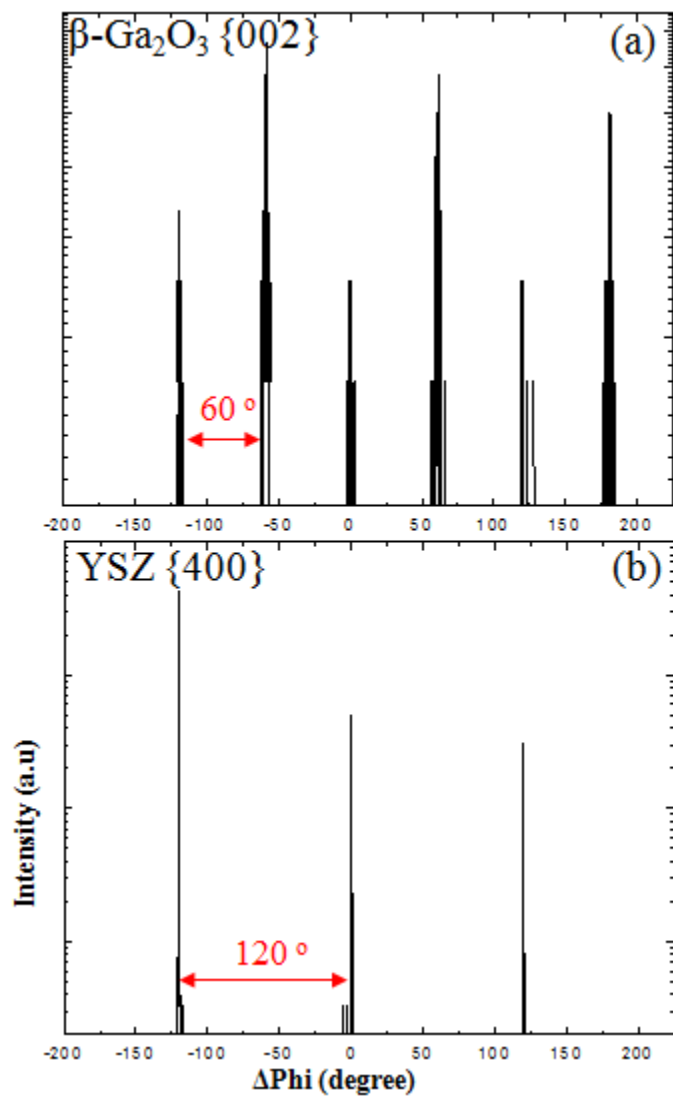


Figure 3.4. (a) XRD patterns of off-specular phi-scans of YSZ  $\{400\}$  and (b) Off-specular phi-scans of  $\beta\text{-Ga}_2\text{O}_3 \{002\}$  planes for the  $\beta\text{-Ga}_2\text{O}_3$  sample grown on YSZ (111).

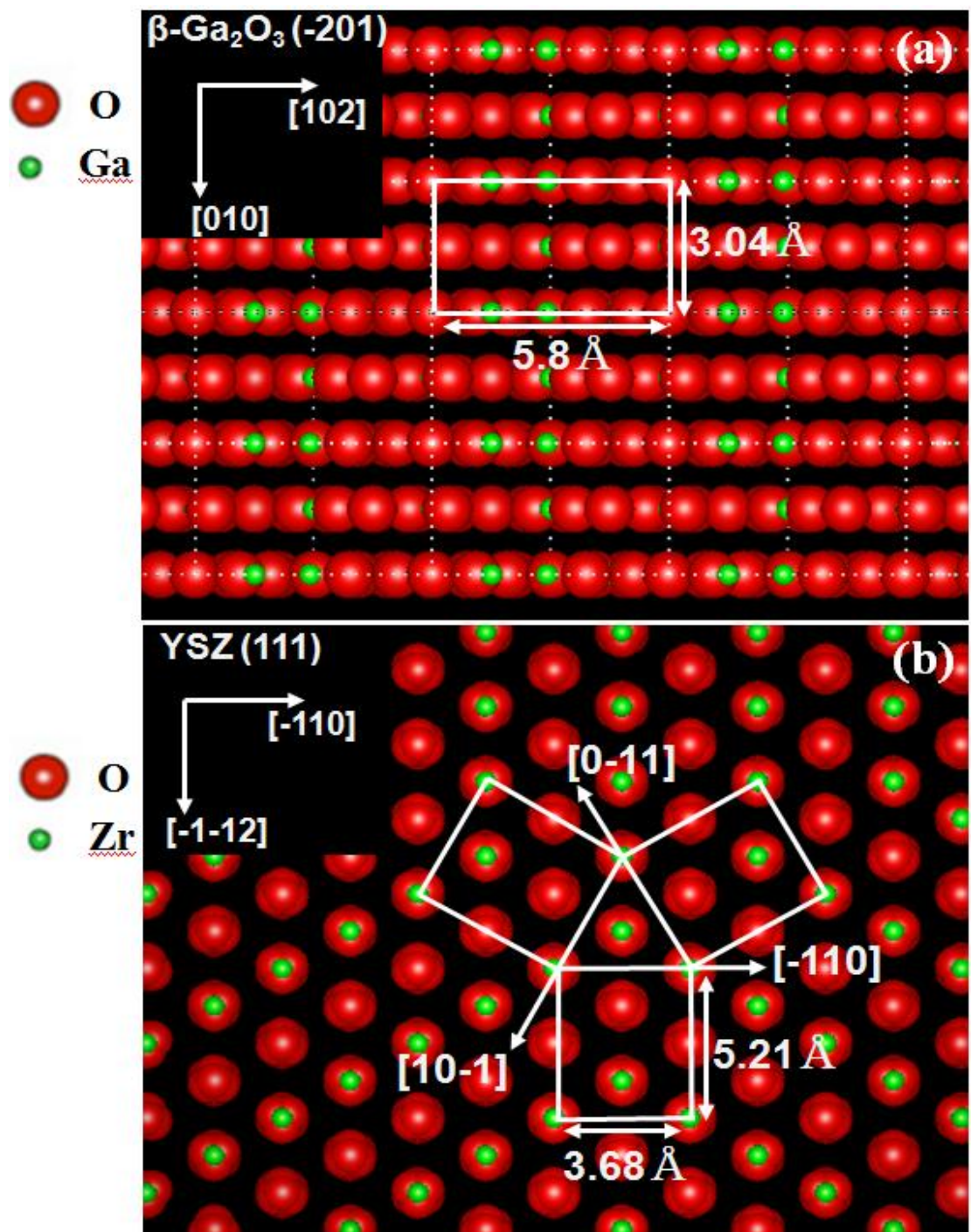


Figure 3.5. Schematic diagram of geometrical epitaxial relationship between the  $\beta\text{-Ga}_2\text{O}_3$  (-201) plane and YSZ (111) substrate face.

Figure 3.6 shows the XRD spectra for off-specular phi-scans of the  $\beta$ -Ga<sub>2</sub>O<sub>3</sub> (002) planes and the YSZ (400) planes for the  $\beta$ -Ga<sub>2</sub>O<sub>3</sub> films grown on YSZ (110). In this figure, two peaks separated by 180° were measured, meaning the existence of two-fold domain structure inside the film. On the other hand, the  $\beta$ -Ga<sub>2</sub>O<sub>3</sub> films grown on YSZ (111) substrates have six-domain structure inside the film as shown in Fig. 3.5 (b). So the crystallinity of the  $\beta$ -Ga<sub>2</sub>O<sub>3</sub> films deposited on YSZ (110) substrate is better than that on YSZ (111) substrate, corresponding to the experimental results.

In order to explain the structure relationship between the film and the substrate, a schematic diagram of geometrical epitaxial relationship between the  $\beta$ -Ga<sub>2</sub>O<sub>3</sub> films and YSZ substrate are shown in Fig. 3.7. The lattice mismatch between the  $\beta$ -Ga<sub>2</sub>O<sub>3</sub> [201] orientation (12.23 Å) and YSZ [-110] orientation (10.42 Å) is 17.4%, while that between the  $\beta$ -Ga<sub>2</sub>O<sub>3</sub> [010] orientation (6.08 Å) and the YSZ [00-1] orientation (5.21 Å) is 16.7%. The experiments revealed that  $\beta$ -Ga<sub>2</sub>O<sub>3</sub> film can grow along the YSZ [00-1] orientation. It should be noted that the  $\beta$ -Ga<sub>2</sub>O<sub>3</sub> belongs to the monoclinic system with the lattice angle  $\beta$  of 103.7°. Therefore, the  $\beta$ -Ga<sub>2</sub>O<sub>3</sub> [010] and [0-10] are different crystal orientations. The  $\beta$ -Ga<sub>2</sub>O<sub>3</sub> [010] growth direction has two equal opportunities along the YSZ [001] and YSZ [00-1] orientations. Therefore, in Fig. 3.7 (a), two peaks 180 ° apart can be seen. The epitaxial relationship can be determined to be the  $\beta$ -Ga<sub>2</sub>O<sub>3</sub> (-102) || YSZ (110) with  $\beta$ -Ga<sub>2</sub>O<sub>3</sub> (010) || YSZ (001).

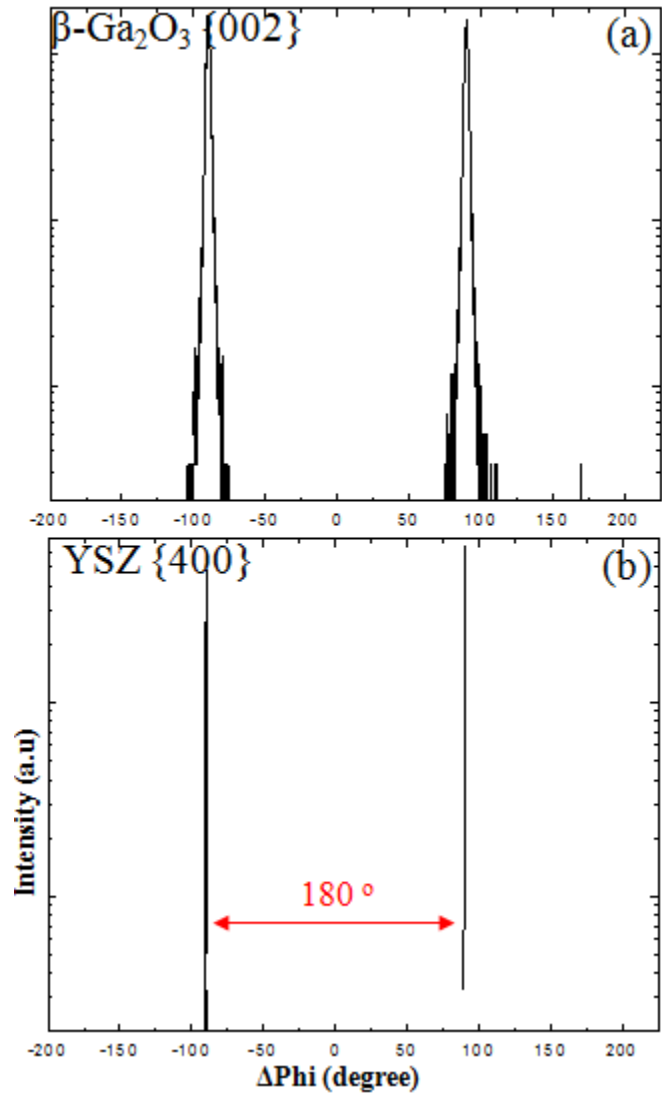


Figure 3.6. (a) Off-specular phi-scans of YSZ  $\{400\}$ . (b) Off-specular phi-scans of  $\beta\text{-Ga}_2\text{O}_3 \{002\}$  planes.

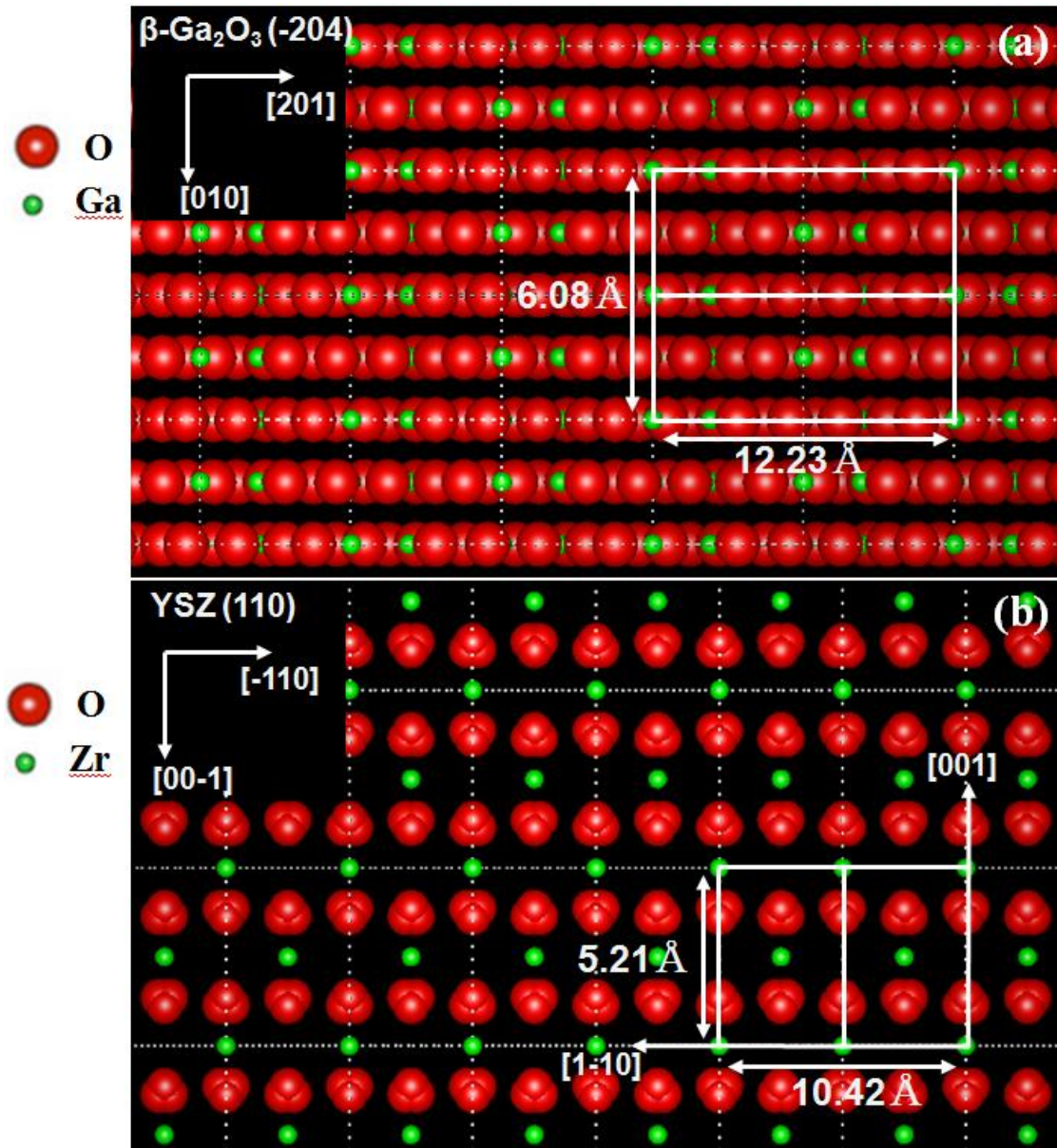


Figure 3.7. Schematic diagram of geometrical epitaxial relationship between the  $\beta\text{-Ga}_2\text{O}_3$  (-204) plane and YSZ (110) substrate face.

In order to understand the mechanism of growth directions of  $\beta$ -Ga<sub>2</sub>O<sub>3</sub> films, schematic images of YSZ and  $\beta$ -Ga<sub>2</sub>O<sub>3</sub> unit cells were illustrated. Figure 3.8 is a schematic images of YSZ and  $\beta$ -Ga<sub>2</sub>O<sub>3</sub> unit cells and YSZ (111) and  $\beta$ -Ga<sub>2</sub>O<sub>3</sub> (-201) planes. The YSZ (111) unit cell formed by oxygen atoms is triangle as shown in Fig. 3.8. Therefore,  $\beta$ -Ga<sub>2</sub>O<sub>3</sub> (-201) was easily grown on YSZ (111) substrate because of similar surface shape formed by oxygen atoms.

On the other hand, in Fig. 3.9, unit cells formed by oxygen atoms on YSZ (100) and  $\beta$ -Ga<sub>2</sub>O<sub>3</sub> (100) planes are both square [13]. Therefore, it is expected that  $\beta$ -Ga<sub>2</sub>O<sub>3</sub> (100) grows on YSZ (100). In the previous report,  $\gamma$ -Ga<sub>2</sub>O<sub>3</sub> was grown on YSZ (100) substrate at lower growth temperature [13], and this is plausible because they have the same crystal structure of cubic. On the other hand, in this results,  $\beta$ -Ga<sub>2</sub>O<sub>3</sub> (-201) was grown on YSZ (100) at higher growth temperature (over 600 °C). The  $\beta$ -Ga<sub>2</sub>O<sub>3</sub> is the most stable phase, so unstable  $\gamma$ -Ga<sub>2</sub>O<sub>3</sub> is transformed to  $\beta$ -phase at high growth temperature. In addition, the area of 3 atoms of oxygen with triangle shape for  $\beta$ -Ga<sub>2</sub>O<sub>3</sub> (-201) is 3.7 Å<sup>2</sup> and the area of 4 atoms of oxygen with square shape for  $\beta$ -Ga<sub>2</sub>O<sub>3</sub> (100) is 8.8 Å<sup>2</sup>. So,  $\beta$ -Ga<sub>2</sub>O<sub>3</sub> (-201) was easily grown on YSZ (100) at higher growth temperature than 600 °C because surface energy of  $\beta$ -Ga<sub>2</sub>O<sub>3</sub> (-201) is lower than that of  $\beta$ -Ga<sub>2</sub>O<sub>3</sub> (100), leading to the XRD data shown in Fig. 3.3.

In case of  $\beta$ -Ga<sub>2</sub>O<sub>3</sub> films on YSZ (110), oxygen atoms in the unit cell take rectangle as shown in Fig. 3.10. The area of 4 atoms of oxygen with rectangle shape for YSZ (110) is 2.56 Å × 3.62 Å. The area of 4 atoms of oxygen with rectangle shape for  $\beta$ -Ga<sub>2</sub>O<sub>3</sub> (-102) is 3.04 Å × 3.94 Å. The estimated lattice mismatch for the above shape is about 10%. Namely,  $\beta$ -Ga<sub>2</sub>O<sub>3</sub> (-102) was easily grown on YSZ (110) substrate because oxygen atoms arrange in the same shape of rectangle.

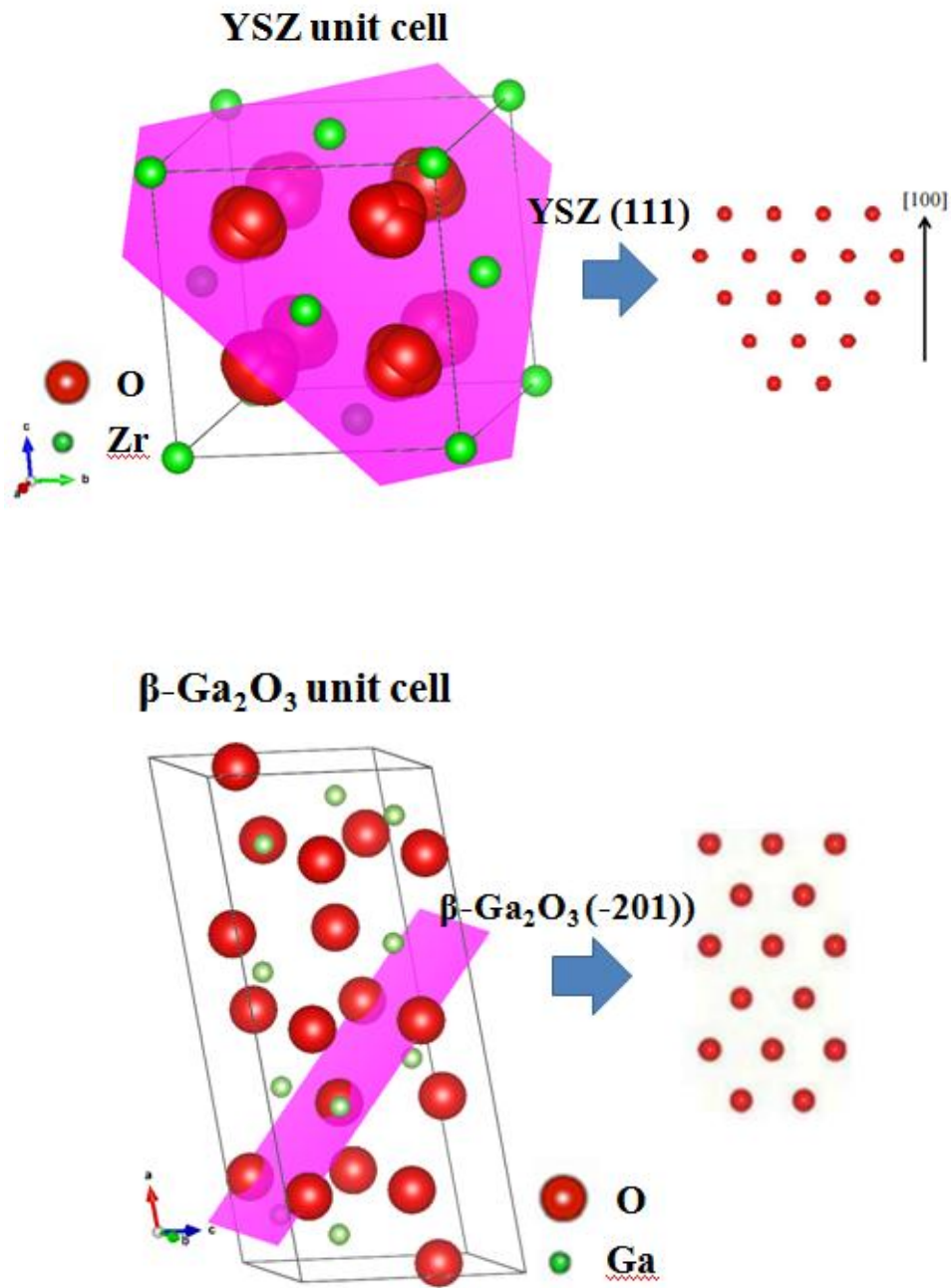


Figure 3.8. Schematic image of YSZ and  $\beta$ -Ga<sub>2</sub>O<sub>3</sub> unit cells with YSZ (111) and  $\beta$ -Ga<sub>2</sub>O<sub>3</sub> (-201) planes. Shape of oxygen atoms of YSZ (111),  $\beta$ -Ga<sub>2</sub>O<sub>3</sub> (-201) planes. (right side)

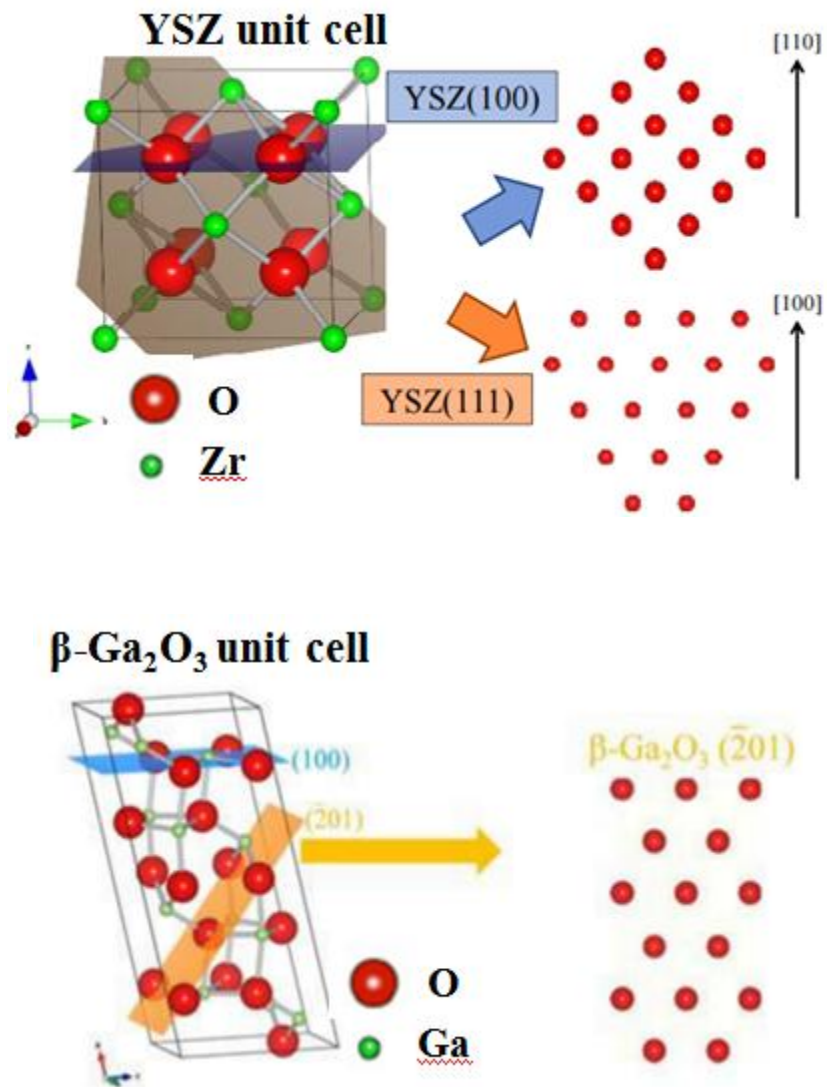


Figure 3.9. Schematic image of YSZ and  $\beta$ -Ga<sub>2</sub>O<sub>3</sub> unit cells with YSZ (100) and  $\beta$ -Ga<sub>2</sub>O<sub>3</sub>(100) planes. Locations of oxygen atoms of YSZ (100), (111),  $\beta$ -Ga<sub>2</sub>O<sub>3</sub> (-201) planes [13].

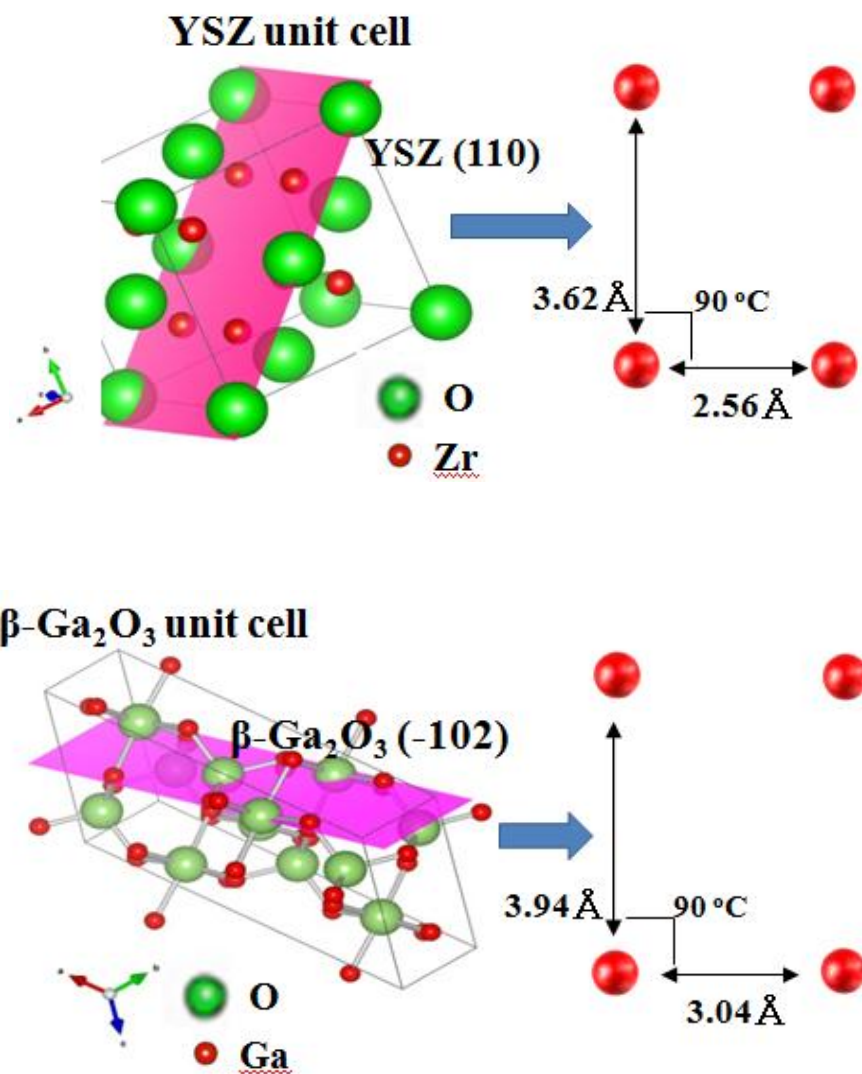


Figure 3.10. Schematic image of YSZ and  $\beta\text{-Ga}_2\text{O}_3$  unit cells. Locations of oxygen atoms of YSZ (110),  $\beta\text{-Ga}_2\text{O}_3 (-102)$  planes. (right side)

In order to see the possibility of controlling electrical conductivity by tin (Sn) doping, Sn-doped  $\beta$ - $\text{Ga}_2\text{O}_3$  films were fabricated on YSZ (110) substrates at 750 °C by the mist CVD method. Sn concentrations in source solution, Sn(II) chloride dihydrate, were changed from  $2.0 \times 10^{-4}$  to  $1.0 \times 10^{-2}$  mol/L. Figure 3.11 shows the XRD  $2\theta/\theta$  scan spectra of Sn-doped  $\beta$ - $\text{Ga}_2\text{O}_3$  on YSZ (110). No marked change or shift of the  $\beta$ - $\text{Ga}_2\text{O}_3$  (-204) peak was seen for the Sn concentration of  $<0.0075$  mol/L in source solution, suggesting incorporation of Sn in the  $\beta$ - $\text{Ga}_2\text{O}_3$  crystal structure. On the other hand, the single-crystalline  $\beta$ - $\text{Ga}_2\text{O}_3$  (-204) peak was disappeared for the Sn concentration of 0.01 mol/L in source solution, indicating severe degradation of crystallinity with excess doping. The results show the possibility of electrical conductivity control by Sn doping, but at the present stage electrical conduction was only confirmed by the simple testing that current flows in the sample: Hall effect measurements have not been able to be carried out. Optimization of the growth conditions and improvement of crystalline quality are the important issues for the electrical conductivity control for  $\beta$ - $\text{Ga}_2\text{O}_3$  on YSZ (110).

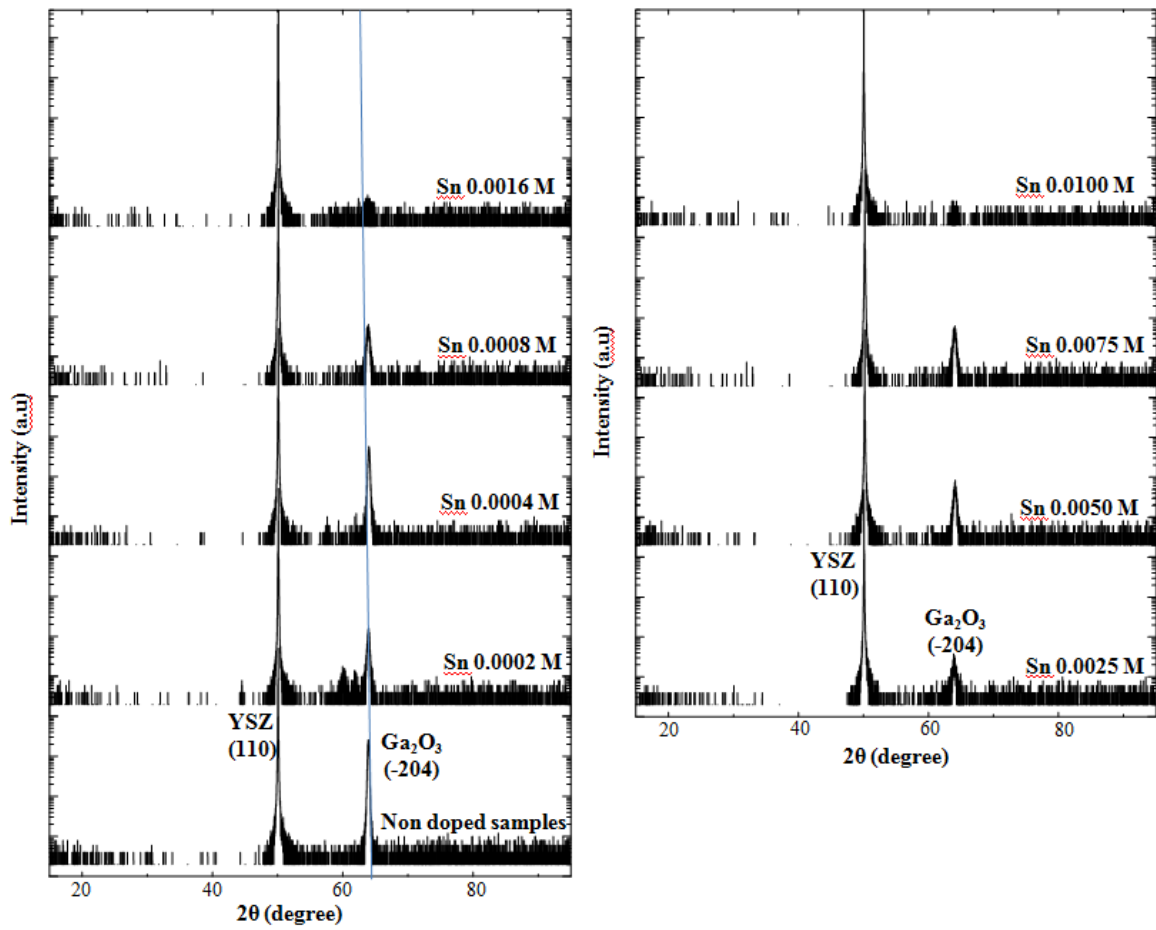


Figure 3.11. XRD 2θ/θ scan spectra of Sn doped β-Ga<sub>2</sub>O<sub>3</sub> on YSZ (110)

### 3.4 Summary

Hetero-epitaxial single-crystal  $\beta$ -Ga<sub>2</sub>O<sub>3</sub> films have been successfully fabricated by mist CVD method on YSZ, MgO, and MgAl<sub>2</sub>O<sub>4</sub> substrates taking cubic crystalline structure. It was found that the crystallinity of the films grown significantly depends on the growth temperature. Single-crystalline  $\beta$ -Ga<sub>2</sub>O<sub>3</sub> (-201) were grown on a YSZ (111) substrate at the growth temperature of 600 to 800 °C. Then growth directions of  $\beta$ -Ga<sub>2</sub>O<sub>3</sub> on cubic (111), (110) and (100) substrates were investigated. On YSZ (111) and MgAl<sub>2</sub>O<sub>4</sub> (111) substrates, single-crystalline  $\beta$ -Ga<sub>2</sub>O<sub>3</sub> (-201) was grown. On YSZ (100) substrate, single-crystalline  $\beta$ -Ga<sub>2</sub>O<sub>3</sub> (-201) was grown at high growth temperature over 600 °C. On YSZ (110) and MgO (110), single-crystalline  $\beta$ -Ga<sub>2</sub>O<sub>3</sub> (-102) was easily grown. The mechanisms determining the growth directions were discussed in terms of the shape of the unit cell on the substrate surface, lattice mismatch, and surface energy. Finally, Sn-doped  $\beta$ -Ga<sub>2</sub>O<sub>3</sub> was fabricated and the activation of Sn donors was speculated by a simple experiment. Detailed characterization of electrical properties was not possible for the present samples. These results exhibit promising growth of  $\beta$ -Ga<sub>2</sub>O<sub>3</sub> by mist CVD. In the next chapter, growth of homo-epitaxial  $\beta$ -Ga<sub>2</sub>O<sub>3</sub> is guided from these results.

## References

- [1] T. Oshima, T. Okuno and S. Fujita, *Jpn. J. Appl. Phys. Lett.* **46**,11 (2007).
- [2] M. Higashiwaki, K. Sasaki, A. Kuramata, T. Masui, and S. Yamakoshi, *Phys. Status Solidi A* **211**, 21 (2014).
- [3] M. Orita, H. Ohta, M. Hirano and H. Hosono, *Appl. Phys. Lett.* **77**,4166 (2000).
- [4] M. Ogita, K. Higo, Y. Nakanishi and Y. Hatanaka, *Appl. Surf. Sci.* **175-176**, (2001).
- [5] H. H. Tippins, *Phys. Rev.* **140**, A316 (1965).
- [6] K. Sasaki, A. Kuramata, T. Masui, E. G. Villora, K. Shimamura, and S. Yamakoshi, *Appl. Phys. Express* **5**, 035502 (2012).
- [7] Y. Tomm, J. M. Ko, A. Yoshikawa, and T. Fukuda, *Sol. Energ. Mat. Sol. C.* **66**, 369 (2001).
- [8] E. G. Villora, K. Shimamura, Y. Yoshikawa, K. Aoki, and N. Ichinose, *J. Cryst. Growth* **270**, 420 (2004).
- [9] Z. Galazka, R. Uecker, K. Irmischer, M. Albrecht, D. Klimm, M. Pietsch, M. Brützam, R. Bertram, S. Ganschow, and R. Fornari, *Cryst. Res. Technol.* **45**, 1229 (2010).
- [10] M. Higashiwaki, K. Sasaki, T. Kamimura, M. H. Wong, D. Krishnamurthy, A. Kuramata, T. Masui, and S. Yamakoshi, *Appl. Phys. Lett.* **103**, 123511 (2013).
- [11] K. Sasaki, M. Higashiwaki, A. Kuramata, T. Masui, and S. Yamakoshi, *J. Cryst. Growth* **378**, 591 (2013).
- [12] H. Murakami, K. Nomura, K. Goto, K. Sasaki, K. Kawara, Q. T. Thieu, R. Togashi, Y. Kumagai, M. Higashiwaki, A. Kuramata, S. Yamakoshi, B. Monemar, and A. Koukitu, *Appl. Phys. Express* **8**, 015503 (2015).

[13] K. Kaneko, H. Ito, S.-D. Lee, and S. Fujita, *Phys. Status Solidi C* **10**, 11 (2013).



## Chapter 4

# Growth of homo-epitaxial and conductive Sn-doped $\beta$ -Ga<sub>2</sub>O<sub>3</sub> thin films

### 4.1 Introduction

Power devices with wide bandgap semiconductors based on such as SiC and GaN have been intensively investigated for enhancement of efficiency in power switching because they can achieve lower power loss and higher electric breakdown voltage at higher power regime compared to conventional Si-based devices [1-3]. However, SiC- and GaN-based devices still possess several remaining problems for mass production and cost.

Beta-gallium oxide ( $\beta$ -Ga<sub>2</sub>O<sub>3</sub>) has become a promising candidate for novel power device applications [4,5]. The  $\beta$ -Ga<sub>2</sub>O<sub>3</sub> has higher wide bandgap of 4.7–4.9 eV at room temperature and estimated higher breakdown electric field of 8 MV/cm compared to SiC and GaN [6-10]. The estimated Baliga's figure of merit, which is a good guideline for an effective power semiconductor material, for  $\beta$ -Ga<sub>2</sub>O<sub>3</sub> is several times greater than those for SiC and GaN as shown in table 2.1 [9,10]. In addition to the above, Ga<sub>2</sub>O<sub>3</sub>-based power devices are more attractive owing to the available high quality single-crystal substrates. Bulk  $\beta$ -Ga<sub>2</sub>O<sub>3</sub> substrates have been fabricated by using the floating zone (FZ), the edge-defined film-fed growth (EFG), and Czochralski (CZ) methods [10-13]. Recently, new power devices with homo-epitaxial  $\beta$ -Ga<sub>2</sub>O<sub>3</sub> film on single-crystal  $\beta$ -Ga<sub>2</sub>O<sub>3</sub> substrates such as metal-oxide-semiconductor field-effect transistors (MOSFETs), metal-semiconductor FETs

(MESFETs), and Schottky barrier diodes (SBDs) were fabricated by molecular beam epitaxy (MBE) and hydride vapor phase epitaxy [14-16].

In this work, the author proposes the application of mist CVD method to fabricate  $\beta$ -Ga<sub>2</sub>O<sub>3</sub> power devices. The details of this method have been described in our previously works [17, 19-21] as well as previous chapters in this thesis. It has been shown that the mist CVD method is a very simple and cost-effective process. In this chapter, the author will show the homo-epitaxial growth of single-crystalline  $\beta$ -Ga<sub>2</sub>O<sub>3</sub> films on  $\beta$ -Ga<sub>2</sub>O<sub>3</sub> (010) substrates by the mist CVD method and crystalline and electrical properties of the  $\beta$ -Ga<sub>2</sub>O<sub>3</sub> homo-epitaxial films together with discussed in terms of their potential for power device applications.

## **4.2 Basic growth conditions of homo-epitaxial $\beta$ -Ga<sub>2</sub>O<sub>3</sub> films**

### **4.2.1 Sample preparation**

For the homo-epitaxial growth of  $\beta$ -Ga<sub>2</sub>O<sub>3</sub> films, gallium acetylacetonate [Ga(C<sub>5</sub>H<sub>8</sub>O<sub>3</sub>)<sub>3</sub>] of 0.05 mol/L solved in deionized water, with slight addition of hydrochloric acid (HCl) to solve the precursor completely was used as the source solution. As substrates,  $\beta$ -Ga<sub>2</sub>O<sub>3</sub> (-201), conductive Sn-doped  $\beta$ -Ga<sub>2</sub>O<sub>3</sub> (010), and semi-insulating Fe-doped  $\beta$ -Ga<sub>2</sub>O<sub>3</sub> (010) were available. Since the number of substrates available for the author's experiments is limited, the author decided to use  $\beta$ -Ga<sub>2</sub>O<sub>3</sub> (-201) substrates for the basic growth experiments and to extend the knowledge to the successive and systematic experiments on conductive Sn-doped  $\beta$ -Ga<sub>2</sub>O<sub>3</sub> (010) and semi-insulating Fe-doped  $\beta$ -Ga<sub>2</sub>O<sub>3</sub> (010) substrates.

As a first trial,  $\beta$ -Ga<sub>2</sub>O<sub>3</sub> films were grown on  $\beta$ -Ga<sub>2</sub>O<sub>3</sub> (-201) substrates at 800 and 900 °C during 30 min and 60 min, under the O<sub>2</sub> gas atmosphere. In order to certain the film growth and to estimate the film thickness, a small area of the substrate was covered by a sapphire substrate during the growth. The thickness of the homo-epitaxial  $\beta$ -Ga<sub>2</sub>O<sub>3</sub> layer was measured by the step height formed after the removal of sapphire. As a result, the thickness of homo-epitaxial  $\beta$ -Ga<sub>2</sub>O<sub>3</sub> layer was about 250 and 500 nm for the growth time of 30 and 60 min, respectively. Structural properties of the  $\beta$ -Ga<sub>2</sub>O<sub>3</sub> films were investigated by X-ray diffraction (XRD). The optical transmittance spectra of the samples were investigated by UV-visible spectrophotometer.

#### **4.2.2 Structural properties of $\beta$ -Ga<sub>2</sub>O<sub>3</sub> as a function of growth temperature**

Figure 4.1 shows XRD  $2\theta/\theta$  scan spectra for the  $\beta$ -Ga<sub>2</sub>O<sub>3</sub> films grown on  $\beta$ -Ga<sub>2</sub>O<sub>3</sub> (-201) substrates. Only  $\beta$ -Ga<sub>2</sub>O<sub>3</sub> (-201) diffraction peak was observed without any other  $\beta$ -Ga<sub>2</sub>O<sub>3</sub> diffraction peaks. To make sure the growth of  $\beta$ -Ga<sub>2</sub>O<sub>3</sub> films, the optical transmittance spectra were investigated as shown in Fig. 4.2. The transmittances of all samples grown were decreased by scattering effect of reflected beams because the surface roughness is increased through growth of thin films. It is considered that the films was successfully grown on  $\beta$ -Ga<sub>2</sub>O<sub>3</sub> substrates.

Of course, it is quite difficult to access the properties of homo-epitaxial layer itself from XRD and optical transmittance measurements because they are veiled by those of the substrates. Detailed characterization of homo-epitaxial  $\beta$ -Ga<sub>2</sub>O<sub>3</sub> films will be reported in the latter sections.

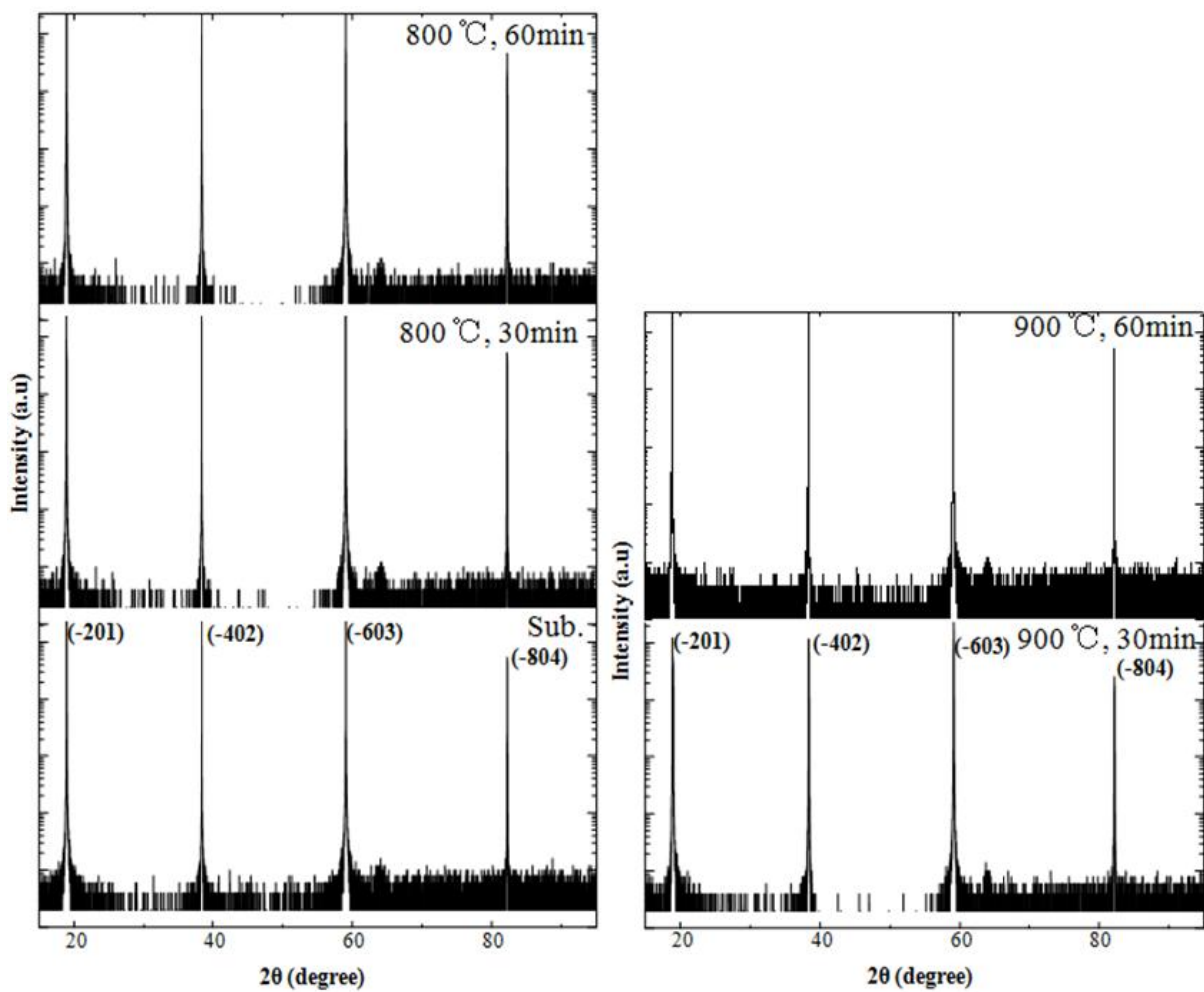


Figure 4.1. XRD  $2\theta/\theta$  scan spectra of  $\beta\text{-Ga}_2\text{O}_3$  films grown on  $\beta\text{-Ga}_2\text{O}_3$  (-201) substrates.

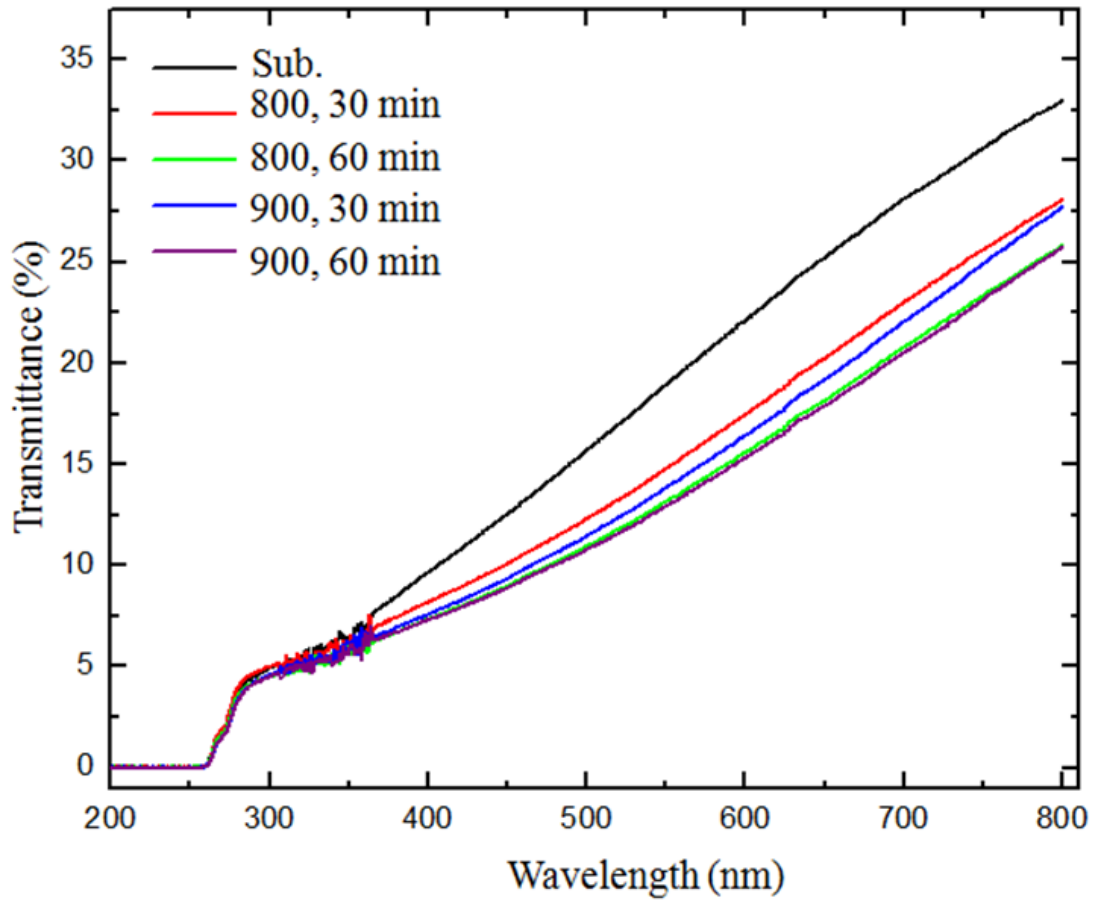


Figure 4.2. The optical transmittance spectra of  $\beta$ -Ga<sub>2</sub>O<sub>3</sub> films grown on  $\beta$ -Ga<sub>2</sub>O<sub>3</sub> (-201) substrates.

## **4.3 Unintentionally doped $\beta$ -Ga<sub>2</sub>O<sub>3</sub> homo-epitaxial films on conductive substrates**

### **4.3.1 Sample preparation**

Based on the preliminary results, the  $\beta$ -Ga<sub>2</sub>O<sub>3</sub> films were grown on Sn-doped  $\beta$ -Ga<sub>2</sub>O<sub>3</sub> (010) substrates at 500, 600, 700, 800, and 900 °C in order for detailed characterization. The source solution was gallium acetylacetonate [Ga(C<sub>5</sub>H<sub>8</sub>O<sub>3</sub>)<sub>3</sub>] of 0.05 mol/L solved in deionized water, with slight addition of hydrochloric acid (HCl).

### **4.3.2 Structural properties of homo-epitaxial unintentionally doped $\beta$ -Ga<sub>2</sub>O<sub>3</sub> films**

Figure 4.3 (a) shows XRD  $2\theta/\theta$  scan spectra for the unintentionally doped (UID)  $\beta$ -Ga<sub>2</sub>O<sub>3</sub> films grown on Sn-doped  $\beta$ -Ga<sub>2</sub>O<sub>3</sub> (010) substrates as a function of the growth temperatures between 500 and 900 °C. It was found that the films grown at the temperatures lower than 600 °C were polycrystalline possessing two other planes of (100) and (102) except for the orientation aligned to the substrate (010). On the other hand, at the temperature higher than 700 °C, homo-epitaxial  $\beta$ -Ga<sub>2</sub>O<sub>3</sub> (010) films were grown without noticeable inclusion of other phases as shown Fig. 4.3 (a). Growth rate at 700 °C was 500 nm/h and the rate was decreased with increasing the temperature to 800 and 900 °C because it seems that the precursors cause pre-reaction before transported to the substrate. In order to estimate the crystalline quality of the films, XRD  $\omega$ -scan rocking curves for the samples was measured for sample grown as shown in Fig. 4.3 (b). The full-width at half maximum

(FWHM) of XRD  $\omega$ -scan for the  $\beta$ -Ga<sub>2</sub>O<sub>3</sub> (010) films grown at 700 °C was as small as 91 arcsec, which it is almost same values to substrate with FWHM of 103 arcsec.

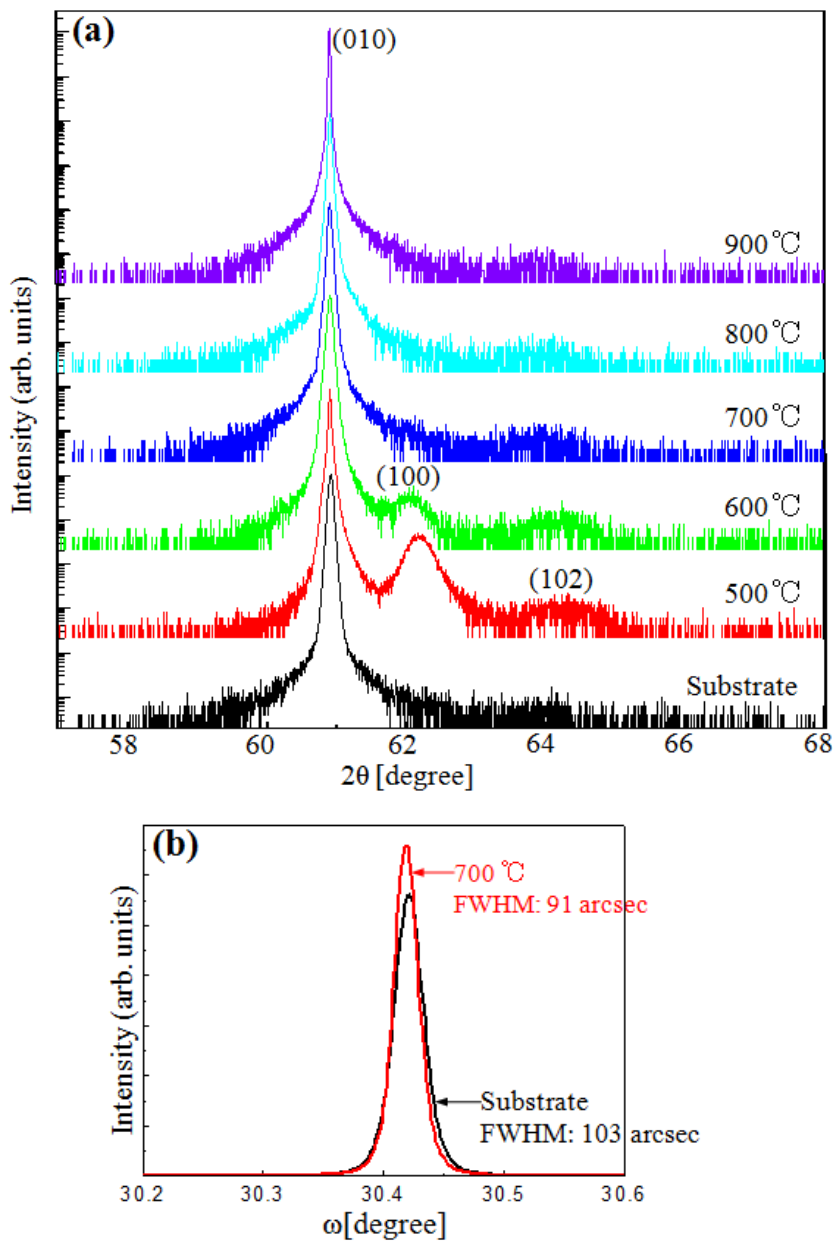


Figure 4.3. (a) XRD  $2\theta/\theta$  scan spectra for the unintentionally doped  $\beta$ -Ga<sub>2</sub>O<sub>3</sub> films grown on Sn-doped  $\beta$ -Ga<sub>2</sub>O<sub>3</sub> (010) substrates as a function of growth temperatures. (b) XRD  $\omega$ -scan for the  $\beta$ -Ga<sub>2</sub>O<sub>3</sub> films grown at 700 °C

It should be noted that in the XRD  $2\theta/\theta$  and  $\omega$ -scan measurements, the diffraction comes from both the homo-epitaxial layer and the substrate, and it is hard to characterize the properties of the homo-epitaxial layer apart from that of the substrate. Therefore, in order to elucidate the properties of the homo-epitaxial layer, in-plane XRD measurements were carried out with low incident angles of the primary x-ray beam, avoiding its penetration to the substrate. Figure 4.4 shows the phi-scans of the  $\beta$ - $\text{Ga}_2\text{O}_3$  (600) planes reflection for the bare substrates and grown sample at 700, 800, 900 °C. Two peaks in all samples separated by  $180^\circ$  were measured, which means the existence of twofold domain structure. It is considered that homo-epitaxial single-crystal  $\beta$ - $\text{Ga}_2\text{O}_3$  films was successfully grown on Sn-doped  $\beta$ - $\text{Ga}_2\text{O}_3$  substrates because the  $\beta$ - $\text{Ga}_2\text{O}_3$  belongs to the monoclinic system. The grown films exhibited an epitaxial relationship with the substrates. As shown in the inset images in Fig 4.4 (a) and (b), FWHM of phi-scan for the  $\beta$ - $\text{Ga}_2\text{O}_3$  (600) films grown at 700 °C was 930 arcsec, which it is almost same values to substrate with FWHM of 900 arcsec. It means that  $\beta$ - $\text{Ga}_2\text{O}_3$  films grown by mist CVD have high crystallinity as well as the substrate.

Figure 4.5 shows AFM surface images of substrates and  $\beta$ - $\text{Ga}_2\text{O}_3$  films grown at 700 °C. Figure 4.5 (a) is surface morphology of substrates. The morphology of deposited  $\beta$ - $\text{Ga}_2\text{O}_3$  thin films are very smooth and uniform with root-mean square (RMS) roughness of 0.53 nm over a  $1\ \mu\text{m} \times 1\ \mu\text{m}$  area as shown in Fig 4.5 (b).

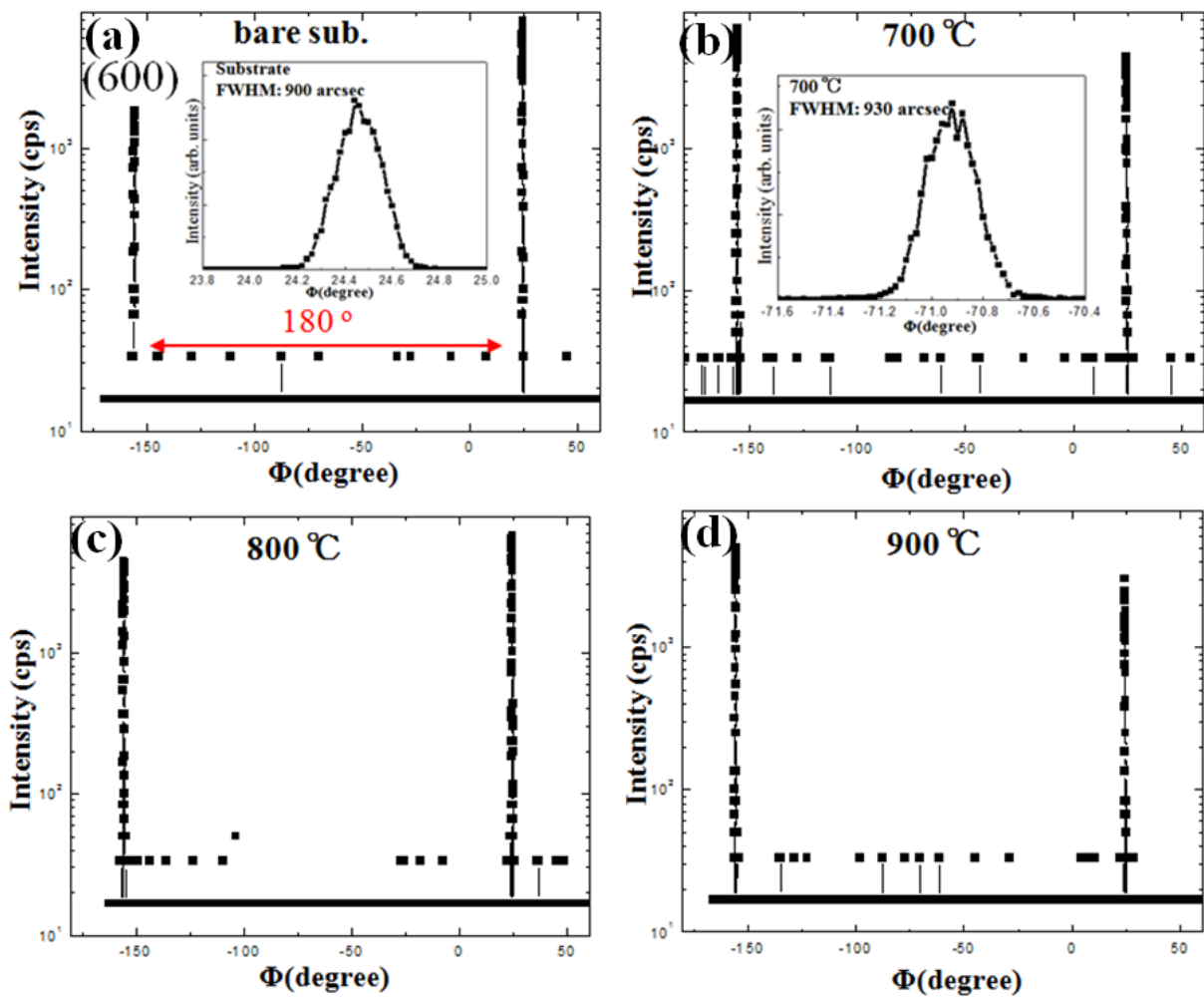


Figure 4.4. phi-scans of  $\beta$ -Ga<sub>2</sub>O<sub>3</sub> (600) planes for (a) bare substrates,  $\beta$ -Ga<sub>2</sub>O<sub>3</sub> films grown at (b) 700 °C, (c) 800 °C, and (d) 900 °C. (Inset images are XRD  $\omega$ -scan rocking curves for the samples)

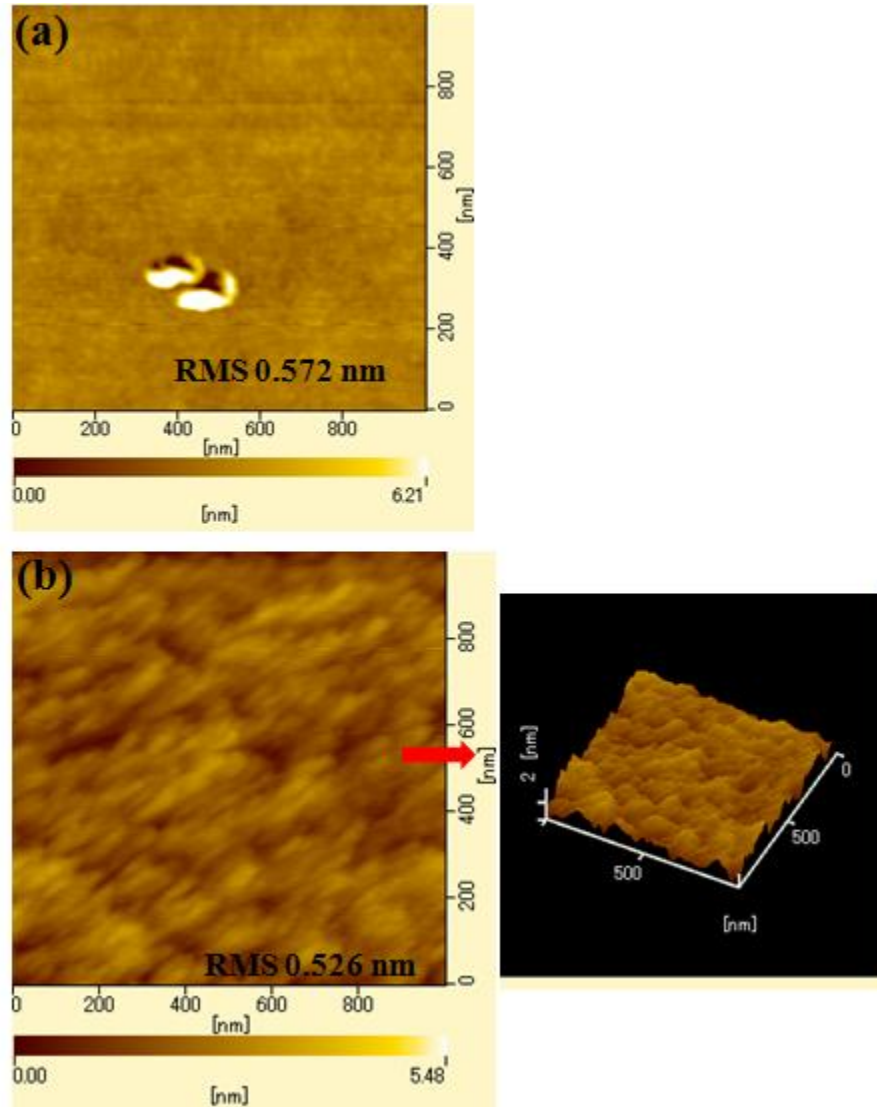


Figure 4.5. AFM images of (a)  $\beta$ -Ga<sub>2</sub>O<sub>3</sub> (010) substrates and (b)  $\beta$ -Ga<sub>2</sub>O<sub>3</sub> films grown at 700 °C.

### 4.3.3 Optical properties of homo-epitaxial unintentionally doped $\beta\text{-Ga}_2\text{O}_3$ films

Figure 4.6 shows optical transmittance spectra of the UID  $\beta\text{-Ga}_2\text{O}_3$  films shown in Fig. 4.3 (a) as a function of the growth temperature. A spectrum of a substrate is also shown for comparison. The film prepared at 600 °C exhibited low transmittance in the entire wavelength region owing to growth of poly crystalline films. However, transmittance of the films deposited at higher than 700 °C was more than 70% in the visible and the UV regions and the spectra were left shift. It was attributed to the enhanced crystallinity and decreased film thickness. There are no significant differences in feature of spectra at higher growth temperature than 700 °C compare with substrate spectrum except slightly reduced transmittance by scattering effect of reflected beams with increasing film thickness.

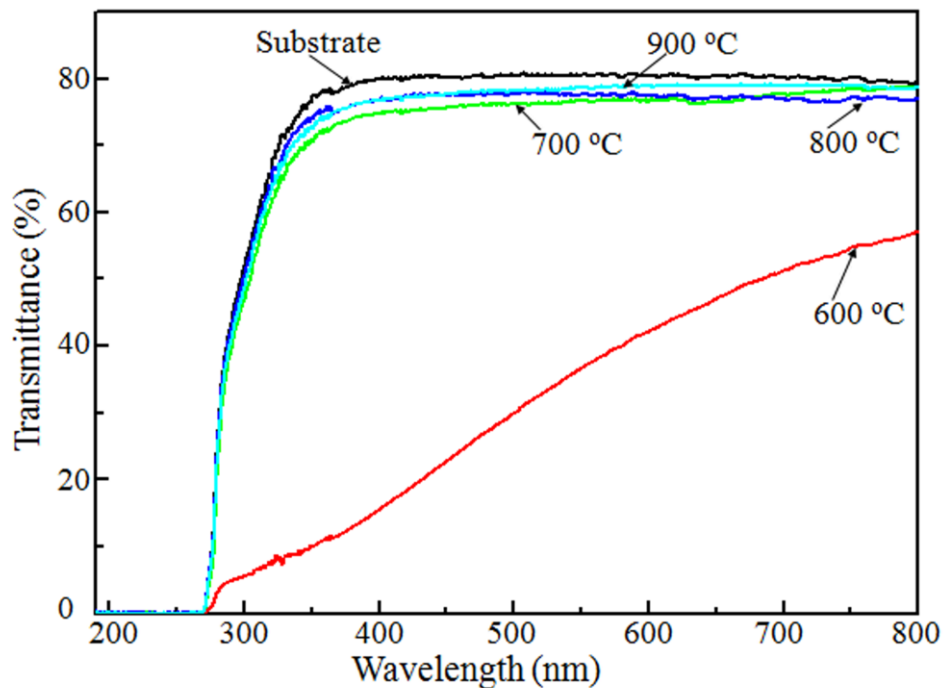


Figure 4.6. Optical transmittance spectra of the unintentionally doped  $\beta\text{-Ga}_2\text{O}_3$  films grown on Sn-doped  $\beta\text{-Ga}_2\text{O}_3$  (010) substrates as a function of the growth temperature.

#### 4.3.4 $\beta$ -Ga<sub>2</sub>O<sub>3</sub>-based Schottky barrier diodes

In order to characterize the electrical properties of the homo-epitaxial  $\beta$ -Ga<sub>2</sub>O<sub>3</sub> films, operation of Schottky barrier diode (SBD) will be demonstrated. An UID  $\beta$ -Ga<sub>2</sub>O<sub>3</sub> film with thickness of 1.2  $\mu\text{m}$  was grown on a Sn-doped  $\beta$ -Ga<sub>2</sub>O<sub>3</sub> ( $n = 6 \times 10^{18} \text{ cm}^{-3}$ ) substrate. Ohmic electrodes were fabricated on the substrate side using pressed indium pellets. The sample was transferred to the rapid thermal annealing chamber and annealed at 950 °C during 1 min under O<sub>2</sub> ambient to achieve ohmic contacts. Next, circular Schottky electrodes of Pt (250 nm) with a diameter of 1 mm were deposited on UID  $\beta$ -Ga<sub>2</sub>O<sub>3</sub> films by electron-beam evaporation. It should be noted that an UID  $\beta$ -Ga<sub>2</sub>O<sub>3</sub> film exhibited high resistivity and therefore the SBD fabricated is recognized as metal-insulator-semiconductor structure where the external voltage was applied to the UID  $\beta$ -Ga<sub>2</sub>O<sub>3</sub> layer.

Figure 4.7 (a) illustrates a schematic homo-epitaxial  $\beta$ -Ga<sub>2</sub>O<sub>3</sub> SBDs structure. Ohmic contact of n-type Sn-doped  $\beta$ -Ga<sub>2</sub>O<sub>3</sub> substrates formed by the rapid thermal annealing of indium actually represented the Ohmic behavior as shown in Fig. 4.7 (b). Figure 4.7 (c) shows a current-voltage ( $I$ - $V$ ) characteristic of the SBD. It exhibited a forward turn-on voltage of 1 V and reverse breakdown voltage of 24 V, which corresponded to 0.2 MV/cm assuming the uniform electric field in the homo-epitaxial UID  $\beta$ -Ga<sub>2</sub>O<sub>3</sub> films. This value is very low probably because of many problems in growth and device processes in the first trial. On the other hand, clear observation of rectifying  $I$ - $V$  characteristics suggests the formation of Schottky barrier and the  $\beta$ -Ga<sub>2</sub>O<sub>3</sub> films may be applicable as devices after the improvements of their structural and electrical properties.

However, it was found that, during the growth of UID  $\beta$ -Ga<sub>2</sub>O<sub>3</sub> films, the resistance of back side of Sn-doped  $\beta$ -Ga<sub>2</sub>O<sub>3</sub> substrate was highly increased probably due to trapping in defects or

compensation of the Sn donors. At the present stage, the reason of this phenomena is unknown but it should be an important issue to be taken into account of in the fabrication of devices.

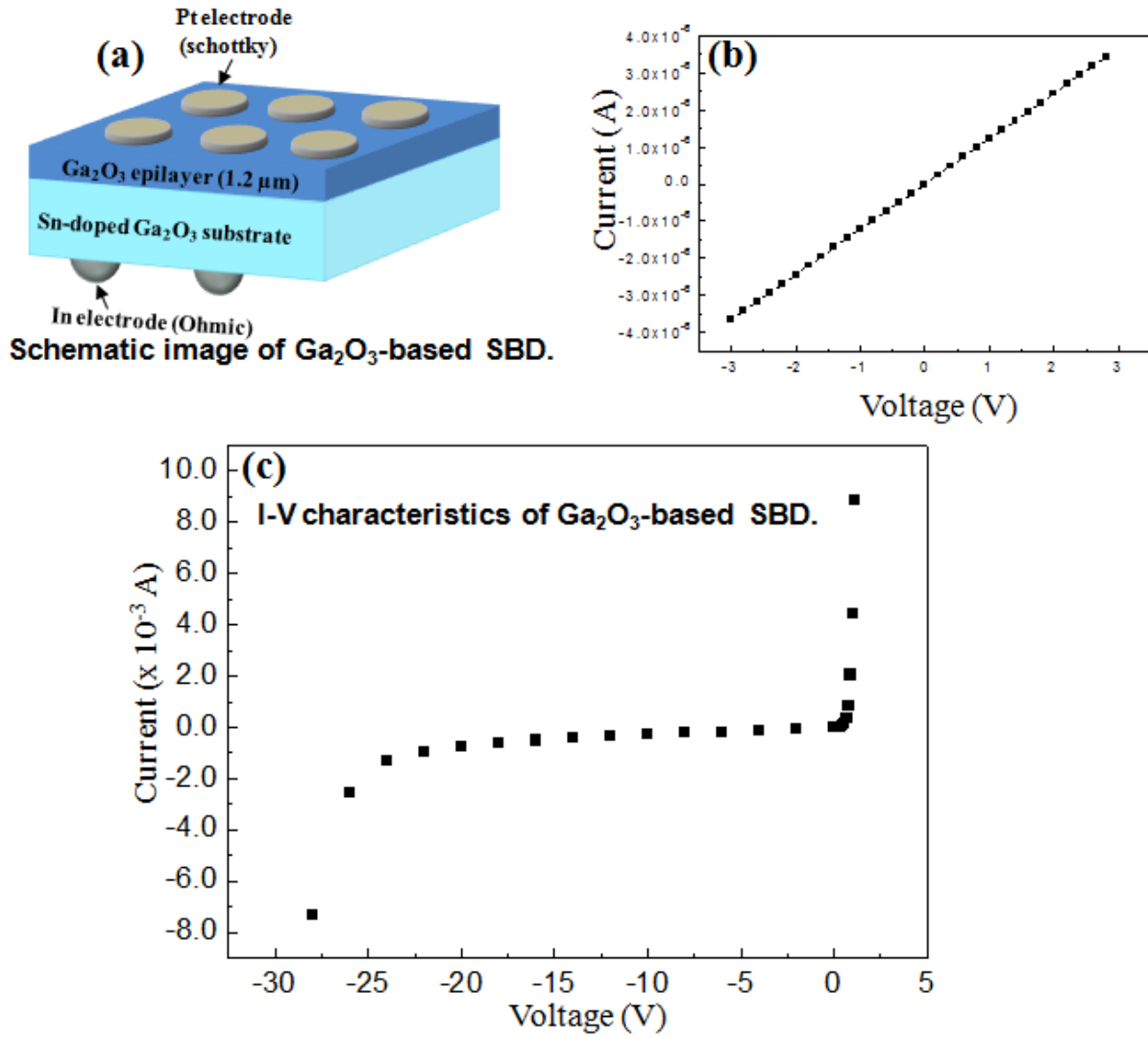


Figure 4.7. (a) Cross-sectional schematic image of  $\beta$ -Ga<sub>2</sub>O<sub>3</sub> SBD. (b) Ohmic property of n-type Sn-doped  $\beta$ -Ga<sub>2</sub>O<sub>3</sub> substrates. (c) I-V characteristic for  $\beta$ -Ga<sub>2</sub>O<sub>3</sub> SBD.

## **4.4 Conductive Sn-doped $\beta$ -Ga<sub>2</sub>O<sub>3</sub> homo-epitaxial films on semi-insulating substrates**

### **4.4.1 Sample preparation**

Sn-doped  $\beta$ -Ga<sub>2</sub>O<sub>3</sub> films were grown by the mist CVD method on semi-insulating Fe-doped  $\beta$ -Ga<sub>2</sub>O<sub>3</sub> substrates at 700 °C. Sn(II) chloride dihydrate was chosen as a dopant source, which was simultaneously solved ion the source solution together with the Ga source. The concentrations in source solution were changed between  $4.0 \times 10^{-21}$  and  $7.5 \times 10^{-4}$  mol/L. Structural and electrical properties of the Sn-doped  $\beta$ -Ga<sub>2</sub>O<sub>3</sub> films were investigated by XRD and Hall measurement.

### **4.4.2 Structural properties of homo-epitaxial Sn-doped $\beta$ -Ga<sub>2</sub>O<sub>3</sub> films**

Figure 4.8 shows XRD  $2\theta/\theta$  scan profiles for the Sn-doped  $\beta$ -Ga<sub>2</sub>O<sub>3</sub> films. Any other peaks except for  $\beta$ -Ga<sub>2</sub>O<sub>3</sub> (010) are seen until the Sn concentration of as high as  $4 \times 10^{-4}$  mol/L in source solution. On the other hand, inclusion of  $\beta$ -Ga<sub>2</sub>O<sub>3</sub> (100) was evident at the Sn concentration of  $7.5 \times 10^{-4}$  mol/L in source solution. In order to estimate the crystalline quality of the films, XRD  $\omega$ -scan rocking curves for the samples was measured. For the samples except for the Sn concentration of  $7.5 \times 10^{-4}$  mol/L in source solution, the full-width at half maximum (FWHM) of XRD  $\omega$ -scan was as small as 35 arcsec, which was almost the same as that of the substrate, though the inclusion of the diffraction from the substrate should be overlapped.

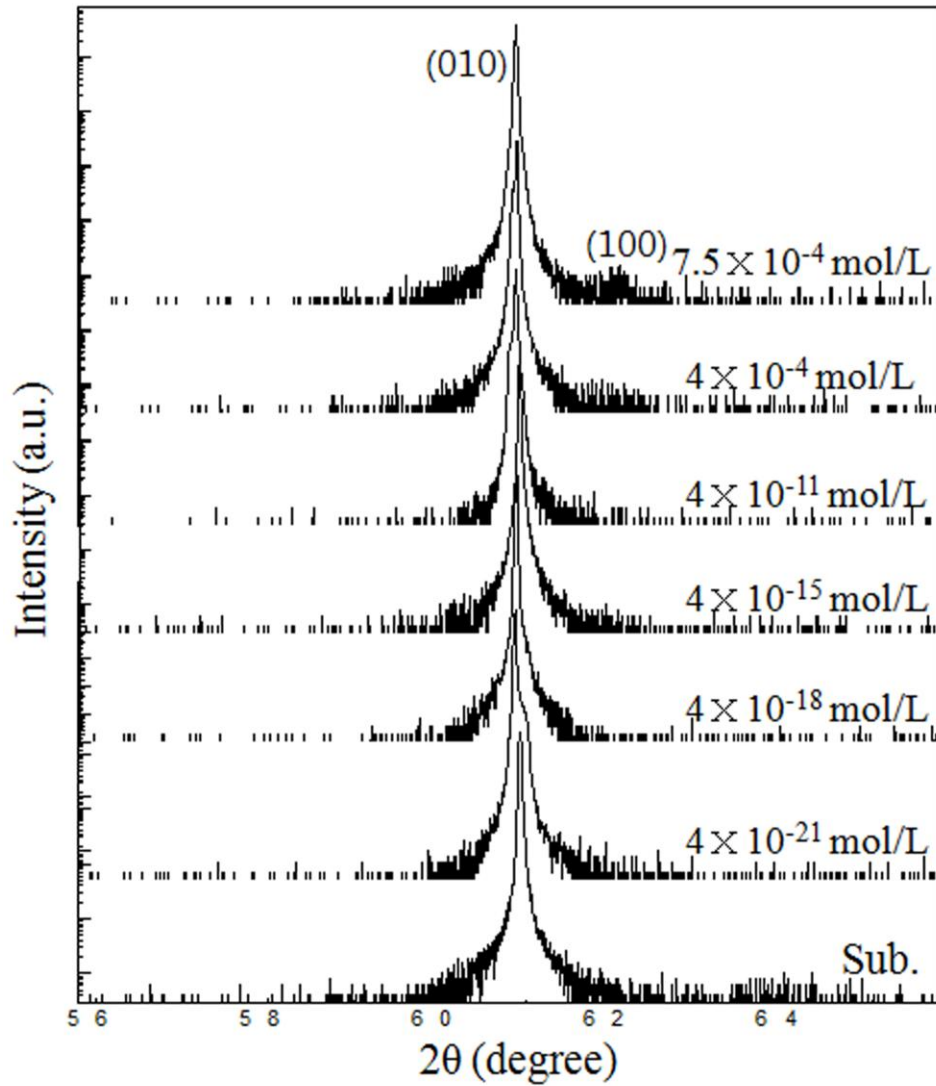


Figure 4.8. XRD  $2\theta/\theta$  scan spectra for the homo-epitaxial Sn-doped  $\beta$ -Ga<sub>2</sub>O<sub>3</sub> films grown as a function of Sn concentration in source solution.

### 4.4.3 Electrical properties of homo-epitaxial Sn-doped $\beta$ -Ga<sub>2</sub>O<sub>3</sub> films

Figure 4.9 (a) shows the carrier concentrations of Sn-doped  $\beta$ -Ga<sub>2</sub>O<sub>3</sub> films grown on semi-insulating  $\beta$ -Ga<sub>2</sub>O<sub>3</sub> substrates. Those were measured by Van der Pauw four-probe technique. The carrier concentration monotonically decreased with the decrease of Sn concentration in source solution. Ideally, in Fig 4.9 (a), the carrier concentration should be decreased almost linearly with decreasing the Sn concentration in source solution. However, the graph is far flat under the Sn concentration of  $4 \times 10^{-7}$  mol/L in source solution. If this is the real, the films are suffered from severe compensation. Note that the author carried out the series of experiments by changing the Sn concentration in source solution from high to low in the same experimental equipment without thermal cleaning process. Therefore, it is considered that the characteristics are severely influenced by memory effect, that is, Sn has remained in the experiment equipment. Therefore, careful experiments eliminating the memory effect is necessary in order to show the controllability of carrier concentration by doping.

However, at the present stage, one may infer that Sn doping resulted in carrier concentration between  $\sim 1.0 \times 10^{18}$  to  $\sim 5.0 \times 10^{20}$  cm<sup>-3</sup>. Since the Sn concentration in source solution is not a reliable parameter for its lower values, the relationship between room-temperature mobility and carrier concentration for the Sn-doped  $\beta$ -Ga<sub>2</sub>O<sub>3</sub> films as shown in Fig. 4.9(b). The mobility of the films was linearly decreased in terms of the carrier concentration, suggesting dominant impurity scattering in the experimental region. The Sn-doped  $\beta$ -Ga<sub>2</sub>O<sub>3</sub> film with carrier concentration of about  $1.0 \times 10^{18}$  cm<sup>-3</sup> showed the Hall mobility of  $45 \text{ cm}^2 \text{V}^{-1} \text{s}^{-1}$ .

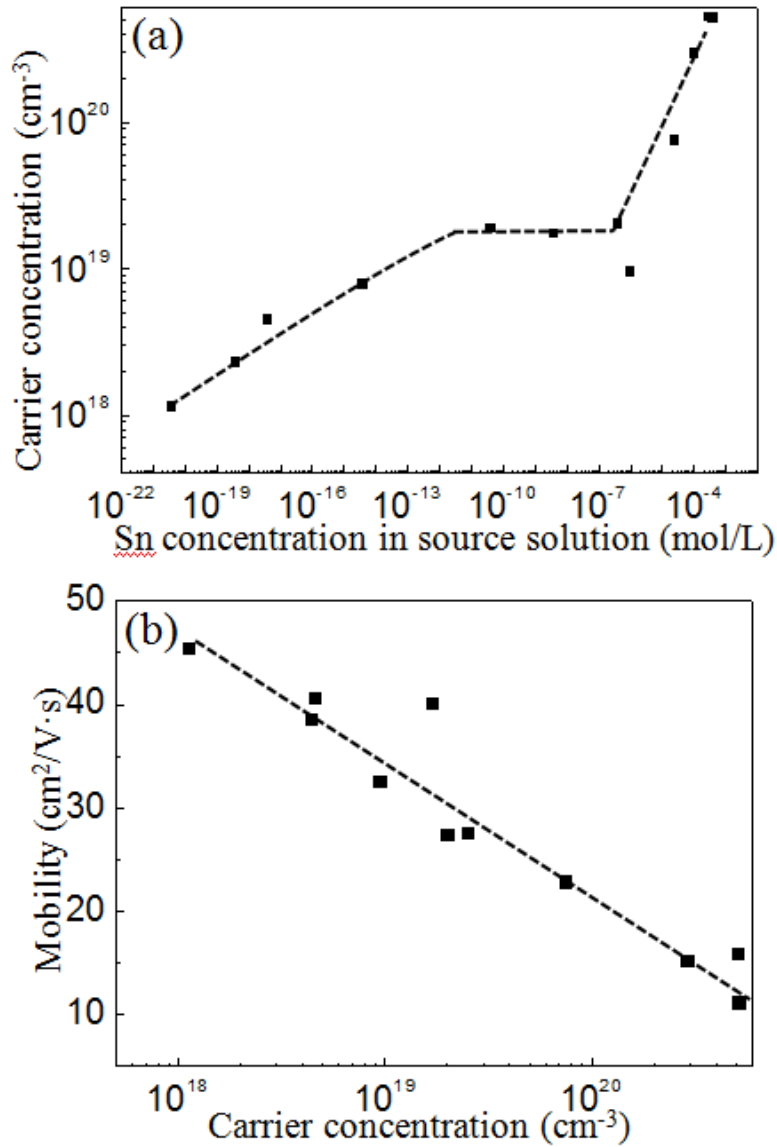


Figure 4.9. (a) Carrier concentration of Sn-doped  $\beta$ -Ga<sub>2</sub>O<sub>3</sub> films grown as a function of Sn concentration in source solution. (b) Relationship between mobility and carrier concentration for Sn-doped  $\beta$ -Ga<sub>2</sub>O<sub>3</sub> films.

Figure 4.10 shows comparison of experimental electron mobility of Sn-doped  $\beta$ -Ga<sub>2</sub>O<sub>3</sub> films grown by MBE [15], Mist CVD and MOCVD [18] as a function of the carrier concentration. The mobility is linearly increased with decreasing the carrier concentration. It should be noted that the mobility achieved by the mist CVD method is not inferior compared to that reported for Sn-doped  $\beta$ -Ga<sub>2</sub>O<sub>3</sub> grown by MBE possessing the similar carrier concentration [5,10], in spite of a very simple growth method. Of course, a severe difference lies in the range of the controllable carrier concentration, that is, it is an important issue for mist CVD to control the lower carrier concentration as well as to eliminate the memory effect. It is noteworthy that the mobility achieved by the mist CVD is higher than that by MOCVD. The author expects the further evolution of the mist CVD technology toward actual applications to devices.

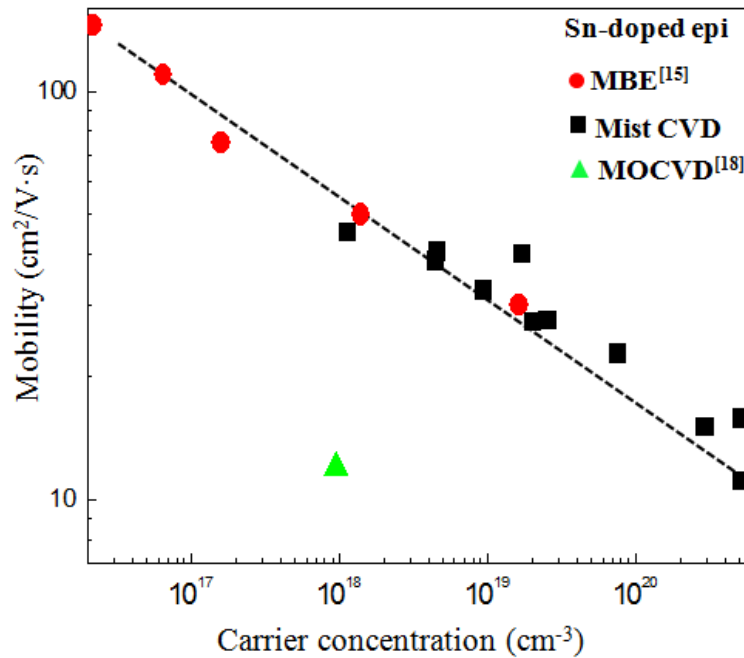


Figure 4.10. Experimental electron mobility of Sn-doped  $\beta$ -Ga<sub>2</sub>O<sub>3</sub> films grown by MBE, Mist CVD and MOCVD as a function of carrier concentration.

## 4.5 Summary

Homo-epitaxial single-crystalline  $\beta$ -Ga<sub>2</sub>O<sub>3</sub> films were successfully grown by mist CVD method. It was found that the crystallinity of the grown films significantly depends on the growth temperature. With UID  $\beta$ -Ga<sub>2</sub>O<sub>3</sub> layer, showing high resistivity, a SBD was fabricated and characterized. It exhibited rectifying characteristics with forward turn-on voltage of 1 V, but the reverse breakdown voltage was as low as 24 V (0.2 MV/cm). Furthermore, electrical conductive Sn-doped  $\beta$ -Ga<sub>2</sub>O<sub>3</sub> films were grown on Fe-doped  $\beta$ -Ga<sub>2</sub>O<sub>3</sub> substrates. The carrier concentration changed between  $\sim 1.0 \times 10^{18}$  and  $\sim 5.0 \times 10^{20}$  cm<sup>-3</sup>. The Hall mobility at room-temperature was higher for lower carrier concentration and achieved 45 cm<sup>2</sup>V<sup>-1</sup>s<sup>-1</sup> at the carrier concentration of about  $10^{18}$  cm<sup>-3</sup>. These results exhibit promising properties for future evolution and the author expects that the mist CVD method will be useful for the practical fabrication of a variety of  $\beta$ -Ga<sub>2</sub>O<sub>3</sub>-based devices.

## References

- [1] H. Morkoç, S. Strite, G. B. GaO, M. E. Lin, B. Sverdlov and M. Burns, *J. Appl. Phys.* **76**, 1363 (1994).
- [2] H. Kambayashi, S. Yoshihiro, S. Ootomo, T. Kokawa, T. Nomura, S. Kato, and T. P. Chow, *Solid State Electron.* **52**, 660 (2010).
- [3] S. Dimitrijević, J. Han, H. A. Moghadam, and A. Aminbeidokhti, *MRS Bull.* **40**, 399 (2015).
- [4] K. Sasaki, M. Higashiwaki, A. Kuramata, T. Masui, and S. Yamakoshi, *IEEE Electr. Device L.* **34**, 493 (2013).
- [5] M. Higashiwaki, K. Sasaki, A. Kuramata, T. Masui, and S. Yamakoshi, *Phys. Status Solidi A* **211**, 21 (2014).
- [6] H. H. Tippins, *Phys. Rev.* **140**, A316 (1965).
- [7] M. Orita, H. Ohta, M. Hirano, and H. Hosono, *Appl. Phys. Lett.* **77**, 4166 (2000).
- [8] H. He, R. Orlando, M. A. Blanco, R. Pandey, E. Amzallang, I. Baraille, and M. Rérat, *Phys. Rev. B* **74**, 195123 (2006).
- [9] M. Higashiwaki, K. Sasaki, A. Kuramata, T. Masui, and S. Yamakoshi, *Appl. Phys. Lett.* **100**, 013504 (2012).
- [10] K. Sasaki, A. Kuramata, T. Masui, E. G. Villora, K. Shimamura, and S. Yamakoshi, *Appl. Phys. Express* **5**, 035502 (2012).
- [11] Y. Tamm, J. M. Ko, A. Yoshikawa, and T. Fukuda, *Sol. Energ. Mat. Sol. C.* **66**, 369 (2001).
- [12] E. G. Villora, K. Shimamura, Y. Yoshikawa, K. Aoki, and N. Ichinose, *J. Cryst. Growth* **270**, 420 (2004).

- [13] Z. Galazka, R. Uecker, K. Irscher, M. Albrecht, D. Klimm, M. Pietsch, M. Brützm, R. Bertram, S. Ganschow, and R. Fornari, *Cryst. Res. Technol.* **45**, 1229 (2010).
- [14] M. Higashiwaki, K. Sasaki, T. Kamimura, M. H. Wong, D. Krishnamurthy, A. Kuramata, T. Masui, and S. Yamakoshi, *Appl. Phys. Lett.* **103**, 123511 (2013).
- [15] K. Sasaki, M. Higashiwaki, A. Kuramata, T. Masui, and S. Yamakoshi, *J. Cryst. Growth* **378**, 591 (2013).
- [16] H. Murakami, K. Nomura, K. Goto, K. Sasaki, K. Kawara, Q. T. Thieu, R. Togashi, Y. Kumagai, M. Higashiwaki, A. Kuramata, S. Yamakoshi, B. Monemar, and A. Koukitu, *Appl. Phys. Express* **8**, 015503 (2015).
- [17] D. Shinohara and S. Fujita, *Jpn. J. Appl. Phys.* **47**, 9311 (2008).
- [18] X. Du, Z. Li, C. Luan, W. Wang, M. Wang, X. Feng, H. Xiao, J. Ma, *J. Mater. Sci.* **50**, 3252 (2015).
- [19] H. Nishinaka, T. Kawaharamura, and S. Fujita, *Jpn. J. Appl. Phys.* **46**, 6811 (2007).
- [20] T. Kawaharamura, H. Nishinaka, and S. Fujita, *Jpn. J. Appl. Phys.* **47**, 4669 (2008).
- [21] K. Kaneko, H. Kawanowa, H. Ito, and S. Fujita, *Jpn. J. Appl. Phys.* **51**, 020201 (2012).



## Chapter 5

### Growth of $\alpha$ -Ga<sub>2</sub>O<sub>3</sub> thin films on c-sapphire substrates

#### 5.1 Introduction

Gallium oxide (Ga<sub>2</sub>O<sub>3</sub>) is a compound semiconductor with wide bandgap of 4.9-5.3 eV. It has been studied for various applications in semiconducting devices such as field-effect transistors, ultraviolet photo-detectors, optical diodes, transparent conducting films, and gas sensors [1-5]. It is generally known that Ga<sub>2</sub>O<sub>3</sub> has five different crystalline phases,  $\alpha$ -,  $\beta$ -,  $\gamma$ -,  $\delta$ -, and  $\epsilon$  [6]. Among them,  $\beta$ -Ga<sub>2</sub>O<sub>3</sub> is the thermodynamically most stable phase. Therefore, previous researches have not received much attention other phases except for  $\beta$ -Ga<sub>2</sub>O<sub>3</sub>. One of the other biggest motivations for promoting the research on  $\beta$ -Ga<sub>2</sub>O<sub>3</sub> may be the fact that  $\beta$ -Ga<sub>2</sub>O<sub>3</sub> bulk substrates are available by the conventional solution methods such as floating zone (FZ) [7-14], edge-defined film-fed growth (EFG) [13,15], and Czochralski (CZ) [16,17] methods.

On the other hand, in previous studies, the Kyoto university research group, where the author belongs, have achieved highly single-crystalline  $\alpha$ -Ga<sub>2</sub>O<sub>3</sub> films with full-width at half maximum (FWHM) values of x-ray diffraction (XRD)  $\omega$ -scanning rocking curves as small as 60 arcsec, or even smaller, by using the mist chemical vapor deposition (CVD) method on *c*-plane sapphire ( $\alpha$ -Al<sub>2</sub>O<sub>3</sub>) substrates [18]. It is expected that this result is a significant step toward the realization of  $\alpha$ -Ga<sub>2</sub>O<sub>3</sub>-based novel electronic devices with low energy consuming processes on large scale substrates. Moreover, in spite of the ideal device structure by homo-epitaxy on  $\beta$ -Ga<sub>2</sub>O<sub>3</sub> substrates, the use of

$\text{Al}_2\text{O}_3$  substrates may be great advantageous for low-cost devices. Unfortunately, however,  $\alpha\text{-Ga}_2\text{O}_3$  is transformable to  $\beta\text{-Ga}_2\text{O}_3$  at high temperatures, so this may limit the process temperature in the device fabrication.

In this chapter, the author reports the effects of thermal annealing on single-crystalline  $\alpha\text{-Ga}_2\text{O}_3$  films on *c*-plane  $\text{Al}_2\text{O}_3$  based on the characterization of the films by XRD analysis and optical transmittance spectroscopy for the understanding of the thermal stability of  $\alpha\text{-Ga}_2\text{O}_3$  films.

## **5.2 $\alpha\text{-Ga}_2\text{O}_3$ films on *c*- $\text{Al}_2\text{O}_3$ substrate**

### **5.2.1 Sample preparation**

$\alpha\text{-Ga}_2\text{O}_3$  films were grown on *c*-plane  $\alpha\text{-Al}_2\text{O}_3$  substrates by the mist CVD. This is a simple, safe, cost-effective, and low energy-consumption solution-source vapor growth process of oxides, whose advantages have been demonstrated in the literatures [18-21]. As a source solution, gallium acetylacetonate [ $\text{Ga}(\text{C}_5\text{H}_8\text{O}_3)_3$ ] solved in deionized water, were used with slight addition of hydrochloric acid (HCl) to solve the precursor completely. The films were synthesized for 60 min at 470 °C of the growth temperature using  $\text{N}_2$  carrier gas in atmospheric pressure. The carrier gas flow rate was found to be one of the most important parameters in the growth. The optimization is important for the growth of higher quality  $\alpha\text{-Ga}_2\text{O}_3$  films.

### **5.2.2 Crystallinity of $\alpha\text{-Ga}_2\text{O}_3$ as a function of carrier gas flow rate**

Figure 5.1 shows XRD  $2\theta/\theta$  scan spectra for the grown  $\alpha\text{-Ga}_2\text{O}_3$  thin films on  $\alpha\text{-Al}_2\text{O}_3$  substrates as a function of the carrier gas flow rate. The growth conditions are summarized in Table 5.1. The

crystallinity of the  $\alpha$ -Ga<sub>2</sub>O<sub>3</sub> films grown at the highest flow rate was worse, as indicated by its broad XRD spectrum and the XRD  $\omega$ -scan rocking curve FWHMs which are displayed in Table 5.1 simultaneously. The FWHM of the rocking curve was as small as 30 arcsec for the  $\alpha$ -Ga<sub>2</sub>O<sub>3</sub> film grown at the lowest carrier gas flow rate (Case 1), where the film thicknesses was 720 nm, On the other hand, for the highest flow rate (Case 3) the rocking curve FWHM was remarkably large as 557 arcsec. The results show that the carrier gas flow has a large influence in crystallinity of  $\alpha$ -Ga<sub>2</sub>O<sub>3</sub> thin films.

The  $\alpha$ -Ga<sub>2</sub>O<sub>3</sub> is thermodynamically a semi-stable oxide material and it is grown at the growth temperature lower than 500 °C by the mist CVD method [18]. The reduction of crystalline quality may be due to hard atomic migration at the low growth temperature. From the growth characteristics of Ga<sub>2</sub>O<sub>3</sub> on YSZ substrate, where the growth rate was very low at 500 °C, it is speculated that the growth on  $\alpha$ -Al<sub>2</sub>O<sub>3</sub> at 500 °C follows surface reaction rate limited growth. This means that adatoms or precursors stay on surface for their decomposition, reaction, and migration, followed by the film growth. Therefore, excess supply of reaction sources may obstruct the sequence of the film growth, especially affect migration, and this can deteriorate crystallinity and surface morphology as well as form defects in the growing film. This seems to be the reason for poor crystal quality for the higher flow rate of carrier gas, shown in Fig. 5.1 and Table 5.1.

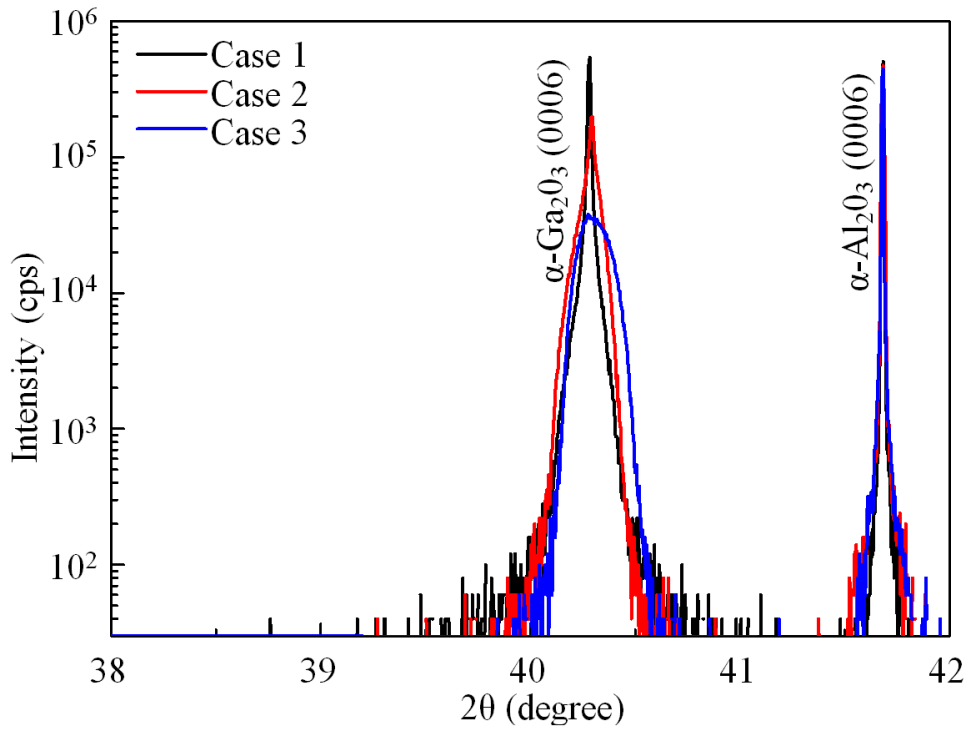


Figure 5.1 (a) Carrier concentration, (b) resistivity and (c) mobility of Sn-doped  $\beta$ -Ga<sub>2</sub>O<sub>3</sub> films grown as a function of Sn concentration in source solution. (d) Relationship between mobility and carrier concentration for Sn-doped  $\beta$ -Ga<sub>2</sub>O<sub>3</sub> films.

Table 5.1 Growth conditions for carrier gas flow.

Growth parameters	Case 1	Case 2	Case 3
Temperature (°C)	470	470	470
Carrier gas (l/min)	1	1.5	2
Dilute gas (l/min)	1	1	1
$\omega$ -scan rocking curve FWHM (arcsec)	30	66	557

## 5.3 Thermal stability of $\alpha$ -Ga<sub>2</sub>O<sub>3</sub> against annealing process

### 5.3.1 Sample preparation

After the growth of  $\alpha$ -Ga<sub>2</sub>O<sub>3</sub> on  $\alpha$ -Al<sub>2</sub>O<sub>3</sub> substrates, the samples were annealed for 60 min at 500, 550, 600, 650, 700, and 950 °C, step by step, under the N<sub>2</sub> gas atmosphere. The morphology of samples was examined by field-emission scanning electron microscopy (FE-SEM). Structural properties of  $\alpha$ -Ga<sub>2</sub>O<sub>3</sub> films were investigated by XRD (Rigaku ATX) with Cu K $\alpha$ <sub>1</sub> radiation ( $\lambda=1.54056$  Å). Optical transmittance spectra were examined by UV-visible spectrophotometer (PharmaSpec UV-1700). The spectra were taken using a double-beam spectrometer with *c*-plane Al<sub>2</sub>O<sub>3</sub> substrates as a reference sample.

### 5.3.2 Structural properties after annealing

Figure 5.2 shows the variation of XRD 2 $\theta$ / $\theta$  scan spectra for the samples grown under the growth condition of case 1 in Table 5.1, showing the smallest FWHM of XRD  $\omega$ -scan rocking curve of 30 arcsec, as a function of the annealing temperature. Any other peaks except  $\alpha$ -Ga<sub>2</sub>O<sub>3</sub> (0006) and  $\alpha$ -Al<sub>2</sub>O<sub>3</sub> substrate are seen until the annealing temperature of 550 °C. On the other hand, the intensity of  $\alpha$ -Ga<sub>2</sub>O<sub>3</sub> (0006) diffraction peak was rapidly decreased and broad and weak peak of  $\beta$ -Ga<sub>2</sub>O<sub>3</sub> (-402) appeared at 600 °C. Finally,  $\alpha$ -Ga<sub>2</sub>O<sub>3</sub> (0006) diffraction peak was completely disappeared and  $\beta$ -Ga<sub>2</sub>O<sub>3</sub> (-402) was only remained at 700 °C. In addition, it was found that the FWHM values of XRD 2 $\theta$ / $\theta$  scan of  $\alpha$ -Al<sub>2</sub>O<sub>3</sub> were increased. This seems to be due to increased interfacial stress caused by deformation of  $\alpha$ -Ga<sub>2</sub>O<sub>3</sub> to  $\beta$ -Ga<sub>2</sub>O<sub>3</sub>, enhancing the mismatch between the film and the substrate. It

was concluded that the single-crystalline  $\alpha$ -Ga<sub>2</sub>O<sub>3</sub> films of meta-stable phase were transformed to  $\beta$ -Ga<sub>2</sub>O<sub>3</sub> of most stable phase above 600 °C.

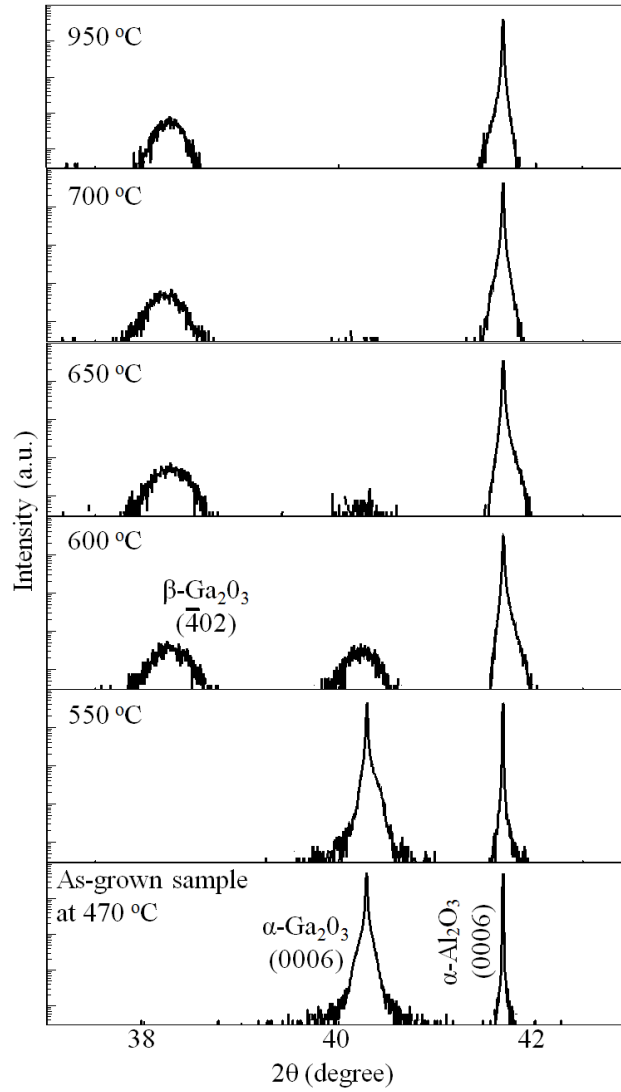


Figure 5.2 XRD 2 $\theta$ / $\theta$  scan spectra of the as-grown and annealed samples.

Figure 5.3 shows the variation of XRD  $\omega$ -scan rocking curves of the samples shown in Fig. 5.2 for the annealing temperature until 550°C. No marked increase of the FWHM is seen, suggesting that the crystal structure is stable until 550°C and the deformation to  $\beta$ -Ga<sub>2</sub>O<sub>3</sub> occurs gradually from the temperature higher than 550°C.

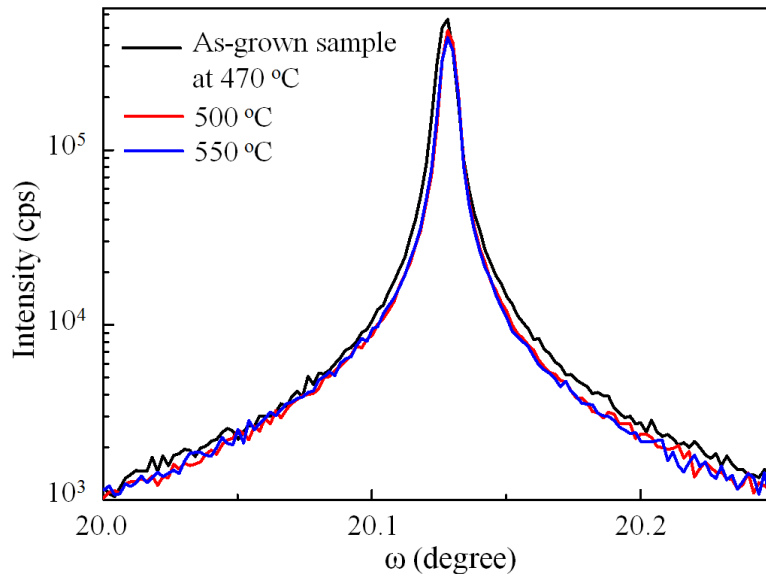


Figure 5.3 Variation of XRD  $\omega$ -scan rocking curves of the samples for the annealing temperatures until 550 °C.

### 5.3.3 Optical properties after annealing

Figure 5.4 is the variation of optical transmittance spectra of the  $\alpha$ -Ga<sub>2</sub>O<sub>3</sub> samples shown in Fig. 5.2 as a function of the annealing temperature. The transmittance spectrum did not show marked change from that of the as-grown  $\alpha$ -Ga<sub>2</sub>O<sub>3</sub> for the annealing temperature upto 550 °C and the optical bandgap energy remained at 5.25 eV as shown in Fig. 5.5, which was that of  $\alpha$ -Ga<sub>2</sub>O<sub>3</sub> [13]. However,

the spectrum drastically changed for the annealing temperature higher than 600 °C. The reduction of transmittance means the rough surface, probably due to appearance of  $\beta$ -Ga<sub>2</sub>O<sub>3</sub>. The optical bandgap energy changed to 4.75 eV as shown in Fig 5.5, which is that of  $\beta$ -Ga<sub>2</sub>O<sub>3</sub>. The variation of optical properties supports the variation of XRD spectra.

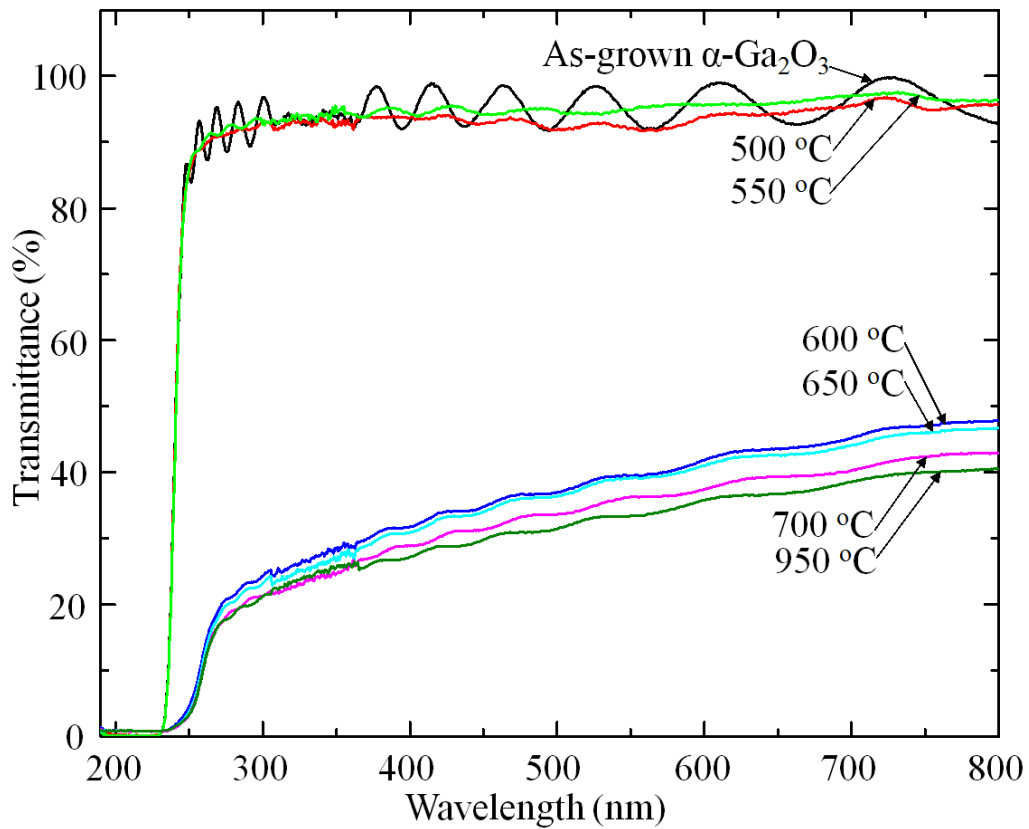


Figure 5.4 Optical transmittance spectra of the as-grown and annealed samples.

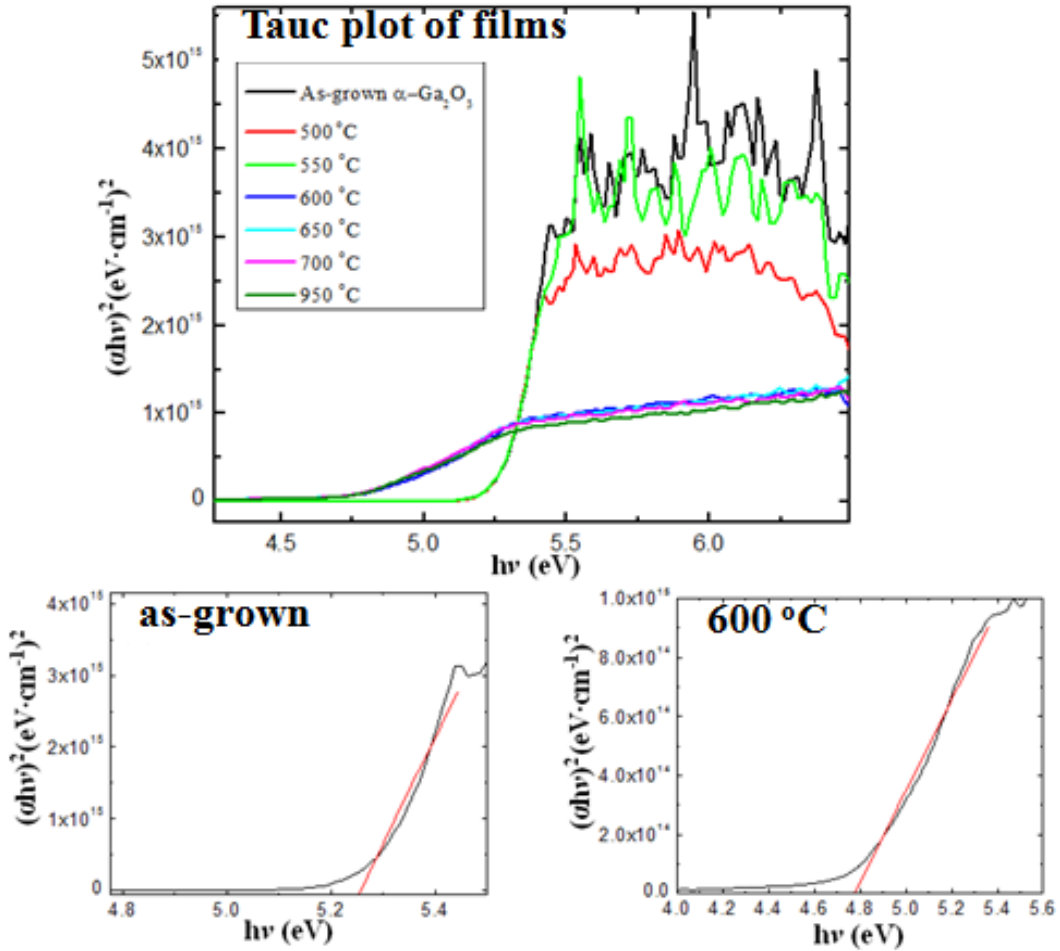


Figure 5.5 Tauc plot for the as-grown and annealed samples.

### 5.3.4 Surface morphology

Figure 5.6 (a) shows FE-SEM images of  $\alpha\text{-Ga}_2\text{O}_3$  films on  $\alpha\text{-Al}_2\text{O}_3$  substrates grown under the condition of case1 in Table 5.1. The as-grown films had very smooth and flat surface. The flat surface corresponds to optical transmittance spectrum with the multiple reflections of as-grown  $\alpha\text{-Ga}_2\text{O}_3$ . The multiple reflections for as-grown  $\alpha\text{-Ga}_2\text{O}_3$  are considered due to strong interference effects within a thin film by the flat surface and interface. In case of annealed samples, the amplitude of multiple reflections was decreased by scattering effect of reflected beams as shown in Fig 5.4. It is

considered that the annealed samples have rough surface because the atomic migration occurs in order to stabilizing during annealing. Unfortunately,  $\alpha$ -Ga<sub>2</sub>O<sub>3</sub> changed to  $\beta$ -Ga<sub>2</sub>O<sub>3</sub> by phase transformation over 600 °C and the surface morphology was also very rough as shown in Fig. 5.6 (b). The rough surface corresponds to results of phase transformation in XRD analysis and reduction in optical transmittance spectroscopy.

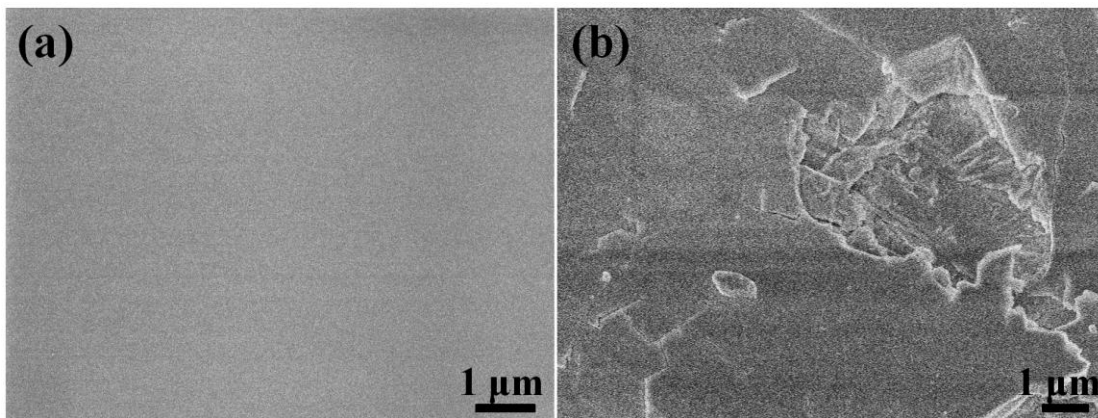


Figure 5.6 FE-SEM images of Ga<sub>2</sub>O<sub>3</sub> films. (a) As-grown sample at 470 °C. (b) Annealed sample at 950 °C.

## 5.4 Summary

It was found that  $\alpha$ -Ga<sub>2</sub>O<sub>3</sub> thin films grown on sapphire substrates at 470 °C remained  $\alpha$ -phase by annealing upto 550 °C, but gradually changed to  $\beta$ -phase at the temperature higher than 600 °C.  $\alpha$ -Ga<sub>2</sub>O<sub>3</sub> thin films on sapphire substrates are advantageous for low-cost devices but It needs careful care for the transformation to  $\beta$ -Ga<sub>2</sub>O<sub>3</sub> in the successive device processes so that the process temperature should kept lower than 550 °C. In other words,  $\alpha$ -Ga<sub>2</sub>O<sub>3</sub> thin films can keep the  $\alpha$ -phase in the successive device processes as far as they were done at the temperature lower than 550 °C.

## References

- [1] M. Orita, H. Ohta, M. Hirano, and H. Hosono, *Appl. Phys. Lett.* 77, 4166 (2000).
- [2] M. Ogita, K. Higo, Y. Nakanishi, and Y. Hatanaka, *Appl. Surf. Sci.* 175, 721 (2001).
- [3] K. Shimamura, E. G. Villora, K. Domen, K. Yui, K. Aoki, and N. Ichinose, *Jpn. J. Appl. Phys.* 44, L7 (2004).
- [4] T. Oshima, T. Okuno, and S. Fujita, *Jpn. J. Appl. Phys.* 46, 7217 (2007).
- [5] M. Higashiwaki, K. Sasaki, A. Kuramata, T. Masui and S. Yamakoshi, *Appl. Phys. Lett.* 100, 013504 (2012).
- [6] R. Roy, V. G. Hill, and E. F. Osborn, *J. Am. Chem. Soc.* 74, 719 (1952).
- [7] V. I. Vasylytsiv, Y. I. Rym, and Y. M. Zakharko, *Phys. Status Solidi B* 195, 653 (1996).
- [8] N. Ueda, H. Hosono, R. Waseda, and H. Kawazoe, *Appl. Phys. Lett.* 70, 3561 (1997).
- [9] Y. Tomm, J. M. Ko, A. Yoshikawa, and T. Fukuda, *Sol. Energy Mater. Sol. Cells* 66, 369 (2001).
- [10] E. G. Villora, Y. Morioka, T. Atou, T. Sugawara, M. Kikuchi, and T. Fukuda, *Phys. Status Solidi A* 193, 187 (2002).
- [11] E. G. Villora, K. Shimamura, Y. Yoshikawa, K. Aoki, and N. Ichinose, *J. Cryst. Growth* 270, 420 (2004).
- [12] J. Zhang, B. Li, C. Xia, G. Pei, Q. Deng, Z. Yang, W. Xu, H. Shi, F. Wu, Y. Wu, and J. Xu, *J. Phys. Chem. Solids* 67, 2448 (2006).
- [13] K. Shimamura, E. G. Villora, K. Muramatsu, K. Aoki, M. Nakamura, S. Takekawa, N. Ichinose, and K. Kitamura, *The Japanese Association for Crystal Growth* 33, 147 (2006) [in Japanese].

- [14] N. Suzuki, S. Ohira, M. Tanaka, T. Sugawara, K. Nakajima, and T. Shishido, *Phys. Status Solidi C* 4, 2310 (2007).
- [15] H. Aida, K. Nishiguchi, H. Takeda, N. Aota, K. Sunakawa, and Y. Yaguchi, *Jpn. J. Appl. Phys.* 47, 8506 (2008).
- [16] Y. Tomm, P. Reiche, D. Klimm, and T. Fukuda, *J. Cryst. Growth* 220, 510 (2000).
- [17] Z. Galazka, R. Uecker, K. Irmischer, M. Albrecht, D. Klimm, M. Pietsch, M. Brutzam, R. Bertram, S. Ganschow, and R. Fornari, *Cryst. Res. Technol.* 45, 1229 (2010).
- [18] D. Shinohara and S. Fujita, *Jpn. J. Appl. Phys.* 47, 7311 (2008).
- [19] H. Nishinaka and S. Fujita, *J. Cryst. Growth* 310, 5007 (2008).
- [20] T. Okuno, T. Oshima, S.-D. Lee, and S. Fujita, *Phys. Status Solidi C* 8, 540 (2011).
- [21] K. Kaneko, H. Kawanowa, H. Ito, and S. Fujita, *Jpn. J. Appl. Phys.* 51, 020201 (2012).

## Chapter 6

### Effect of Al doping for enhanced thermal stability of $\alpha$ -Ga<sub>2</sub>O<sub>3</sub> thin films

#### 6.1 Introduction

Corundum-structured  $\alpha$ -Ga<sub>2</sub>O<sub>3</sub> is a thermodynamically semi-stable phase [1]. Therefore, it has not attracted much attention owing to the difficulty of film growth. Nevertheless, the Kyoto University group (where the author is belonging) has shown that high-quality single-crystalline  $\alpha$ -Ga<sub>2</sub>O<sub>3</sub> films can be grown on sapphire ( $\alpha$ -Al<sub>2</sub>O<sub>3</sub>) substrates by the mist chemical vapor deposition (CVD) method [2-5]. This has opened the door to research on  $\alpha$ -Ga<sub>2</sub>O<sub>3</sub>-based power devices [6,7] that possess the potential advantages of low-cost sapphire substrates and low-cost growth technology. In addition, corundum-structured  $\alpha$ -Ga<sub>2</sub>O<sub>3</sub> is attractive for fabricating alloys with other corundum-structured oxide materials such as Al<sub>2</sub>O<sub>3</sub>, In<sub>2</sub>O<sub>3</sub>, Cr<sub>2</sub>O<sub>3</sub>, and Fe<sub>2</sub>O<sub>3</sub> for bandgap and function engineering [8,9]. However, owing to its semi-stable phase, the inclusion of the  $\beta$ -phase was seen at growth temperatures higher than 550 °C [2] and at successive annealing temperatures higher than 600 °C [10]. This is a severe limit for  $\alpha$ -Ga<sub>2</sub>O<sub>3</sub>-based device processes because it needs to keep the process temperatures lower than 600 °C. A higher thermal stability is expected for  $\alpha$ -(Al<sub>x</sub>Ga<sub>1-x</sub>)<sub>2</sub>O<sub>3</sub> alloy films [11] because Al<sub>2</sub>O<sub>3</sub> is in the stable  $\alpha$ -phase. However, the increased bandgap in  $\alpha$ -(Al<sub>x</sub>Ga<sub>1-x</sub>)<sub>2</sub>O<sub>3</sub> will make the control of electrical conductivity difficult.

Ehrenreich and Hirth [12] proposed solution hardening effects in gallium arsenide (GaAs) by doping a solution of 3 to 4% indium (In), which is an isovalent impurity in GaAs and substitutes for Ga atoms. Similar effects upon doping a slight amount of aluminum (Al) to  $\alpha$ -Ga<sub>2</sub>O<sub>3</sub> were expected without markedly enhancing the bandgap energy, which will contribute to stabilizing the crystal structure against the thermal processes. In this chapter, the author reports that the doping of a slight amount of Al in  $\alpha$ -Ga<sub>2</sub>O<sub>3</sub> is effective for the improvement of thermal stability against the transition to the  $\beta$ -phase.

## **6.2 Fabrication and characterization of Al-doped $\alpha$ -Ga<sub>2</sub>O<sub>3</sub> films**

### **6.2.1 Sample preparation**

The growth and annealing conditions are briefly shown in Table 6.1. A mist CVD system was used, and its detail has been reported in previous literatures [2-5]. To grow  $\alpha$ -Ga<sub>2</sub>O<sub>3</sub>:Al thin films, the precursor solutions were prepared by dissolving gallium acetylacetonate [Ga(C<sub>5</sub>H<sub>8</sub>O<sub>3</sub>)<sub>3</sub>] and aluminum acetylacetonate [Al(C<sub>5</sub>H<sub>7</sub>O<sub>2</sub>)<sub>3</sub>] into deionized water as the solvent solution, with the addition of a slight amount of hydrochloric acid to dissolve the precursor completely. The parameters of the growth were the molar ratio of [Al]/[Ga] in the source solution and the growth temperature ( $T_g$ ). The molar ratios were 0 (ref.), 1 (case 1), and 3 (case 2), as shown in Table 6.1. One may argue that the molar ratios are too high to achieve the slight doping of Al rather than alloying, but this is because of the much weaker dissociation of the Al source [Al(C<sub>5</sub>H<sub>7</sub>O<sub>2</sub>)<sub>3</sub>] than of the Ga source [Ga(C<sub>5</sub>H<sub>8</sub>O<sub>3</sub>)<sub>3</sub>] at various growth temperatures. Discussions on Al composition will be given later based on the X-ray diffraction (XRD) spectra.

The growth temperature was varied between 550 and 800 °C. After the main growth, the grown films were annealed from 550 to 900 °C at 50 °C intervals for 60 min, step by step, under N<sub>2</sub> gas atmosphere.

The structural properties of the prepared samples were investigated by XRD with Cu K<sub>α1</sub> radiation (Rigaku ATX). The optical transmittance spectra were evaluated using a UV-visible spectrophotometer (PharmaSpec UV-1700). The atomic densities of Al in the grown films were estimated by secondary ion mass spectroscopy (SIMS).

### 6.2.2 Structural properties

Figure 6.1 shows the XRD  $2\theta/\theta$  scan spectra of the Al-doped  $\alpha$ -Ga<sub>2</sub>O<sub>3</sub> film grown at 550 °C under the condition of case 1 and the unintentionally doped (UID)  $\alpha$ -Ga<sub>2</sub>O<sub>3</sub> film grown at 470 °C. No marked difference in the XRD peak position was seen between these samples, suggesting that the Al concentration in the Al-doped  $\alpha$ -Ga<sub>2</sub>O<sub>3</sub> film was lower than 1%. Hereafter, the author denotes Al-doped  $\alpha$ -Ga<sub>2</sub>O<sub>3</sub> as  $\alpha$ -Ga<sub>2</sub>O<sub>3</sub>:Al as long as the Al concentration is low enough not to cause any marked change in the lattice constant (and bandgap). However, the full-width at half-maximum (FWHM) of the XRD  $\omega$ -scan rocking curve for the  $\alpha$ -Ga<sub>2</sub>O<sub>3</sub>:Al film was 140 arcsec, which was larger than that (40 arcsec) for the UID  $\alpha$ -Ga<sub>2</sub>O<sub>3</sub> film, probably because of the slight degradation of the crystallinity upon the incorporation of foreign atoms. Nevertheless, it is interesting to note that the  $\alpha$ -phase is dominant without the marked incorporation of the  $\beta$ -phase for the  $\alpha$ -Ga<sub>2</sub>O<sub>3</sub>:Al film grown at 550 °C, in contrast to our previous report indicating that the  $\beta$ -phase was incorporated in UID  $\alpha$ -Ga<sub>2</sub>O<sub>3</sub> at growth temperatures higher than 550 °C [2].

Table 6.1 Growth and annealing conditions.

Solute	Ga(C <sub>5</sub> H <sub>8</sub> O <sub>3</sub> ) <sub>3</sub> Al(C <sub>5</sub> H <sub>7</sub> O <sub>2</sub> ) <sub>3</sub>
Solvent	Deionized water
Solution concentration (Ref.)	0.05 M of Ga(C <sub>5</sub> H <sub>8</sub> O <sub>3</sub> ) <sub>3</sub>
Solution concentration (Case 1)	0.05 M of Ga(C <sub>5</sub> H <sub>8</sub> O <sub>3</sub> ) <sub>3</sub> 0.05 M of Al(C <sub>5</sub> H <sub>7</sub> O <sub>2</sub> ) <sub>3</sub>
Solution concentration (Case 2)	0.05 M of Ga(C <sub>5</sub> H <sub>8</sub> O <sub>3</sub> ) <sub>3</sub> 0.15 M of Al(C <sub>5</sub> H <sub>7</sub> O <sub>2</sub> ) <sub>3</sub>
Growth temperature ( $T_g$ )	550 – 800 °C (intervals: 50 °C)
Growth time	30 min
Substrate	$\alpha$ -Al <sub>2</sub> O <sub>3</sub>
Carrier gas, flow rate	O <sub>2</sub> , 3.0 L/min
Dilution gas, flow rate	O <sub>2</sub> , 0.5 L/min
Annealing temperature ( $T_a$ )	550 – 900 °C (intervals: 50 °C)
Annealing time	60 min (at each step)
Atmospheric gas, flow rate	N <sub>2</sub> , 2 L/min

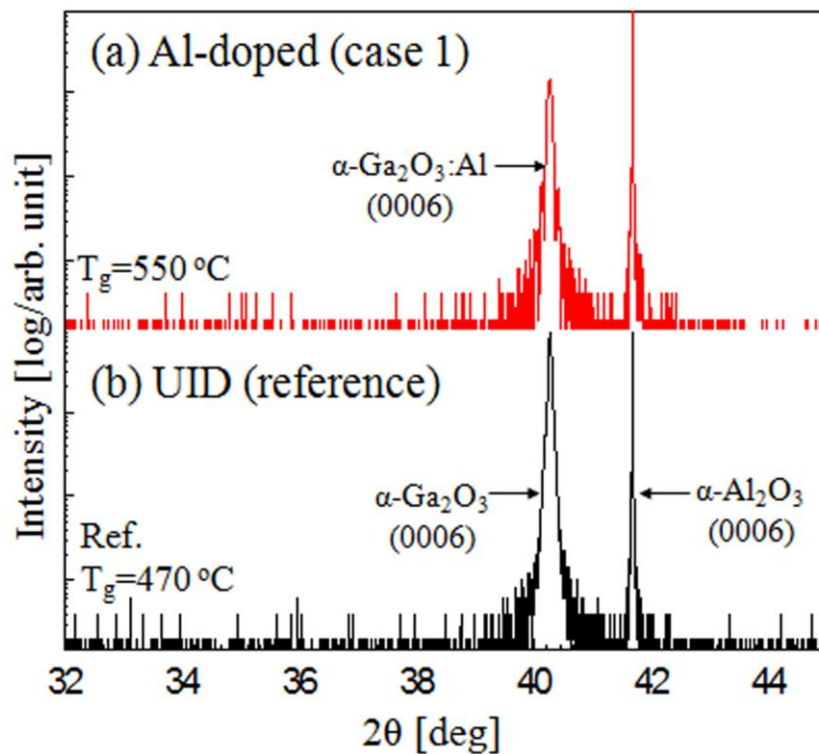


Figure 6.1 XRD  $2\theta/\theta$  scan spectra of (a) Al-doped  $\alpha$ - $\text{Ga}_2\text{O}_3$  film grown at 550 °C under the condition of case 1 and (b) UID  $\alpha$ - $\text{Ga}_2\text{O}_3$  film grown at 470 °C (reference sample).

### 6.3 Thermal stability for Al-doped $\alpha$ - $\text{Ga}_2\text{O}_3$ films

The UID  $\alpha$ - $\text{Ga}_2\text{O}_3$  and  $\alpha$ - $\text{Ga}_2\text{O}_3$ :Al films, discussed above, were subjected to thermal annealing in order to compare their thermal stabilities. Variations of the XRD  $2\theta/\theta$  scan spectra against the annealing temperatures are shown in Fig. 6.2. In Fig. 6.2 (b) [10], the UID  $\alpha$ - $\text{Ga}_2\text{O}_3$  film clearly exhibited the inclusion of the  $\beta$ -phase at annealing temperatures above 600 °C. On the other hand, as shown in Fig. 6.2 (a) for the  $\alpha$ - $\text{Ga}_2\text{O}_3$ :Al film, the  $\beta$ -phase was

not seen at annealing temperatures up to 650 °C, but became apparent at annealing temperatures above 700 °C. It is reasonable to claim that Al doping allows the higher temperature growth of  $\alpha$ -Ga<sub>2</sub>O<sub>3</sub>, followed by a higher thermal stability.

In order to confirm the contribution of Al doping into  $\alpha$ -Ga<sub>2</sub>O<sub>3</sub> to the thermal stability,  $\alpha$ -Ga<sub>2</sub>O<sub>3</sub>:Al films were prepared at a higher Al flow rate. Figure 6.3 shows the XRD  $2\theta/\theta$  scan spectra of the  $\alpha$ -Ga<sub>2</sub>O<sub>3</sub> films grown at different temperatures under the condition of case 2, where the Al flow rate is three times higher than that in case 1. As shown in Fig. 6.3 (b), no marked XRD peak shift was seen for the  $\alpha$ -Ga<sub>2</sub>O<sub>3</sub>:Al film grown at a growth temperature as high as 650 °C. When the  $\alpha$ -Ga<sub>2</sub>O<sub>3</sub>:Al film was grown at 650 °C under the condition of case 1, the  $\beta$ -phase was apparently seen (not shown). This implies that the doping of more Al yields the  $\alpha$ -phase Ga<sub>2</sub>O<sub>3</sub> at higher growth temperatures. On the other hand, the sample grown at 800 °C clearly exhibits the peak shift of the XRD spectrum, as shown in Fig. 6.3 (a). From the peak position, the film composition was estimated to be  $\alpha$ -(Al<sub>0.2</sub>Ga<sub>0.8</sub>)<sub>2</sub>O<sub>3</sub>, assuming Vegard's law. This means that the Al concentration in the film is higher than what author call a doping level, and the film should be identified as an alloy material. The optical bandgap estimated from the optical absorption spectra with the Tauc plot was 5.95 eV, which was consistent with the previous result [11,13]. The reason for the inclusion of more Al in the film grown at a higher temperature, 800 °C compared with 650 °C, may be the greater decomposition of the Al precursor.

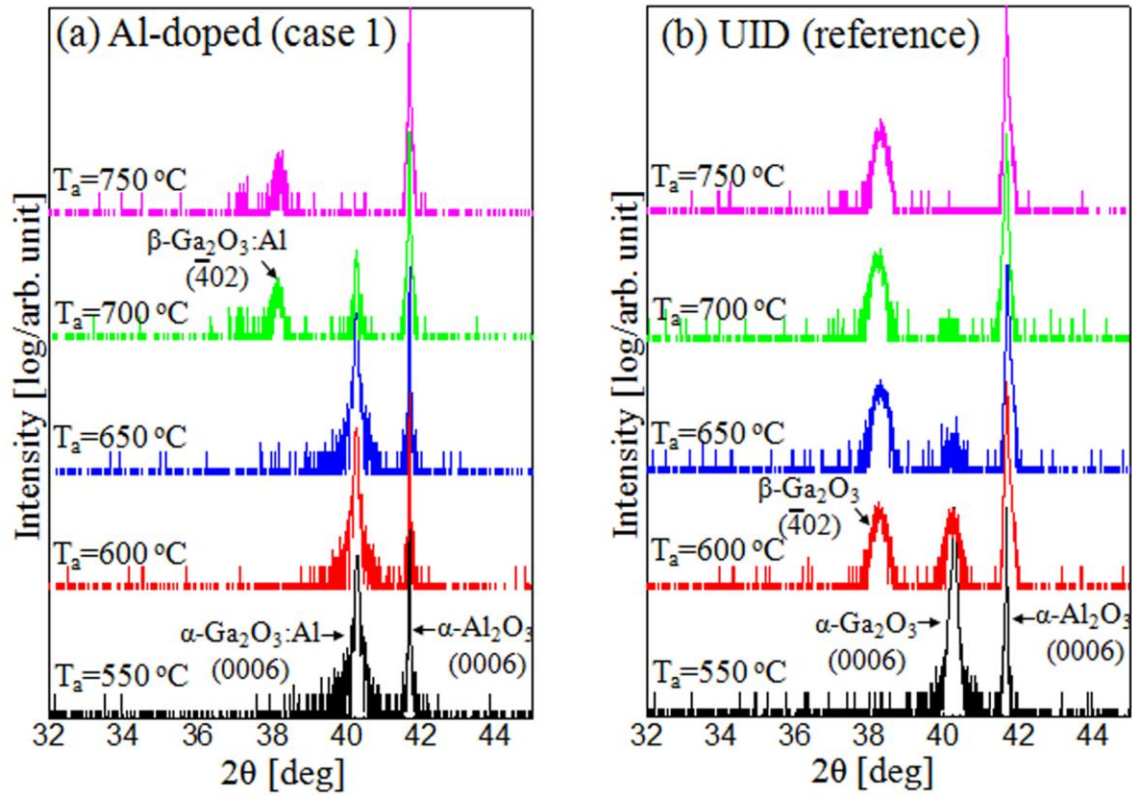


Figure 6.2 XRD  $2\theta/\theta$  scan spectra of stepwise annealed samples as a function of annealing temperature ( $T_a$ ). The samples were the same as those shown in Fig. 6.1, that is, (a) Al-doped  $\alpha\text{-Ga}_2\text{O}_3$  film grown at 550 °C under the condition of case 1 and (b) UID  $\alpha\text{-Ga}_2\text{O}_3$  film grown at 470 °C (reference sample).

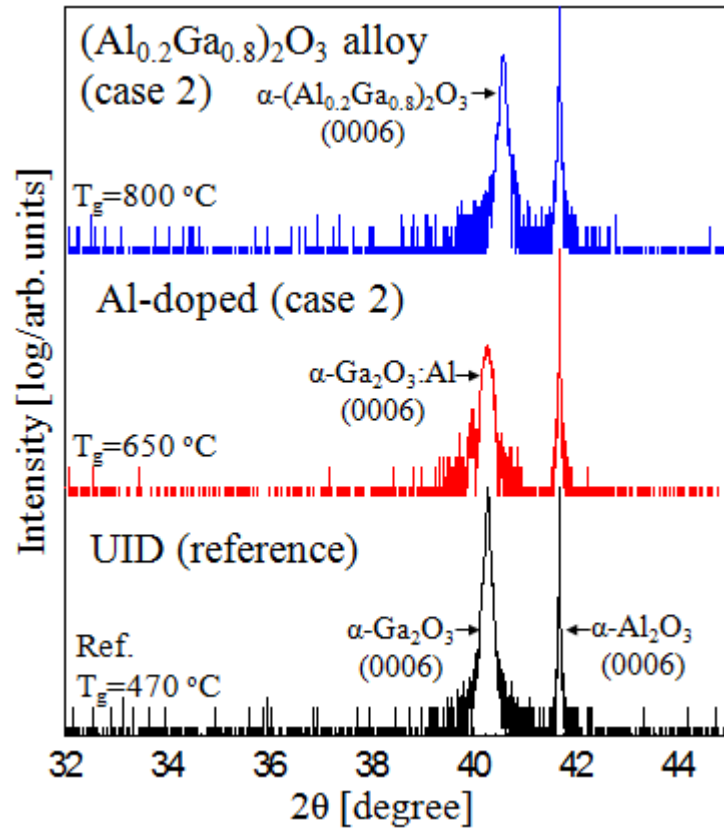


Figure 6.3 XRD  $2\theta/\theta$  scan spectra of Al-doped  $\alpha\text{-Ga}_2\text{O}_3$  films grown at (a)  $800\text{ }^\circ\text{C}$  and (b)  $650\text{ }^\circ\text{C}$  under the condition of case 2, and of (c) UID  $\alpha\text{-Ga}_2\text{O}_3$  film grown at  $470\text{ }^\circ\text{C}$  (reference sample).

Figure 6.4 shows the XRD  $2\theta/\theta$  scan spectra of the samples discussed above, that is, those grown at 650 and 800 °C under the condition of case 2. As shown in Fig. 6.4 (b), the sample grown at 650 °C, where the Al concentration in the film was as low as the doping level, maintained the  $\alpha$ -phase for annealing temperatures up to 750 °C. The sample grown at 800 °C can no longer be referred to as “Al-doped  $\alpha$ -Ga<sub>2</sub>O<sub>3</sub>” but is “(Al<sub>x</sub>Ga<sub>1-x</sub>)<sub>2</sub>O<sub>3</sub> alloy”, although it exhibited up to  $\alpha$ -phase for the annealing temperature of 850 °C, as shown in Fig. 6.4 (a). This is because the effects of Al doping are considerably enhanced by the higher amount of incorporation.

In order to analyze the atomic density of Al in the grown films, the samples were investigated by SIMS measurements as shown in Fig. 6.5. The Al atomic densities in the films were  $2 \times 10^{20}$  and  $5 \times 10^{20}$  cm<sup>-3</sup> for the growth conditions of case 1 ( $T_g=550$  °C) and case 2 ( $T_g=650$  °C), respectively. From these results, the Al concentration in the Al-doped  $\alpha$ -Ga<sub>2</sub>O<sub>3</sub> film could be calculated to be about 1 and 2.5% for case 1 ( $T_g=550$  °C) and case 2 ( $T_g=650$  °C), respectively. These results are in close agreement with estimated Al composition  $x$  from the XRD peak position shown in Figs. 6.1 (0.8% of XRD peak shift) and 6.3 (1.4% of XRD peak shift). It is indicated that the thermal stability of the films was enhanced by the increased Al doping concentration.

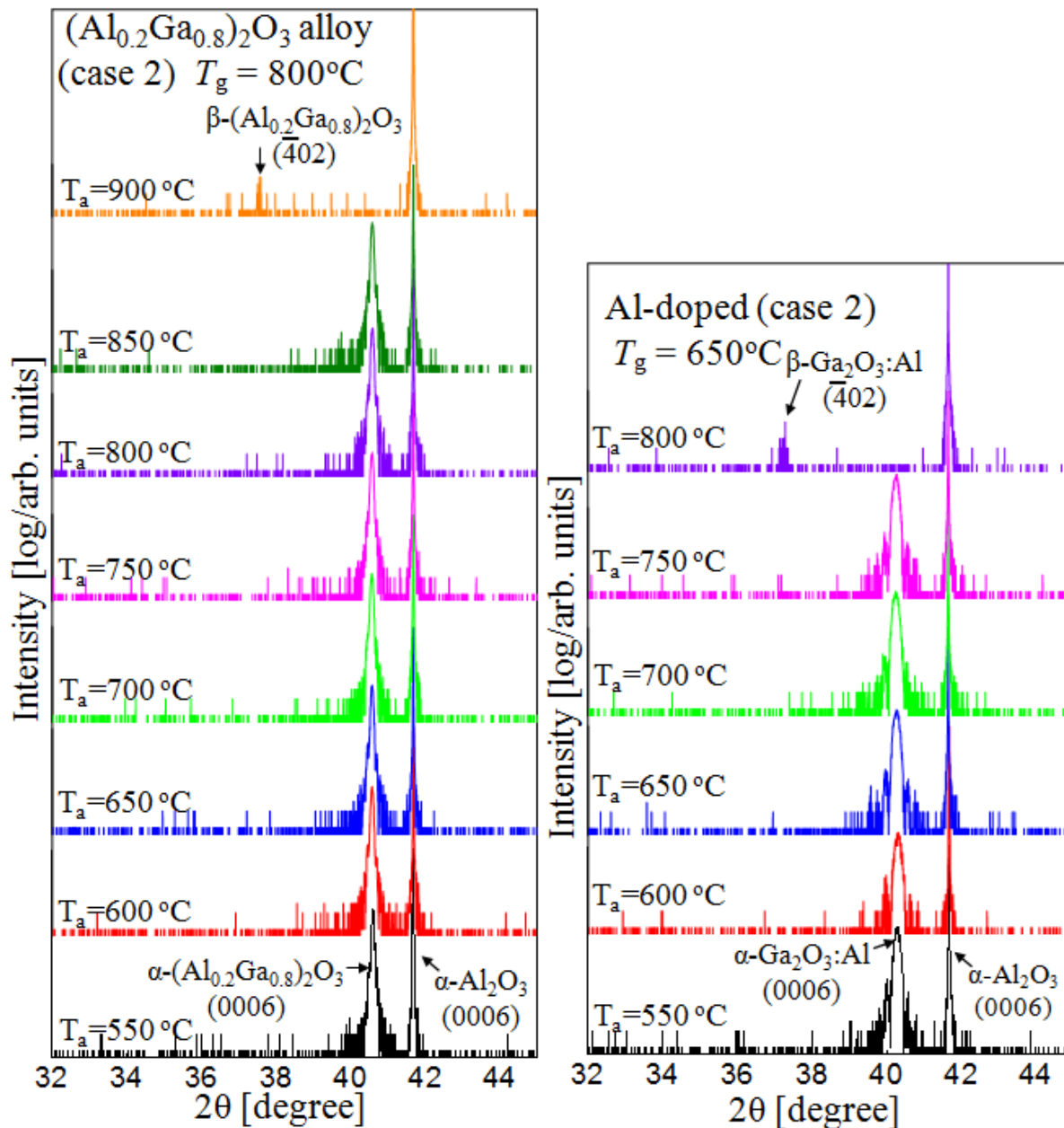


Figure 6.4 XRD  $2\theta/\theta$  scan spectra of stepwise annealed samples as a function of annealing temperature ( $T_a$ ). The samples were the same as those shown in Fig. 6.3, that is, Al-doped  $\alpha-Ga_2O_3$  films grown at (a) 800 and (b) 650  $^\circ C$  under the condition of case 2.

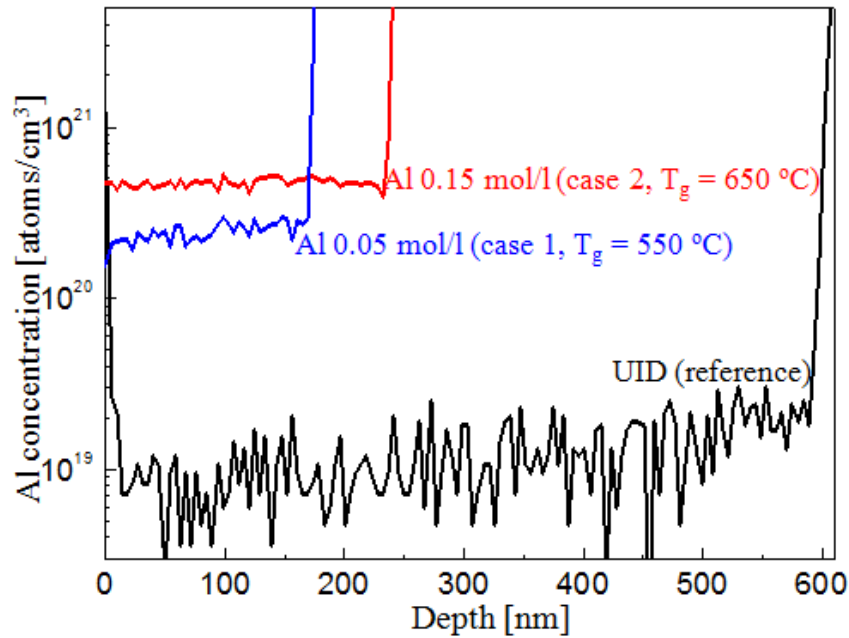


Figure 6.5 Depth profiles of Al in films grown as a function of Al concentration in source solution by SIMS.

Figure 6.6 shows the data presented above, that is, whether the phase transformation occurs at the annealing temperature in terms of the growth temperature. Without Al doping,  $\alpha$ -Ga<sub>2</sub>O<sub>3</sub> should be grown at 470 °C in order to avoid the inclusion of the  $\beta$ -phase. This sample retains the  $\alpha$ -phase up to the annealing temperature of 550 °C. With Al doping, the growth temperature can be increased to 550 and 650 °C for the growth conditions of case 1 and case 2, respectively. These samples were thermally stable, that is, the inclusion of the  $\beta$ -phase was negligible, as determined from the XRD spectra for thermal annealing up to 650 and 750 °C, respectively. The sample grown under the condition of case 2 becomes the  $\alpha$ -phase at the growth temperature of 800 °C and the annealing temperature of 850 °C, though the Al concentration in the film is higher; the solid composition is  $\alpha$ -(Al<sub>0.2</sub>Ga<sub>0.8</sub>)<sub>2</sub>O<sub>3</sub> with the optical bandgap of 5.95 eV.

Figure 6.7 shows the temperature of phase transition to the  $\beta$ -phase as a function of the Al composition  $x$  in the  $\alpha$ -phase films. The Al composition  $x$  in the films was estimated, assuming Vegard's law, from the XRD peak position. The temperature of phase transition to the  $\beta$ -phase increased with Al composition  $x$  up to about 40%. However, above the 40% Al composition in films, the phase transition temperature decreased owing to the low crystallinity of the grown films.

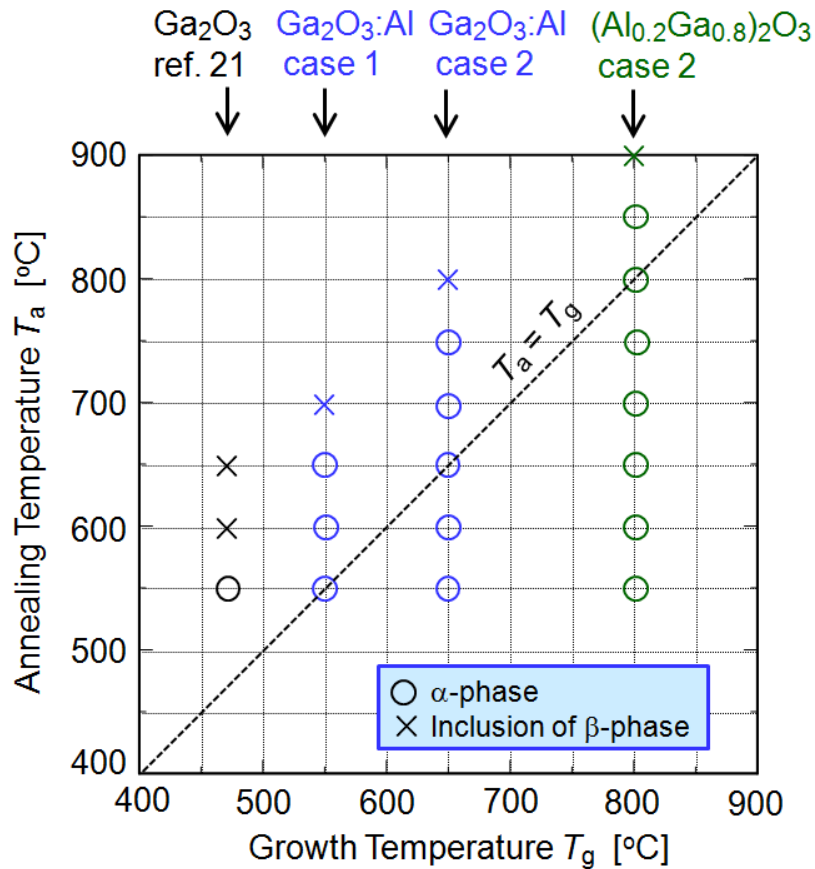


Figure 6.6 Summary of the experimental data showing whether the phase transformation occurs at the annealing temperature in terms of the growth temperature

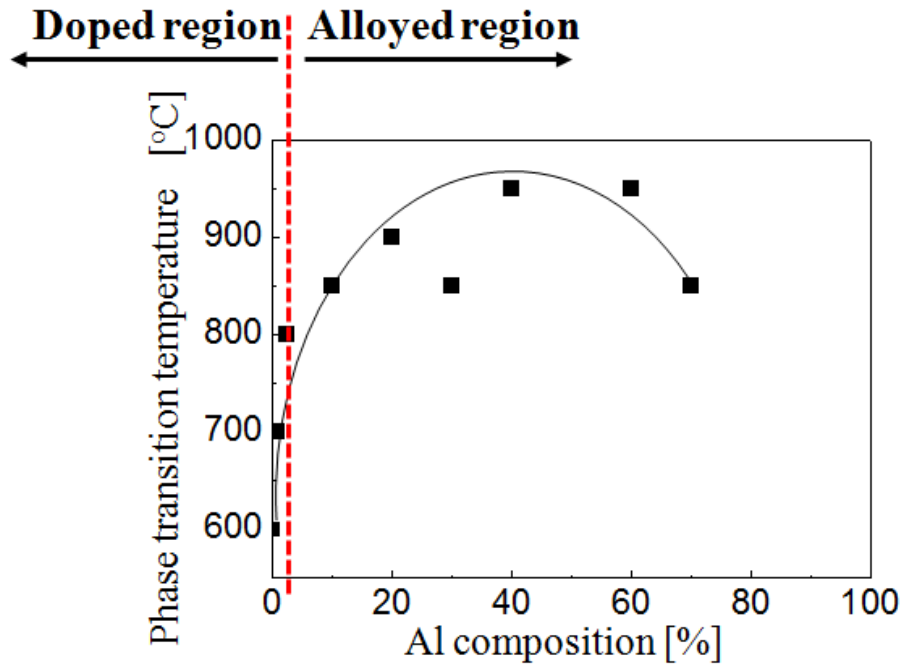


Figure 6.7 Temperature of phase transition to the  $\beta$ -phase as a function of Al composition in the  $\alpha$ -phase films.

## 6.4 Summary

Enhancement of the thermal stability of  $\alpha$ - $\text{Ga}_2\text{O}_3$  films on sapphire substrates were described upon Al doping. In the previous studies,  $\alpha$ - $\text{Ga}_2\text{O}_3$  films were grown at temperatures lower than 500 °C to avoid formation of the  $\beta$ -phase. This also has limited the successive process temperatures, that is, the process windows of, for example, thermal annealing and overlayer growth, have been significantly narrowed. On the other hand, slight doping of Al allows the growth at higher temperatures (for example, by 50–150 °C), and this enhances thermal stability for the successive thermal treatments without markedly modifying the basic chemical composition of  $\text{Ga}_2\text{O}_3$ . If the inclusion of more Al, which results in an enhanced bandgap energy of  $\sim 6$  eV, does not obstruct the target application, the

film can be grown at a temperature as high as 800 °C and can withstand an annealing temperature as high as 850 °C without formation of the  $\beta$ -phase. These results indicate that wide process windows, which will be useful for the evolution of various  $\alpha$ -Ga<sub>2</sub>O<sub>3</sub>-based devices, are possible.

Very recently, Takemoto in Kyoto University (who is in the same research group as the authors') succeeded in the Sn doping to (Al<sub>0.03</sub>Ga<sub>0.97</sub>)<sub>2</sub>O<sub>3</sub> achieving n-type conductivity with carrier concentration of  $2.7 \times 10^{18} \text{ cm}^{-3}$  and Hall mobility of  $4.7 \text{ cm}^2 \text{ V}^{-1} \text{ s}^{-1}$  [14]. The solid composition of Al in that sample (3%) was in the doping range without markedly changing bandgap and lattice constant from those of Ga<sub>2</sub>O<sub>3</sub> but the enhanced thermal stability is expected for it based on the results shown in this chapter. The author believes that the present results can contribute to the actual device processes of Ga<sub>2</sub>O<sub>3</sub>-based power devices for higher performance.

## References

- [1] R. Roy, V. G. Hill, and E. F. Osborn, *J. Am. Chem. Soc.* **74**, 719 (1952).
- [2] D. Shinohara and S.F Fujita, *Jpn. J. Appl. Phys.* **47**, 7311 (2008).
- [3] H. Nishinaka, T. Kawaharamura, and S. Fujita, *Jpn. J. Appl. Phys.* **46**, 6811 (2007).
- [4] T. Kawaharamura, H. Nishinaka, and S. Fujita, *Jpn. J. Appl. Phys.* **47**, 4669 (2008).
- [5] K. Kaneko, H. Kawanowa, H. Ito, and S. Fujita, *Jpn. J. Appl. Phys.* **51**, 020201 (2012).
- [6] M. Oda and T. Hitora, presented at 2013 Materials Research Society Fall Meet. **GG3.21** (2013)
- [7] M. Oda, A. Takatsuka, T. Hitora, J. Kikawa, K. Kaneko, and S. Fujita, presented at Int. Conf. Solid State Devices and Materials **N-1-5** (2014)
- [8] K. Kaneko, T. Nomura, and S. Fujita, *Phys. Status Solidi C* **7**, 2467 (2010).
- [9] K. Kaneko, I. Takeya, S. Komori, and S. Fujita, *J. Appl. Phys.* **113**, 233901 (2013).
- [10] S.-D. Lee, K. Akaiwa, and S. Fujita, *Phys. Status Solidi C* **10**, 1592 (2013).
- [11] H. Ito, K. Kaneko, and S. Fujita, *Jpn. J. Appl. Phys.* **51**, 100207 (2012).
- [12] H. Ehrenreich and J. P. Hirth, *Appl. Phys. Lett.* **46**, 668 (1985).
- [13] S. Fujita and K. Kaneko, *J. Cryst. Growth* **401**, 588 (2014).
- [14] S. Takemoto, B.S. Thesis of Kyoto University (2016) [unpublished].



## Chapter 7

### Conclusions

In this study, crystalline properties of gallium oxide thin films epitaxially grown by mist chemical vapor deposition have been investigated to achieve high quality thin films for Ga<sub>2</sub>O<sub>3</sub>-based novel device application. Systematic realization of alpha and beta gallium oxide ( $\alpha$ -Ga<sub>2</sub>O<sub>3</sub> and  $\beta$ -Ga<sub>2</sub>O<sub>3</sub>, respectively) with high quality was proposed and successfully demonstrated by mist CVD. Structural properties of Ga<sub>2</sub>O<sub>3</sub> films were investigated in detail. The conclusions accomplished for this thesis are summarized as follows.

In chapter 2, the author summarized the fundamental properties of gallium oxide and discussed the issues for commercial power devices from the viewpoints of substrate and growth technologies. Mist CVD was highlighted as a promising growth technology for device applications.

In chapter 3, hetero-epitaxial single-crystalline  $\beta$ -Ga<sub>2</sub>O<sub>3</sub> films has been successfully fabricated by mist CVD method. It was found that the crystallinity of films grown depends on growth temperature. Single-crystal  $\beta$ -Ga<sub>2</sub>O<sub>3</sub> (-201) were grown on YSZ (111) at the growth temperature of 600-800 °C. In addition, the growth direction of  $\beta$ -Ga<sub>2</sub>O<sub>3</sub> on cubic (111), (110) and (100) substrates were structurally discussed in terms of the unit-cell structures and surface energy. On YSZ (111) and MgAl<sub>2</sub>O<sub>4</sub> (111) substrates, single-crystal  $\beta$ -Ga<sub>2</sub>O<sub>3</sub> (-201) was grown. On YSZ (100) substrate, single-crystal  $\beta$ -Ga<sub>2</sub>O<sub>3</sub> (-201) was grown at high growth temperature over 600 °C. On YSZ (110) and MgO (110), single-crystal  $\beta$ -Ga<sub>2</sub>O<sub>3</sub> (-102) were easily grown. These growth behaviors were also explained in terms of

the unit-cell structures and surface energy. Conductive Sn-doped  $\beta$ -Ga<sub>2</sub>O<sub>3</sub> was fabricated, showing promising potential of mist CVD for device fabrication..

In chapter 4, homo-epitaxial single-crystalline  $\beta$ -Ga<sub>2</sub>O<sub>3</sub> films was successfully grown by mist CVD method on  $\beta$ -Ga<sub>2</sub>O<sub>3</sub> substrates. It was found that the crystallinity of the films significantly depended on growth temperatures. For unintentionally doped  $\beta$ -Ga<sub>2</sub>O<sub>3</sub> on conductive  $\beta$ -Ga<sub>2</sub>O<sub>3</sub> substrates, Schottky barrier diodes were fabricated and a device showed rectifying characteristics with turn-on voltage of 1 V and reverse breakdown voltage of 24 V (0.2 MV/cm) as a preliminary data. Electrical conductive Sn-doped  $\beta$ -Ga<sub>2</sub>O<sub>3</sub> films were grown on Fe-doped semi-insulating  $\beta$ -Ga<sub>2</sub>O<sub>3</sub> substrates, achieving n-type conductivity with carrier concentrations between  $\sim 1.0 \times 10^{18}$  and  $\sim 5.0 \times 10^{20}$  cm<sup>-3</sup>. The Hall mobility was 45 cm<sup>2</sup>V<sup>-1</sup>s<sup>-1</sup> at the Sn concentration of 10<sup>18</sup> cm<sup>-3</sup>.

In chapter 5,  $\alpha$ -Ga<sub>2</sub>O<sub>3</sub> on c-face sapphire ( $\alpha$ -Al<sub>2</sub>O<sub>3</sub>) substrates was synthesized by mist CVD and thermal stability of the  $\alpha$ -Ga<sub>2</sub>O<sub>3</sub> films was investigated. It was found that  $\alpha$ -Ga<sub>2</sub>O<sub>3</sub> thin films grown on sapphire substrates at 470 °C remained  $\alpha$ -phase by annealing upto 550 °C, but gradually changed to  $\beta$ -phase at the temperature higher than 600 °C.  $\alpha$ -Ga<sub>2</sub>O<sub>3</sub> thin films on sapphire substrates are advantageous for low-cost devices but the author pointed out that thermal stability of  $\alpha$ -Ga<sub>2</sub>O<sub>3</sub> is an important issue to overcome for the successive device fabrication processes.

In chapter 6, enhancement of the thermal stability of  $\alpha$ -Ga<sub>2</sub>O<sub>3</sub> films on sapphire substrates was achieved upon Al doping. In the previous chapter 5,  $\alpha$ -Ga<sub>2</sub>O<sub>3</sub> films were grown at temperatures lower than 500 °C to avoid formation of the  $\beta$ -phase. This also has limited the successive process temperatures, that is, the process windows of, for example, thermal annealing and overlayer growth, have been significantly narrowed. On the other hand, slight doping of Al allowed the growth at

higher temperatures (for example, by 50–150 °C), and this enhances thermal stability for the successive thermal treatments without markedly modifying the basic chemical composition of Ga<sub>2</sub>O<sub>3</sub>. If the inclusion of more Al, which results in an enhanced bandgap energy of ~6 eV, does not obstruct the target application, the film can be grown at a temperature as high as 800 °C and can withstand an annealing temperature as high as 850 °C without formation of the β-phase.

Throughout the work, the author showed the promising potential of mist CVD, which is a simple, safe, energy-effective, and low-cost growth technology. The author recognizes that this technology is applicable and contributes to both for α-Ga<sub>2</sub>O<sub>3</sub> and β-Ga<sub>2</sub>O<sub>3</sub> devices on sapphire and β-Ga<sub>2</sub>O<sub>3</sub> substrates for their future development.

Finally, the author points out the future issues to be investigated for the future evolution of Ga<sub>2</sub>O<sub>3</sub>-based devices.

1. In chapter 4, the author reported electrical conductive Sn-doped β-Ga<sub>2</sub>O<sub>3</sub> films with n-type conductivity. However, in the present thesis, the carrier concentration of the Sn-doped β-Ga<sub>2</sub>O<sub>3</sub> films could not be controlled under the Sn concentration of 10<sup>18</sup> cm<sup>-3</sup> because of impurities or defects in the film. Reduction of impurities and defects by optimized growth conditions is necessary for the conductivity control under 10<sup>18</sup> cm<sup>-3</sup>. In addition, in the present thesis, the author handled only Sn as the n-type doping materials. A theoretical and experimental study suggested that Sn is an efficient n-type dopant in Ga<sub>2</sub>O<sub>3</sub>, but Ge and Si could also be intentionally incorporated into Ga sites. Those dopants may be represented with different electrical properties compared to Sn dopant. Moreover, Zn could be a potential p-type dopant for

$\beta$ -Ga<sub>2</sub>O<sub>3</sub>. The Zn-doped  $\beta$ -Ga<sub>2</sub>O<sub>3</sub> will lead to interesting possibilities in p-n junction  $\beta$ -Ga<sub>2</sub>O<sub>3</sub> devices.

2. In the present work, crystalline properties of gallium oxide thin films epitaxially grown by mist CVD have been investigated. To achieve  $\alpha$ -Ga<sub>2</sub>O<sub>3</sub>-based devices with high efficiency,  $\alpha$ -Ga<sub>2</sub>O<sub>3</sub> thin films should be of high crystallinity.  $\alpha$ -Ga<sub>2</sub>O<sub>3</sub> films have been grown c-plane sapphire substrate. Therefore, there are lattice mismatch between  $\alpha$ -Ga<sub>2</sub>O<sub>3</sub> and a substrate. It is worth noticing that, in chapter 6, Al-doped  $\alpha$ -Ga<sub>2</sub>O<sub>3</sub> and (Al<sub>0.2</sub>Ga<sub>0.8</sub>)<sub>2</sub>O<sub>3</sub> alloy films were successfully grown on c-plane sapphire substrate. The insertion of buffer layer(s) of (Al<sub>x</sub>Ga<sub>1-x</sub>)<sub>2</sub>O<sub>3</sub> between  $\alpha$ -Ga<sub>2</sub>O<sub>3</sub> and c-plane sapphire substrate will reduce the lattice mismatch. The reduced lattice mismatch is expected to higher crystallinity  $\alpha$ -Ga<sub>2</sub>O<sub>3</sub> films.
3. The results of present thesis will pave the way for Ga<sub>2</sub>O<sub>3</sub>-based power devices such as MESFETs and MOSFETs with wide bandgap semiconductor. The MESFETs will be fabricated using electrical conductive Sn-doped  $\beta$ -Ga<sub>2</sub>O<sub>3</sub> films from the results of chapter 4. In chapter 6, Al-doped  $\alpha$ -Ga<sub>2</sub>O<sub>3</sub> films with enhanced thermal stability were successfully grown on c-sapphire substrate. To fabricate the  $\alpha$ -Ga<sub>2</sub>O<sub>3</sub>-based MOSFETs, n-type conductive channel and insulating films should be grown by mist CVD. N-type conductive channel can be realized with (Sn, Al)-doped  $\alpha$ -Ga<sub>2</sub>O<sub>3</sub>.  $\alpha$ -Al<sub>2</sub>O<sub>3</sub> can be used to insulate films. MOSFETs with film of all corundum structure will be achieved by mist CVD. The author anticipates that Ga<sub>2</sub>O<sub>3</sub> will be of global interest by energy saving power devices.
4. Mist CVD has many advantages in simple growth, low energy consuming process, large area growth, high quality film growth, and non-vacuum system. However, the growth system has not

been fully optimized for its materials and flow controllers. Purity of source materials may not be sufficient for semiconductor grade. The development of mist CVD is continuing for film growth with high quality and uniformity.

It is the authors' sincere wish that the achievements of this study can, even somewhat, contribute to sustainable progress of our society for our children, grandchildren, and all descendants.

# LIST OF ACHIEVEMENTS

## [PUBLICATIONS]

1. **S-D Lee**, and S. Fujita

“Homo-epitaxial growth of beta gallium oxide films by mist chemical vapor deposition”

(in progress)

2. **S.-D Lee**, Y. Ito, K. Kaneko, and S. Fujita

“Enhanced thermal stability of alpha gallium oxide films by supported aluminium”

Jpn. J. Appl. Phys. 54, 030301 (2015)

3. **S.-D Lee**, K. Akaiwa, and S. Fujita

“Thermal stability of single crystalline alpha gallium oxide films on sapphire substrates”

Phys. Status Solidi C. 10, 1592 (2013)

4. K. Kaneko, H. Ito, **S.-D. Lee**, and S. Fujita

“Oriented growth of beta gallium oxide thin films on yttrium-stabilized zirconia substrates”

Phys. Status Solidi C. 10, 1596 (2013)

5. T. Okuno, T. Osihma, **S.-D. Lee**, and S. Fujita

“Growth of SnO<sub>2</sub> crystalline thin films by mist chemical vapour deposition method”

Phys. Status Solidi C. 8, 540 (2011)

## [INTERNATIONAL CONFERENCES]

### 1. S.-D. Lee and S. Fujita

“Homo-epitaxial growth of beta gallium oxide by mist chemical vapor deposition”

2015 Materials Research Society Fall Meeting, Boston, USA, Nov. 29 – Dec. 4, 2015

### 2. S.-D. Lee and S. Fujita

“Fabrication of conductive Sn-doped  $\beta$ -Ga<sub>2</sub>O<sub>3</sub> films by mist chemical vapor deposition”

2015 International Workshop on Gallium Oxide and Related Materials, Japan, Nov. 3-6, 2015

### 3. S. Fujita, S.-D. Lee, K. Akaiwa, Y. Ito, M. Kitajima, and K. Kaneko

“Crystal stability and electrical defects in corundum-structured  $\alpha$ -Ga<sub>2</sub>O<sub>3</sub>-based semiconductor thin films”

2015 Materials Research Society Spring Meeting, San Francisco, USA, Apr. 6-10, 2015

### 4. S. Fujita, K. Kaneko, K. Akaiwa, S.-D. Lee, and N. Suzuki

“Wide band gap oxide semiconductors for novel device applications”

6th Asia-Pacific Workshop on Widegap Semiconductors, Tamsui, New Taipei City, Taiwan, May 12-15, 2013

### 5. S.-D. Lee and S. Fujita

“Thermal stability for single crystalline alpha gallium oxide films on sapphire substrate”

40th Int. Symp. Compound Semiconductors, Kobe, Japan, May 19-23, 2013

**6.** K. Kaneko, H. Ito, **S.-D. Lee**, and S. Fujita

“Epitaxial growth of beta gallium oxide thin films on yttrium-stabilized zirconia substrates”

40th Int. Symp. Compound Semiconductors, Kobe, Japan, May 19-23, 2013

**7.** K. Kaneko, K. Akaiwa, **S.-D. Lee**, N. Suzuki, and S. Fujita

“Band gap engineering and property engineering with gallium oxide-based compounds and alloys”

2012 Materials Research Society Fall Meeting, Boston, USA, Nov.25-30, 2012

**8.** S. Fujita, K. Kaneko, K. Akaiwa, **S.-D. Lee**, and N. Suzuki

“Wide bandgap gallium oxide-based compound and alloy semiconductors for novel functions”

Workshop on Frontier Photonic and Electronic Materials and Devices, 2012 German-Japanese-

Spanish Joint Workshop, Berlin, Germany, July 21-22, 2012

**9.** K. Kaneko, K. Akaiwa, **S.-D. Lee**, and S. Fujita

“Band gap engineering and function engineering with corundum-structured gallium oxide-based compounds and alloys”

55th Electronic Materials Conference, South Bend, IN, USA, June 26-28, 2012

**10. J. Piao, S.-D. Lee, S. Katori, T. Ikenoue, K. Kaneko, and S. Fujita**

“Ultrasonic spray-assisted vapor-deposition method as a cost-effective and environmental-friendly technology for fabrication of novel devices”

2012 European Materials Research Society Spring Meeting, strasbourg, France, May 14-18, 2012

**11. S. Fujita, K. Kaneko, T. Ikenoue, H. ito, T. Igawa, J. Piao, S.-D. Lee, and S. Katori**

“Solution-based vapor deposition of green materials: oxides and organic thin films and nanomaterials”

2011 Materials Research Society Fall Meeting, Boston, USA, Nov.28-Dec.2, 2011

**12. S. Fujita, K. Kaneko, T. Ikenoue, H. ito, J. Piao, S.-D. Lee, and S. Katori**

“Solution-based vapor deposition of oxide and organic thin films”

2nd Int. Conf. Green & Sustainable Chemistry, Singapore, Nov.14-16, 2011

**13. S. Fujita, T. Ikenoue, K. Kaneko, H. ito, T. Igawa, J. Piao, S.-D. Lee, and S. Katori**

“Solution-source vapor-phase synthesis of oxide and organic thin films”

UPAC 7th Int. Conf. Novel Materials and Synthesis, Shanghai, China, Oct. 16-21, 2011

**14. S. Fujita, K. Kaneko, Y. Fukui, T. Nomura, H. ito, S.-D. Lee, and S. Katori**

“Mist deposition technique as a green-chemical-route for oxide thin films and nanostructures”

International Conference on Materials and Advanced Technologies, Singapore, June 26-July 1, 2011

15. T. Okuno, T. Oshima, **S.-D. Lee**, and S. Fujita

“Characteristics of high quality SnO<sub>2</sub> thin films grown by novel mist chemical vapor deposition method”

37th Int. Symp. Compound Semiconductors, Takamatsu, Japan, May 31-June 4, 2010

## **[DOMESTIC MEETINGS]**

1. K. Akaiwa, **S.-D. Lee**, K. Kaneko, and S. Fujita

“Electrical properties of Sn-doped Ga<sub>2</sub>O<sub>3</sub> films grown by mist-CVD”

The 62nd JSAP spring meeting, Japan, March 11 – 14, 2015

2. K. Kaneko, N. Suzuki, **S.-D. Lee**, M. Kitajima, K. Akaiwa and S. Fujita

“Electrical characterization of corundum-structured oxides for device applications”

The 62nd JSAP spring meeting, Japan, March 11 – 14, 2015

IEICE CPM-ED-SDM meeting, Japan, May 28 – 29, 2014

3. Y. Ito, **S.-D. Lee**, and S. Fujita

“Modification in crystal structures of  $\alpha$ -Ga<sub>2</sub>O<sub>3</sub> grown on sapphire substrates”

The 32th Electronic Material Symposium, Japan, July 10 – 12, 2013

## ACKNOWLEDGEMENTS

I am very indebted to my advisor, Professor Shizuo Fujita, for his invaluable advice, guidance, supports on private difficulties during my long study at Kyoto University. I had such a level of self-confidence, when I first came to Japan, but I lost self-confidence a short time later from the ordeals and difficulties of relationships. This thesis would not have been possible without his concern, encouragement, and effort. Again, I would like to express my sincere gratitude to Professor Shizuo Fujita.

I wish to express my deep gratitude to Professor Gikan Takaoka and Associate Professor Jun Suda for their critical comments and valuable advice in this work. I am much obliged to Associate Professor Mitsuru Funato for training of experimental equipments. I would like to thank Assistant Professor Takayoshi Oshima at Tokyo Institute of Technology for his continuous concerns to me. I would like to express my sincere appreciation to Assistant Professor Kentaro Kaneko for his supports on both public and private difficulties and concerning experimental details. I also thank Assistant Professor Takumi Ikenoue at Graduate School of Energy Science, Kyoto University for his continuous concerns.

Special thanks are due to Dr. Kazuaki Akaiwa for his valuable discussions and his kind instructions on the operation of the experimental equipments. I am also grateful to Mr. Sachio Komori for photolithography operation. I would like to express his gratitude to Mr. Hiroshi Ito, Mr. Takuto Igawa, Mr. Daisuke Harada, Mr. Norihiro Suzuki, Mr. Kenji Shibayama, Kenta Suzuki, Yoshito Ito, Mr. Takayuki Uchida, Mr. Masashi Kitajima, Mr. Ryosuke Takagi, Mr. Masashi Uchida,

Ms. Riena Jinno, Mr. Shu Takemoto, Mr. Keiichi Tsumura for their kindness and support in the Fujita Laboratory including graduated members. In addition, I would like to thank Ms. Harumi Yoshimoto, Secretary of Fujita Laboratory for her help on practical difficulties in the Kyoto University.

I am very grateful to Professor Sang-Woo Kim at Sungkyunkwan University, Korea, who encouraged and advised me from my master course. I would like to thank Dr. Yoon-Seok Kim and Dr. Yoon-Seok Lee for their encouragement and concern.

Finally, I would like to express deeply gratitude to my parents, my wife's parents, my sisters, my brothers, my lovely son Ho-Hyun and all of my family for the support and their understanding. Especially, I must acknowledge my wife, Sung-Eun Kim, without whose love, encouragement, forbearance, and her understanding, I would not have finished this thesis.